The University of Southern Mississippi
The Aquila Digital Community

Dissertations

Fall 12-2009

Investigation of the Relationship Between Polymer Structures and Thermal, Mechanical, Viscoelastic Properties

Ethem Kaya
University of Southern Mississippi

Follow this and additional works at: https://aquila.usm.edu/dissertations

Part of the Materials Chemistry Commons, and the Polymer Chemistry Commons

Recommended Citation

Kaya, Ethem, "Investigation of the Relationship Between Polymer Structures and Thermal, Mechanical, Viscoelastic Properties" (2009). *Dissertations*. 1081.
https://aquila.usm.edu/dissertations/1081

This Dissertation is brought to you for free and open access by The Aquila Digital Community. It has been accepted for inclusion in Dissertations by an authorized administrator of The Aquila Digital Community. For more information, please contact aquilastaff@usm.edu.

The University of Southern Mississippi

INVESTIGATION OF THE RELATIONSHIP BETWEEN POLYMER STRUCTURES AND THERMAL, MECHANICAL, VISCOELASTIC PROPERTIES

by

Ethem Kaya

A Dissertation
Submitted to the Graduate School
of The University of Southern Mississippi
in Partial Fulfillment of the Requirements
for the Degree of Doctor of Philosophy

Approved:

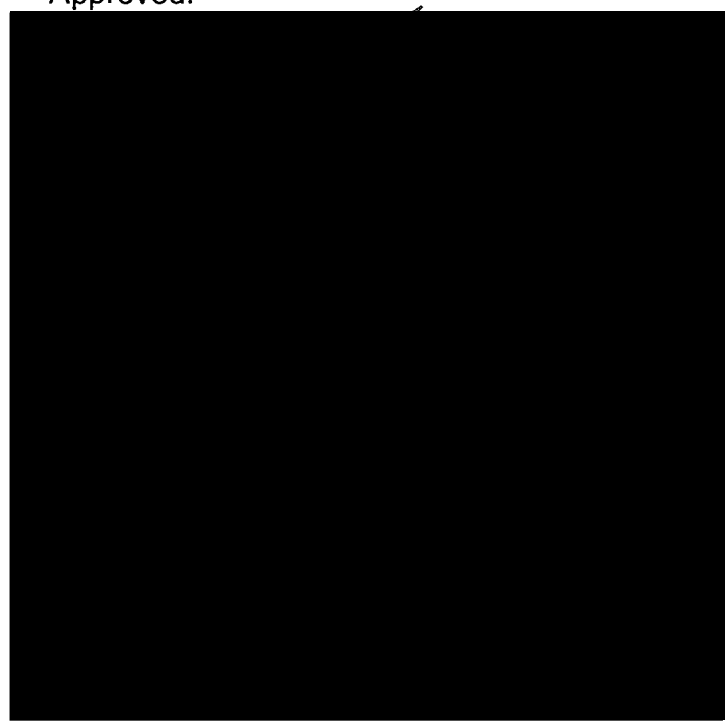

December 2009

COPYRIGHT BY

ETHEM KAYA

2009

The University of Southern Mississippi

INVESTIGATION OF THE RELATIONSHIP BETWEEN POLYMER STRUCTURES AND THERMAL, MECHANICAL, VISCOELASTIC PROPERTIES

by

Ethem Kaya

Abstract of a Dissertation
Submitted to the Graduate School
of The University of Southern Mississippi
in Partial Fulfillment of the Requirements
for the Degree of Doctor of Philosophy

December 2009

ABSTRACT

INVESTIGATION OF THE RELATIONSHIP BETWEEN POLYMER STRUCTURES AND THERMAL, MECHANICAL, VISCOELASTIC PROPERTIES

by Ethem Kaya

December 2009

The research presented in this dissertation involves four distinct areas: physical crosslinking systems, UV curable coatings for enhanced oxygen and carbon dioxide barrier properties, synthesis, and investigation of melting behavior/crystallinity relations of linear polyamides with long alkyl chains, and synthesis and characterization of cyclic diamides as precursors to linear polyamides 6 4.

The physical crosslinking section involves synthesis of monomers and polymers bearing cyclodextrin and adamantane pendent groups, and investigation of non-covalent interactions between these polymers (Chapter II). Two methacrylate monomers bearing cyclodextrin and adamantane were synthesized, and copolymerized with poly(ethylene glycol) methyl ether methacrylate. The specific interaction between copolymers bearing pendent cyclodextrin and adamantane were examined. The viscoelastic properties of supramolecular assemblies were investigated with frequency and temperature sweep experiments. The specific host-guest interaction between pendent adamantyl and cyclodextrin lead to large increases of viscosity, and depending on the concentration of these groups, also to gel formation.

The second section involves the investigation of methyl (α-hydroxymethyl)acrylate (MHMA) and its various copolymers as coatings for barrier improvement (Chapter III). The UV curable coating of MHMA gives excellent barrier improvement when coated onto PET biaxially oriented thin films. Blown bottle side walls from coated PET preforms show 2-3 times improvement over uncoated side walls. The affect of photoinitiator concentration, initiator types, and temperature on photopolymerization kinetics of MHMA was investigated. The photopolymerization kinetics of MHMA with methyl methacrylate was also studied.

The third section involves synthesis and characterization of long alkyl chain nylons (Chapter IV), and investigation of melting and crystallinity of nylons with high aliphatic content (Chapter V). Nylon 18 18 and nylon 18 ADA (1,3-adamantanedicarboxylic acid) have been synthesized via melt polycondensation and characterized by thermal and spectroscopic techniques. Crystallization and melting behaviors of both polymers were investigated. There is no observed melting for nylon 18 ADA by DSC. However, solution cast samples of nylon 18 ADA shows some ordered structures that can grow into more stable crystals with annealing.

The fourth section involves synthesis and characterization of cyclic diamides and exploration of the affect of the reaction conditions on yield and final cyclic formation. Ring-opening polymerization of these novel cyclic diamides was also investigated with different methods. Copolymerization of cyclic diamides with ε-caprolactam via an anionic route gave a block copolyamide with a two distinct

endotherms in DSC analysis. However, copolymerization by the hydrolytic route gave only nylon 6 with a terminal 6 4 units.

DEDICATION

To my brother and my mom, for their love and constant support

ACKNOWLEDGEMENTS

There are a number of people that I would like to thank for helping me throughout my graduate career. First, I wish to thank my advisor, Dr. Lon J. Mathias for being a great educator, and for his endless enthusiasm for teaching, his patience, and his support. Doc, you have given me the best education a person could ask for, and more importantly transferred some of your passion for science and education to me.

Next, I would like to acknowledge my committee members for their advice and recommendations over the past years: Dr. Charles Hoyle, Dr. Sergei Nazarenko, Dr. Jeffrey S. Wiggins, and Dr. James W. Rawlins. I am especially grateful to Dr. Rawlins for his time and friendly advice when I really needed it. I also thank Dr. Douglas J. Wicks for being part of my committee.

I also acknowledge Dr. William Jarrett for a number of discussions about NMR problems, and Dr. Robert Lochhead for the discussions about rheological behaviors of gels.

There are a number of other scientists that I have had the pleasure of working with, and learning from including Dr. Sanjay Mehta, whom I collaborated with on improving the barrier properties of PET, along with Vamsi Prattipati, Dr. Anne Hiltner, and Dr. Eric Baer. I would also like to thank the scientist from Solutia, Inc., Dr. Scott Osborn, Dr. Steven Manning, and Dr. Roger Ayotte for their insights and advice about the high performance polyamide projects, and providing the laboratory to carry out the experiments in their facilities.

Without the assistance of the people in the Department of Polymer Science, my life would have been much harder. Thanks to you all. There is a special person, Beverly McNeese, to whom I am especially thankful for her help in many problems I have faced.

I would like to thank the members of the Mathias Research Group, past and present, and fellow students for their support and friendship. Former MRG group members that helped me during my education include Tara Smith, Carl Bennett, Allison M. Sikes, Bianca Shemper, Paul Wheeler, Jean-Francois Morizor, Bishua Nayak, and Shailesh Goswami. I would also like to express special thanks to a former MRG member, Louis Somlai, for being a great friend and helping with many problems of my research. And to present MRG members, Chris and Ted, I always feel so lucky to be friends with you and to be in the same research group.

Huseyin and Eylem, you are the greatest, and I really do not know what I would do without you.

Dr. Brian Olson, you are the best friend a guy can ask for. Thanks Brian for being always around for me.

Finally, a very special thanks to Leigh Anne Sims for being in my life and for her support.

TABLE OF CONTENTS

ABSTRACT..... ii

DEDICATION.....v

ACKNOWLEDGMENTS.....vi

LIST OF ILLUSTRATIONS.....x

LIST OF TABLES.....xvii

LIST OF EQUATIONS.....xix

CHAPTER

I. INTRODUCTION.....1

Supramolecular Crosslinking Systems
Barrier Coatings for Poly(ethylene terephthalate)
Low Amide Density Nylons
Cyclic Diamides as Precursors to Linear Polyamides
References

II. SYNTHESIS AND CHRACTERIZATION OF PHYSICAL CROSSLINKING SYSTEMS BASED ON CYCLODEXTRIN INCLUSION/HOST-GUEST COMPLEXATION.....31

Abstract
Introduction
Experimental
Instrumental Analysis
Results and Discussion
Conclusion
References

III. UV CURABLE COATINGS FOR IMPROVED GAS BARRIER PROPERTIES OF POLY(ETHYLENE TEREPHTHALATE).....69

Abstract
Introduction
Results and Discussion
Conclusions
Acknowledgments
Experimental

References

IV. SYNTHESIS AND CHARACTERIZATION OF NYLON 18 18 AND NYLON 18 ADAMANTANE.....112

Abstract
Introduction
Experimental
Results and Discussion
Conclusions
Acknowledgments
References

V. INVESTIGATION OF MELTING BEHAVIORS AND CRSYTALLINITY OF LINEAR POLYAMIDE WITH HIGH ALIPHATIC CONTENT 145

Abstract
Introduction
Experimental
Results and Discussion
Conclusions
References

VI. PREPARATION, CHARACTERIZATION, AND COPOLYMERIZATION OF 12-MEMBERED CYCLIC DIAMIDE: 6-DIAZACYCLICDODECANE-2,5-DIONE.....173

Abstract
Introduction
Experimental
Results and Discussion
Conclusions
Acknowledgments
References

LIST OF ILLUSTRATIONS

Figure

1.1. (a) Complementary base pairing in helical DNA and (b) examples of specific pairs in DNA.....2

1.2. Chemical structure of β-cyclodextrin 3

1.3. Proposed structures of the (a) α-CD-PEA and (b) γ-CD-PEA complexes.....5

1.4. Molecular structure of adamantyl substituted monomer.....7

1.5. Crystal structures of nylon 6 in a) α forms and b) γ forms. 18

2.1. ^{13}C solution NMR of P(PEGMA) (top) and P(PEGMA-co-15APM) (bottom) in DMSO-d_6.....40

2.2. ^{1}H solution NMR of P(PEGMA) (top) and P(PEGMA-co-15APM) (bottom) in DMSO-d_6.....41

2.3. ^{13}C solution NMR of P(PEGMA-co-15MCD) in DMSO-d_6.....42

2.4. ^{1}H solution NMR of P(PEGMA-co-15MCD) in DMSO-d_6.....43

2.5. FTIR spectra of a) P(PEGMA-co-10MCD), b) P(PEGMA-co-10APM), c) P(PEGMA), and d) PEGMA.....45

2.6. DSC thermograms of copolymers a) P(PEGMA-co-5APM), b) P(PEGMA-co-10APM) , c) P(PEGMA-co-15APM), d) P(PEGMA-co-5MCD), e) P(PEGMA-co-10MCD), f) P(PEGMA-co-15MCD).....47

2.7. TGA thermograms of copolymers a) P(PEGMA-co-5APM), b) P(PEGMA-co-15APM), c) P(PEGMA-co-5MCD), d) P(PEGMA-co-15MCD) in N2.....48

2.8. Cloud point vs. comonomers feed ratio of copolymer bearing MCD, and APM.....50

2.9. ^{1}H NMR analysis of P(PEGMA-co-15APM) in D_2O (bottom) and DMSO-d_6 (top).....51

2.10. ^{1}H NMR analysis of inclusion complex formation between P(PEGMA-co-10APM) with various concentrations of free cyclodextrin.....53

2.11. Photograph and schematic representation of gel formation as a result of inclusion complexation between adamantyl and cyclodextrin pendent groups of copolymers. 54

2.12. Angular frequency dependence on complex viscosity for the mixture of 10 wt-% P(PEGMA-co-5APM)/P(PEGMA-co-5MCD) (■,□), P(PEGMA-co-10APM)/P(PEGMA-co-10MCD) (▲,△), P(PEGMA-co-15APM)/P(PEGMA-co-15MCD) (●,○), and P(PEGMA)/P(PEGMA-co-10MCD) (♦,◇) at 20 (open symbols) and 30 °C (filled symbols).....56

2.13. Frequency dependence on storage (filled symbols) and loss moduli (open symbols) for the mixture of 10 wt-% P(PEGMA-co-5APM)/P(PEGMA-co-5MCD) (■,□), P(PEGMA-co-10APM)/P(PEGMA -co-10MCD) (▲,△), P(PEGMA-co-15APM)/P(PEGMA-co-15MCD) (●,○), and P(PEGMA)/ P(PEGMA-co-10MCD) (♦,◇) at 30 °C.....57

2.14. Viscosity dependence on temperature for the mixture of P(PEGMA-co-10APM)/P(PEGMA-co-10MCD) (▲) and P(PEGMA-co-10MCD) (△) alone.....59

3.1. Structure of the supramolecular assembly of melamine.....72

3.2. Structure of methyl (α-hydroxymethyl)acrylate (MHMA).....74

3.3. A) Rate versus time and B) conversion versus time plots for MHMA with various Irgacure 819® initiator concentrations at 30 °C.....78

3.4. A) Rate versus time and B) Conversion versus time plots for MHMA with various Irgacure 819® initiator concentrations at 50 °C.....80

3.5. Structure of Irgacure 651® and Irgacure 819® photoinitiators 81

3.6. Rate versus time plots for MHMA with Irgacure 819® vs. 651® initiator at 30°C.....82

3.7. FTIR spectra of MHMA/MMA (50/50) mixture exposed to UV for various time intervals.....87

3.8. RT-FTIR plot of % conversion as a function of irradiation time for (a) MHMA, (b) MHMA:MMA with a ratio of (90:10), (c) MHMA:MMA (75:25), (d) MHMA:MMA (50:50), (e) MHMA:MMA (10:90), and (f) MMA.....88

3.9. DSC thermograms of homopolymers and copolymers.....90

3.10. The synthesis routes for MF and DF monomers.....93

3.11. Rate versus time plots for MHMA with MF and DF using 1 mol-% Irgacure 819® at 30 °C.....94

3.12. DSC thermograms for poly(MHMA-co-MMA) (50/50) with a) 1 mol-% MF, b) 5 mol-% MF, c) 10 mol-% MF, d) 1 mol-% DF, e) 5 mol-% DF, and f) 10 mol-% DF.....96

3.13. TGA for homo- and copolymers of a) poly(MHMA),

b) poly(MMA), c) poly(MHMA-co-MMA) (50/50),
d) poly(MHMA-co-MMA) (50/50) with 10 mol-% MF, and e)
poly(MHMA-co-MMA) (50/50) with 10 mol-% DF.....97

3.14. ^{1}H NMR spectra in DMSO-d_6 of (A) thermally polymerized viscous solution and (B) UV cured coating removed from a preform.....99

4.1. Repeat units of nylons with progressively higher aliphatic content. As amide density decreases and the spacing becomes more uniform, the polymer chain more resembles a functionalized polyethylene 114

4.2. FTIR spectrum of nylon 18 18.....119

4.3. ^{13}C solution NMR of the aliphatic and carbonyl (inset) regions of nylon 18 18. Sample was dissolved in a mixture of HFIP:$CDCl_3$.....120

4.4. Non-isothermal DSC heating traces of nylon 18 18 recorded at different heating rates 122

4.5. Non-isothermal DSC cooling traces of nylon 18 18 at different cooling rates 124

4.6. Graph of T_m and T_c for nylons X 18. The AB analogs nylon 16 and nylon 18 are shown for comparison.....125

4.7. Solid state ^{15}N CP/MAS NMR of nylon 18 18.....127

4.8. FTIR spectrum of nylon 18 ADA.....128

4.9. ^{13}C solution NMR of Nylon 18 ADA.....130

4.10. Solid state ^{15}N CP/MAS NMR of nylon 18 ADA.....131

4.11. DSC thermograms of solution-cast nylon 18 ADA annealed at various temperatures for 2 h.....132

4.12. DSC thermograms of solution-cast nylon 18 ADA annealed at 80 °C for various times.....134

4.13. The WAXD patterns of solution-cast nylon 18 ADA annealed at various temperatures for 2 h.....135

4.14. TGA thermograms in N_2 with heating rates of 10 °C/min.....136

4.15. Stress-strain curve for a) nylon 18 18, b) nylon 18 ADA, c) nylon 8 18, and d) nylon 6 18.....137

4.16. DMA curves of a) nylon 6 18, b) nylon 8 18, and c) nylon 18 18.....139

5.1. DSC thermograms of nylon18 18 annealed for 2 h at a) 80 °C, b) 90 °C, c) 100 °C, d) 110 °C, e) 120 °C, f) 130 °C, and g) 135 °C (samples annealed in DSC). 151

5.2. DSC thermograms of nylon18 18 annealed for 2 h at a) 140 °C, b) 145 °C, c) 150 °C, d) 155 °C, and e) 158 °C (samples annealed in DSC)..... 153

5.3. DSC heating thermograms of nylon18 18 annealed at 145 °C for 15, 60, 120, 360, 1440, and 2880 mins from bottom to top 156

5.4. DSC thermograms of nylon18 18 isothermally crystallized from melt for 2 h at a) 80 °C, b) 100 °C, c) 110 °C, d) 130 °C , e) 140 °C, and f) 150 °C (cooling rate is 60 °C/min).....157

5.5. DSC thermograms of nylon18 18 annealed at 145 °C for 2 h

and scanned with different heating rates 159

5.6. DSC thermograms of nylon18 18 sequentially annealed a) 80 °C, 100 °C, 135 °C, 145 °C, and finally 155 °C for 2 h each, b) first 155 °C then 145 °C, and 135 °C for 6 h each, and c) first 155 °C then 145 °C, 135 °C, 100 °C, and 80 °C for 2 h each.....161

5.7. The WAXD patterns of the nylon 18 18 annealed at various temperatures for 2 h from bottom to top: quenched, 80, 110, 120, 130, 140, 145, 150, and 155 °C.....162

5.8. The solid state ^{15}N CP/MAS NMR spectrum of nylon 18 18 samples a) quenched, b) annealed at 145 °C, and c) annealed at 155 °C for 2 h.....164

5.9. The solid state ^{13}C CP/MAS NMR spectrum of nylon 18 18 samples a) quenched, b) annealed at 145 °C, and c) annealed at 155 °C for 2 h.....165

5.10. Partial FTIR spectrum of annealed nylon 18 18 with increasing annealing temperature (arrows indicate direction of increasing temperature).....166

6.1. ^{13}C solution NMR spectrum of 1,6-diazacyclododecane-2,5-dione.....180

6.2. ^{1}H solution NMR of 1,6-diazacyclododecane-2,5-dione.....181

6.3. FTIR spectrum 1,6-diazacyclododecane-2,5-dione.....182

6.4. ^{13}C solution NMR of the 50/50 mixture (top) and

cyclic diamide II (bottom). 184

6.5. ^{1}H solution NMR of 50/50 mixture (top) and cyclic diamide II (bottom).....185

6.6. Partial FTIR spectra of the 50/50 mixture (solid line) and cyclic diamide II (dashed line).....186

6.7. The WAXD patterns of 50/50 mixture (bottom) and cyclic diamide II (middle), and cyclic diamide I (top).....187

6.8. ^{13}C solution NMR of neat nylon 6 (top) and nylon (6-co-64) (bottom) by anionic polymerization method.....189

6.9. Chemical structures of a) HAD-bisimide and b) HAD-bisamide acid 190

6.10. ^{13}C solution NMR nylon (6-co-64) by hydrolytic polymerization method 191

6.11. DSC heating thermograms of nylon (6-co-64) by hydrolytic polymerization (dashed line), and anionic polymerization (solid line).....192

Scheme

2.1 Synthesis of monomers.....39

2.2 General route for synthesis of copolymers.....39

6.1 Synthesis of 1,6-diazacyclododecane-2,5-dione.....179

LIST OF TABLES

Table

2.1 Mn, Mw, PDI, compositions, and yield of copolymers 44

2.2 T_g1 and T_g2 values of copolymers.....47

3.1 Density comparison for methacrylate monomers.....74

3.2 Oxygen permeation results for PET thin films coated with MHMA and photocured.....75

3.3 Carbon dioxide permeation results for PET thin films coated with MHMA and photocured.....75

3.4 Oxygen barrier of MHMA on PET thin films UV cured with varied initiator concentration and cure times.....83

3.5 Carbon dioxide barrier of MHMA on PET thin films UV cured with varied initiator concentration and cure time.....83

3.6 Effect of thickness of MHMA coating on PET permeability at 0 % RH.....85

3.7 Effect of thickness of MHMA coating on PET permeability at 85 % RH.....85

3.8 Water absorption and transmittance changes.....86

3.9 Compositions and T_g values of homopolymers and copolymers.....90

3.10 Oxygen barrier of MHMA with various MMA concentrations ranging from 1 mol-% to 25 mol-%.....91

3.11 Carbon dioxide barrier of MHMA on PET thin films UV cured with varied initiator concentration and cure times.....95

3.12 T_g values for copolymers with MF and DF.....97

3.13 Oxygen barrier results of blown bottle sidewalls.....100

4.1 ^{13}C solution NMR chemical shifts for nylon 18 18.....121

4.2 Thermal data for nylons X 18 recorded at a scan rate of 10 °C/min.....126

5.1 DSC parameters of nylon 18 18 samples annealed between 80 to 135 °C.....151

5.2 DSC parameters of nylon 18 18 samples annealed between 140 to 158 °C 154

5.3 DSC parameters of nylon 18 18 samples annealed 145 °C for two hours and scanned with different heating rates.....159

6.1 Synthesis of 1,6-diazacyclododecane-2,5-dione.....179

LIST OF EQUATIONS

Equation

1.1. Permeability as the product of solubility (S) and diffusivity (D).....11

3.1. Apparent oxygen permeability of coated film.....91

3.2. Instantaneous rates of polymerization.....106

3.3. Conversion.....107

CHAPTER I

INTRODUCTION

The research presented in this dissertation involves three distinct areas, physical crosslinking systems, UV curable coatings for enhanced oxygen and carbon dioxide barrier properties, synthesis, and investigation of melting behavior/crystallinity relations of linear polyamides with long alkyl chains, and finally synthesis of cyclic diamides as linear polyamide's precursor. The chapters in this dissertation were formatted to be submitted for publication, therefore each chapter contains an abstract, introduction, result and discussion, experimental, conclusion, and references section. The physical crosslinking chapter involves synthesis of monomers and polymers bearing cyclodextrin and adamantane pendent groups, and investigation of non-covalent interactions between these polymers (Chapter II). The second section involves the investigation of methyl (α-hydroxymethyl)acrylates and its various copolymers as a coating for gas barrier improvement (Chapter III). The third section involves synthesis and characterization of long alkyl chain nylons (Chapter IV), and investigation of melting and crystallinity of nylons with high aliphatic content (Chapter V). The fourth section involves synthesis and characterization of novel cyclic diamides and their copolymerization (Chapter VI).

Supramolecular Crosslinking Systems

Supramolecular materials are formed through reversible non-covalent interactions which may include ionic, or dipole interactins, metal-ligand associations, and/or hydrogen bonding. Because of the responsive features of

these interactions to external stimuli, supramolecular materials can undergo dynamic self-assembly and disassembly processes. This reversible characteristic makes such assemblies dynamic materials.[1] In nature, this type of structure and behavior is abundant. Naturally occurring DNA is one of the best examples for self-assembled structures. In DNA, two single strands are held together via a number of very selective hydrogen bonds (shown in Figure 1.1).[2]

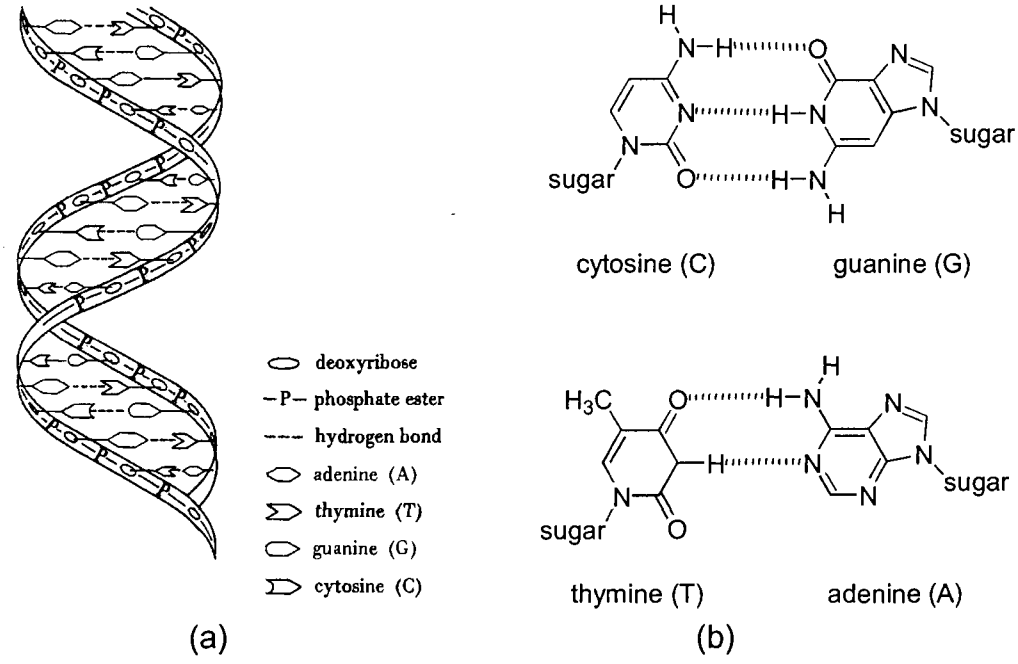

Figure 1.1. (a) Complementary base pairing in helical DNA and (b) examples of specific pairs in DNA.

Cyclodextrins (CDs) have been extensively used for industrial applications in many fields from laundry soap to food and pharmaceuticals. They also have been investigated as building blocks for supramolecular chemistry because they can form complexes with a number of different molecules and polymers through host-guest interaction.[3,4] The most widely used CDs are α-CD, β-CD (Figure 1.2), and γ-CD, which respectively consist of six, seven, or eight D-glucopyranose

units. They possess truncated, cone-shaped hydrophobic cavities in which the narrow end has primary and the wide end secondary hydroxyl groups. Since the inner cavity does not have any hydroxyl groups,[5] it can bind a number of different hydrophobic moieties. The driving forces for complex formation are the expulsion of high energy water from the cyclodextrin cavity, the release of ring strain, van der Waals interaction, and hydrogen bonding.[6]

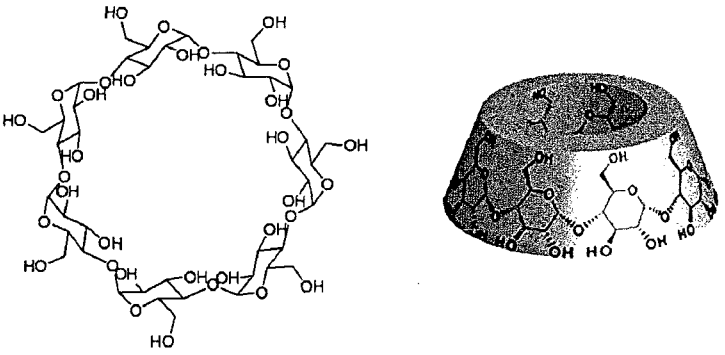

Figure 1.2. Chemical structure of β-cyclodextrin.

Because CDs have non-covalent interactions with host molecules, they are easily affected by changes in solvent, temperature, and other external stimuli. A cyclodextrin-based molecular shuttle is based on the fact that cyclodextrins, threaded along a polymer chain (polyrotaxane), move between different blocks of the polymer chain in response to various stimuli.[7,8]

Polyrotaxane Type Host-guest Interactions

Polyrotaxanes are topological structures that are usually made of one or more cyclic compounds threaded around another linear chain. Cyclodextrins, crowns, and porphyrins have been used as host cyclic units with several organic and inorganic polymers as linear guests.[9] In 1990, the first polymer-cyclodextrin inclusion complexes were reported by Harada.[10] Poly(ethylene glycol) (PEG) with

average molecular weight between 400 and 10000 was used to form inclusion complexes with α-cyclodextrin by addition of an aqueous solution of PEG to a saturated α-cyclodextrin aqueous solution at room temperature. The solution became turbid and precipitated complexes were obtained.[11] However, no complex formation was observed if poly(ethylene glycol) was replaced with poly(propylene glycol). Evidently, the presence of pendent CH_3 groups in poly(propylene glycol) increases the cross sectional dimension of the linear chains, which become too large to penetrate into the relatively narrow cavity of α-cyclodextrin.[12] These results indicate that the size of the cyclodextrin cavity and the cross sectional area of the included polymer are both important parameters for inclusion complex formation.

It has been reported[12] that poly(ethylene glycol) (PEG) does not form inclusion complexes with β-CD. The β-CD cavity (diameter of the cavity= 7.0 Å) may be too large for the cross sectional dimension of PEG to form a stable complex. Although the cavity of γ-CD is bigger (8.5 Å), inclusion complexes of γ-CD have been reported with several polyethers and polyesters such as poly(ethylene glycol) (PEG)[12,13], poly(ethylene adipate) (PEA)[14] as well as poly(ε-caprolactone) (PEC)[15]. It was proposed that two linear chains are included into each γ-CD cavity (as shown in Figure 1.3). PEG derivatives with γ-CD give crystalline compounds with columnar structures,[16] which seems to contradict this hypothesis, C_{60}-end-capped poly(ethylene oxide), on the other hand, formed a thermo-reversible gel structure presumably involving highly hydrophobic C_{60} ends

in hydrophilic solvent forming micelle-like core-shell aggregates which create another physical linkage besides cyclodextrins threaded PEGs.[13]

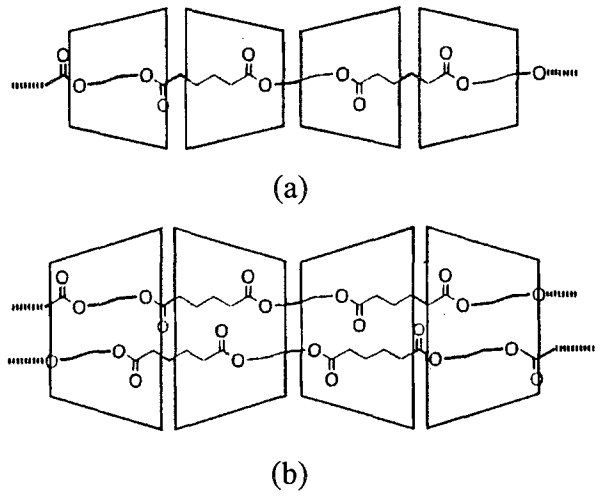

Figure 1.3. Proposed structures of the (a) α-CD-PEA and (b) γ-CD-PEA complexes.

Several crosslinking systems have been reported utilizing cyclodextrins. Yui, et al.,[17] reported supramolecular hydrogels based on inclusion complexation between α-cylodextrin and poly(ethylene glycol)-grafted dextran. α-Cyclodextrin threaded PEG chains come together to form channel-type crystalline micro-domains. These crystalline microphases create physical junctions between dextran main chains. The sol-gel transition is based on physical threading-dethreading of α-CDs from the polymeric guests. The process is strongly affected by temperature changes, making gelation thermo-reversible. The transition temperature can be varied by changing the solution concentrations, the PEG content in the graft polymer, and the stoichiometric ratio between guest and host molecules.

Another interesting crosslinking system was proposed by Okumura and Ito.[18] They synthesized polyrotaxanes in which PEG chains with molecular weights between 20,000 and 100,000 were included into α-cyclodextrins, then end-capped with bulky groups to prevent de-threading. These cyclodextrins were then chemically connected with cyanuric chloride crosslinker to give a transparent gel with good tensile strengths and large swellability in water. The polymer chains in this gel are neither covalently bonded like chemical gels nor attractively interacting like physical gels.

Specific Host-guest Interaction

Yui, et al.,[5] published a study in which both ionic and hydrophobic interactions were used to obtain sol-gel systems with rapid phase transitions. They modified poly(ε-lysine) (PL) with β-CD to give biocompatible and biodegradable polymeric hosts (β-CDPL). The guest, 3-trimethylsilylpropionic acid (TPA), containing both hydrophobic and ionic groups, was chosen specifically to provide dual interactions with the polymeric host and each other. In this system, TPA is included into the CD cavity by host-guest interaction to create physical crosslinks through co-operative hydrophobic and ionic interactions. The system showed a very rapid phase transition with small change in temperature across their upper critical solution region. Because of the ionic character, all systems are profoundly affected by pH changes.

The stability of an adamantane and cyclodextrin inclusion complexes have also been examined.[19] An acrylamide monomer substituted with an adamantyl group was synthesized (as shown in Figure 1.4).

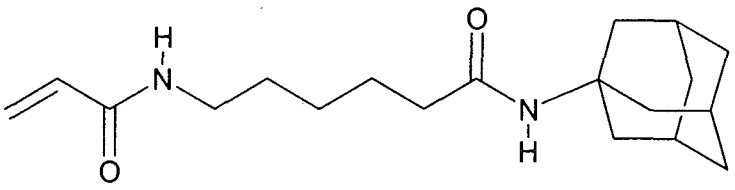

Figure 1.4. Molecular structure of adamantyl substituted monomer.

The copolymerization of an inclusion complex formed between adamantyl substituted monomer and 2,6-dimethyl-β-CD *N*-isoproplyacrlyamide (NIPAAM) was carried out in aqueous media. After copolymerization, the mixture was dialyzed for two days and then freeze dried. GPC analysis of the copolymer showed that it retained the original amount of β-CD, which implies that the complex was stable during both synthesis and dialysis. On the other hand, GPC using DMF as a solvent indicated detachment from CD during elution; clearly, DMF shifted the equilibrium back to the uncomplexed state.

Organic-inorganic polymer hybrids have been prepared using the strong host-guest interaction between adamantane and β-cyclodextrin.[20] Supramolecular assembles of adamantane-modified poly(acrylic acid) (ADA-PAA) and β-cyclodextrin mixed with an aqueous solution of tetramethoxysilane (TMSO) gave the first example of a transparent and homogenous polymer hybrid. A homogenous aqueous solution of ADA-PAA cannot be achieved because of poor solubility of adamantane moiety in water, but after addition of β-CD to the mixture, a transparent and homogenous solution was obtained. This results from strong host-guest interaction between adamantane and cyclodextrin which increases aqueous solubility of the adamantane groups.

The host-guest interactions between adamantane and β-cyclodextrin have also been proven by fluorescence using a dansyl group that exhibits strong fluorescence in a hydrophobic environment, but not in water.[21] Because the cyclodextrin cavity is hydrophobic, complexation of the dansyl group with β-cyclodextrin gives an intense peak around 480 nm. The peak intensity decreases with addition of ADA-PAA, because adamantane forms a stronger complex with the β-CD, causing the dansyl groups to be excluded from the hydrophobic cavity into water and decreasing the fluorescence peak.

Many studies have been performed to understand the mechanism of molecular recognition and molecular assembly by cyclodextrins to obtain more selective and functional supramolecular systems.[22,23,24,25] Studies showed that some substituents can self-include into the cavity of the parent cyclodextrin scaffold to form an intramolecular inclusion complex.[22] However, depending on the substituted structure, either two modified cyclodextrins can interact with each other (heterodimerization)[23] or modified cyclodextrin can interact with unmodified cyclodextrin (homodimerization).[24]Oligomeric supramolecular structures can also form in aqueous medium,[26] generating a supramolecular helical column possessing inclusion complexes between modified cyclodextrins.

Biomedical Applications

Controlled drug release is one of the main goals of polymeric drug delivery systems. It is known that polymeric systems can modify drug release through generic mechanisms involving dissolution, diffusion, and erosion. Cyclodextrin is well known for being a host for many drugs. It has been reported

that physically mixing cyclodextrin with drugs can modify drug solubility, and diffusivity, and can change the hydration behavior of a polymer matrix to promote erosion.[6]

Paclitaxel is known for its tumor inhibitory properties.[27] However, its poor water solubility is a significant problem in clinical applications. To increase its solubility, paclitaxel was complexed with simple or modified cyclodextrins. Limited water solubility and stability are also problems for anti-tumor drugs such as doxorubicin[28] and chlorambucil.[29] In addition to increasing water solubility, cyclodextrins can allow simultaneous delivery of two or more drugs at the targeted site. Although cyclodextrins have been extensively used as host molecules for individual drugs and as building blocks for supramolecular gel formation, no report to date has described bringing those properties together. A supramolecular gel made with adamantyl-cyclodextrin conjugated polymers could be used as gels for single drug delivery or for host-guest complex formation with several drugs for synergistic treatment.

Cyclodextrins are also used for supramolecular hydrogel formation. Biodegradable hydrogels are very important for delivery of hydrophobic therapeutic drugs and proteins. Erosion of hydrogels via hydrolysis makes surgery unnecessary to remove the implanted hydrogel. Another important issue with hydrogels is the erosion time, the time necessary for complete disappearance, and it is crucial to control erosion time for many biomedical applications. Yui, et al.,[30] described a series of PEGs crosslinked by polyrotaxanes that consisted of PEGs chain-threaded with α-CDs and end-

capped with bulky groups via ester linkages. It has been shown that the time for complete gel erosion is prolonged by decreasing the polyrotaxane content and increasing the PEG/α-CD ratio, indicating that the number of PEG chains linked to one CD is important.

The work described in this dissertation involves preparation of supramolecular hydrogel for possible drug delivery applications. Two novel monomers and their polymers bearing adamantane and cyclodextrin pendant groups were synthesized. These monomers were copolymerized with poly(ethylene glycol) methyl ether methacrylate (PEGMA, 300 g/mol) at three different compositions by conventional free radical polymerization techniques. The host-guest interactions and viscoelastic properties of these new physical networks between PEG and adamantane units with pendent cyclodextrin units were investigated.

Barrier Coatings for Poly(ethylene terephthalate)

Poly(ethylene terephthalate) (PET) is widely used in food packaging because of its cost efficiency and good mechanical properties compared to other polymeric materials. PET has reasonably good gas barrier properties, but still the barrier performance of PET must be improved for certain applications such as bottles used for beer or juices. Therefore, there has been a significant interest in research to obtained PET with enhanced barrier properties. However, it is important not to compromise the mechanical properties, and in some cases the transparency of PET, while improving the barrier performance. In addition, the improvement has to be achieved with minimal cost to be applicable to industry.

Permeabilities of small molecule penetrants through polymer films was described in the late 1800's using a "solution-diffusion" mechanism. The permeability, P, depends on a small molecule penetrant entering the film by dissolving in the upstream face and diffusing to the downstream face. This mechanism still holds today, and describes the permeability as the product of solubility (S) and diffusivity (D).[31]

Equation 1.1 $P = D \cdot S$

Most semicrystalline polymers like PET show decreasing permeability with increasing crystallinity. Crystallites are considered impermeable and create a torturous pathway for the penetrant molecules which, in turn, decreases D. In addition to this factor, increased crystalline domain content would decrease the amount of amorphous domain which can dissolve the penetrant molecules and, in turn, decrease S. However, the decrease of S is not directly proportional to decrease in amorphous domain content. This observation was discussed by Nazarenko, et al.,[32] for semicrystalline PET and attributed to formation of rigid amorphous fraction.

Because permeability depends on diffusivity and solubility, a number of approaches to lowering D and S in PET systems have been investigated. One approach to enhance the gas barrier performance of PET is silica coating. The gas barrier of silica coating is governed by chemical composition of silica layers in addition to pinholes and cracks.[33] The surface composition affects the gas adsorption, while the inner composition is associated with gas diffusion through the Si-O-Si network. Plasma-enhanced chemical vapor deposition (PECVD) has

also been utilized to deposit silica coating on PET substrates. Silica coating on PET prepared by PECVD has been reported to have serious drawbacks as a result of impurities such as Si-CH_3, Si-H, and Si-OH which prevent completion of the Si-O-Si network and therefore increase the permeability of the coating.[34] Takai, et al.,[35] utilized a second layer composed of a different organosilane on the silica coating. This was deposited by PECVD and enhanced the gas barrier performance of PET. Organosilanes, such as n-ocdecyltrimethoxysilane (ODS), and heptadefluoro-1,1,2,2-tetrahydrodecyl-1-trimethoxysilane (FAS), were deposited on the silica layer by a low-temperature CVD method, and lead to slight decreases in oxygen transmission rates compared to the original silica layer. However, water vapor transmission rates for the FAS deposited substrate showed a significant decrease compared to the initial silica layer.

Blending PET with a high barrier polymer is another approach that has been explored for a number of different polymers such as ethylene-vinyl alcohol copolymer,[36] liquid crystalline polyester,[37]and polyamides.[38] Unlike aliphatic polyamides, aromatic polyamides retain barrier performance even under high humidity conditions which makes them suitable for blending with PET. However, incompatibility could be an issue for blending, and a compatibilizer may need to be incorporated to obtain optimum barrier properties. Work by Hiltner, et al.,[39] explored the effect of the compatibilizer content, polyamide content, and humidity on gas barrier of PET. This study demonstrated that 5-10 wt-% high barrier aromatic polyamides noticeably improved gas barrier performance of PET. However, orientation is essential to obtain barrier, since unoriented blends of

PET/polyamides show only very small changes in oxygen permeability. Biaxial orientation of the blend converted spherical polyamide domains into high aspect ratio platelets which in turn improved gas barrier properties by creating a more torturous pathway for penetrant molecules (decreasing D).

Poly(ethylene 2,6-naphthalate) (PEN) is a very interesting high-barrier thermoplastic. It gives a 4-5 times lower air permeation than PET. However, the application of PEN in the packaging industry is limited due to its much higher cost (4-5 times more than that of PET). It has been of great interest to use this high-barrier thermoplastic with PET to reduce cost. Again, blending is one alternative to improve the barrier performance of PET. Compatibility can be obtained at the interface by transesterification which leads an indistinct interface between PET and PEN, and to smaller PEN particles. However, barrier improvement can only be achieved if the blend will biaxial. Baer, et al.,[40] investigated the effect of the copolymer composition and the various comonomers including naphthalate units on PET barrier. The incorporation of naphthalate units reduced the permeability to lower values, and gas barrier performance of PET improved with the increasing amounts of comonomers.

Recently, there has been increasing emphasize on inorganic fillers on barrier properties of several polymers including PET. The improved gas barrier performance depends on both crystallinity and filler loading level. One typical filler is Montmorillonite (MMT), and it has to be organically modified to obtain high levels of interaction with the polymer matrix. It is assumed that exfoliation of clay platelets is crucial to obtaining high barrier since the aligned and exfoliated MMT

sheets would create a torturous pathway (decreasing D). This observation was reported for a number of polymer matrices.[41,42] However, exfoliation for PET is difficult at the processing temperature of PET which is higher than the decomposition temperature of most surfactants used to organically modify the clay. Yongping, et al.,[43] investigated barrier properties of PET/MMT nanocomposites in which MMT was organically modified with a surfactant containing –COOH group to incorporate the surfactant as an end group in the PET. Although biaxially oriented films of PET/MMT nanocomposites showed lower permeability to O_2, there were no detailed studies to establish the effect of clay on permeability of PET. Hwang, et al.,[44] on the other hand, attempted to intercalate an esterification catalyst directly into MMT interlayers (instead of using organic modification of the clay) to avoid the thermal degradation of surfactant. Oxygen permeability of PET/clay-supported catalyst composite films was found to be considerably lower compared to neat PET films.

A reduction in free volume in the amorphous regions would also reduce the diffusion rate of the penetrant molecules. Moolman, et al.,[45] studied the effect of hydrogen bonding interactions between poly(vinyl alcohol) (PVOH) and poly(methyl vinyl ether-co-maleic acid) (PMVE-MA) blends on barrier properties of PVOH. PVOH with 20 wt-% (PMVE-MA) showed almost 4 times lower oxygen permeability compared to PVOH. Since the crystallinity of PVOH with 20-30 wt-% (PMVE-MA) was not significantly changed, the decrease in permeability was attributed to a denser amorphous region due to hydrogen bonding between the two polymers causing a decrease in free volume. Further increase in (PMVE-MA)

content, on the other hand, resulted in decreased barrier performance since the hydrogen bonding and crystalinity were both reduced by increasing the (PMVE-MA) content.

All these methods has been shown to improve the barrier properties of PET, yet they have not been widely used in industry because of a substantial increase in investment in equipment, very complicated manufacturing processes, an increase in material cost, decrease in transparency, and loss of mechanical properties. An alternative second barrier, such as, a silica coating, requires complex processing such as vacuum deposition. Inorganic fillers such as clays must be aligned and dispersed throughout a PET matrix to effectively reduce permeation, and dispersion of clay platelets is difficult due to thermal degradation of surfactants used for organic modification of clays. Blending and incorporation of comonomers can affect bulk properties of PET, but substantially increase the cost and may require changes in processing conditions. In addition, such materials must be approved for contact with food and beverages.

In this work we investigate the use of a UV-curable coating based on methyl (α-hydroxymethyl)acrylate for improved PET barrier properties. The solvent free coating does not alter bulk properties of PET, and is applied as an outer layer, so it does not contact food or beverages inside. The work presented here was accomplished by the collaboration with Tara Smith.

Low Amide Density Nylons

Nylons are an important family of polymers due to their unique properties including relatively high modulus, toughness and strength; and good temperature

resitantance, which makes them widely used as fibers and engineering thermoplastics. Mechanical properties of nylons depend on backbone symmetry, total amide density and processing conditions. The backbone symmetry determines if the polymer is highly crystalline or amorphous while the processing controls the orientation of the polymer chains and final the degree of crystallinity.

The most important characteristic of nylons is the hydrogen bonding capabilities of – NH – and – CO – moieties in the amide groups. Therefore, the properties of a specific nylon will vary depending on amide density within the nylon's molecular chains. Amide density affects T_m, and to some extent, T_g. In recent years, there have been several reports on nylons with low and high amide unit density to investigate the effect of amide density on the performance of these novel polyamides.[46,47,48,49] The low amide density nylons have lower melting points depending on the concentration of amide units. They show good impact properties, a lower dielectric constant, and improved hydrophophobicity. These nylons may be thought as backbone functionalized polyethylene, possessing the hydrophobic characteristics of polyethylene, but with improved thermal properties due to the hydrogen bonding amide units. These long alkyl chain nylons have also been considered as compatibilizers between polyamides and polyolefins.[50]

Crystallinity of Nylons

The most important feature of nylon structure is the organization of the polymer chains in two dimensional hydrogen bonded sheets which are held together by van der Waals interactions in a three dimensional lattices.[51] Crystallization requires the optimization of interactions of amide groups, and

methylene groups combined with chain folding. Hydrogen bonds have the lowest energy when they are linear, perpendicular to chain axis. Most even-even nylons can progressively shear by 13° parallel to the chain axis (c direction) to form chain-folded sheets called p-sheets with linear hydrogen bonds. However, nylons with equal numbers of methylene units in both diamine and diacid segments can also fold over amides units to create alternatively sheared chains called a-sheets. As in the case of hydrogen-bonded sheets formation, these hydrogen bonded sheets can also be stacked together either progressive or alternating manners via van der Waals forces.

Depending on the type of hydrogen-bonded sheet formation, and stacking of sheets, two main crystalline structures denoted α and γ can be identified for nylons. There are other types of crystalline structures that can be regarded as variations of these two main types.[52] In the α structure, the chains are hydrogen bonded with a fully extended planar zigzag conformation. The amide groups in γ structures are rotated about 60° with respect to the polymethylene chain axis resulting shorter chain axis than that of the fully extended zigzag conformation. The energy lost by twisting amide groups in the γ structure can be compensated by the stability of fully hydrogen bonded structures.[53] Crystal structures of nylon 6 in α forms and γ forms are given in Figure 1.5 as examples. For even-even nylons, the α form is the stable phase, while the γ form is the stable phase for even-odd, odd-even, and odd-odd nylons at room temperature. Even nylons with short methylene groups such as PA-4, and PA-6 mainly crystallize into the α

form, while even nylons with more than seven methylene groups adopt the γ form as the stable phase.

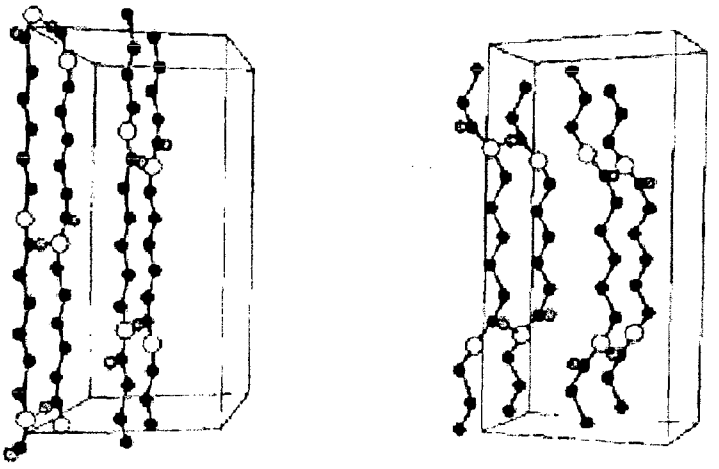

Figure 1.5. Crystal structures of nylon 6 in a) α forms and b) γ forms.

The α and γ crystallites can be easily identified using x-ray techniques. In addition to x-ray, ^{15}N nuclear magnetic resonance (NMR) techniques is also used to differentiate α and γ forms, as well as to quantitate the relative amorphous content.[54,55,56] Different crystal forms can be obtained under specific conditions and one type of crystal can be transformed into another type by changing these conditions. The α crystal form can usually be obtained by slow crystallization from the melt, or by crystallization from a solvent, while the γ crystal form can be produced by kinetically-trapping via rapid crystallization. The transformation from γ to α can be achieved by heat, drawing, solvent, or a combination of these factors. For instance, the α crystal form of even nylons can be transformed into the γ form by treating the sample with an aqueous iodine-potassium iodide solution, while the reverse transformation is possible by treatment with phenol.

Mo, at el.,[57] investigated the crystal transition of nylon 12 12 under drawing and annealing. The α form was obtained for nylon 12 12 by crystallization from the melt or annealing at high temperature. The γ form, on the other hand, can be obtained by crystallizing from the melted state at 90 °C, or drawing at 90 and 160 °C.

In recent years, there have been several reports by our group and others, which emphasize synthesis and crystal structures of nylons with long alkyl chains.[58,59,60] The hydrogen bonded amide units of nylons control the crystal structures and overall characteristic of polyamides. However, van der Waals interactions would be expected to be more and more important with decreasing amide density in specific nylons. Therefore, one would expect that below a certain amide density, nylons would adopt polyethylene-like crystal structures.

In this work, the synthesis and characterization of two new long alkyl chain nylons are reported along with the effect of adamantyl backbone units in combination with a long alkyl chain on the thermal and mechanical properties of nylons. Additionally, the affect of crystallization conditions on melting behavior of long alkyl chain nylons was studied. The work presented in Chapter IV was accomplished by the collaboration with Carl Bennett.

Cyclic Diamides as Precursors to Linear Polyamides

Cyclic monomer and oligomers are part of many step-growth polymerization or Depolymerization reactions, and their presence and chemistry are well-known.[61] Because of their low viscosity, and easy in situ poymerizability with an appropriate catalyst, they give high molecular weight polymers, that are

of interest to industry. For instance, anionic polymerization of caprolactam can be done in reaction injection molding since the monomer has a much lower melting temperature compared to the polymer. The process thus provides many economical and processing advantages.[62] Cyclic monomers and oligomers are also of interest in host-guest supramolecular chemistry, since they can recognize inorganic, and organic cations as well as strongly bind neutral substances.[63]

The melting temperature of nylon 6 4 was reported[64] as being 278 °C, which is much higher then commercial nylon 6 6 (260 °C). Since amide density is higher then the amide density of nylon 6 6, the mechanical properties of nylon 6 4 would be expected to be enhanced. Although there are economical advantages for the starting materials for nylon 6 4 compared to other high melting commercial nylons, it has not yet been commercialized. To date, there have been only reports of thermal properties and crystal structures of this promising polymer.[51,64.66,67] This may be due to the fact that high molecular weight nylon 6 4 can not be obtained with traditional polycondensation reactions.

In this work, the synthesis and characterization of a 12-membered cyclic diamide as potential precursor of nylon 6 4 was explored. Additionally, ring-opening polymerization of the cyclic diamide was investigated.

References

1 Berl, Volker; Schmutz, Marc; Krische, Michael J.; Khoury, Richard G.; Lehn, Jean-Marie. Supramolecular Polymers Generated from Heterocomplementary Monomers Linked through Multiple Hydrogen-Bonding Arrays-Formation, Characterization, and Properties. *Chemistry-A European Journal,* **2002**, 8, 1227-1244.

2 Stryer, L. Biochemistry; Fourth Edition Ed.; W. H. Freeman And Company: New York, **1995**.

3 Wenz, Gerhard. Cyclodextrins as Synthons for Supramolecular Structures and Functional Units. *Angewandte Chemie,* **1994**, 106, 851-870.

4 Rusa, Cristian C.; Tonelli, Alan E.. Separation of Polymers by Molecular Weight through Inclusion Compound Formation with Urea and α-Cyclodextrin Hosts. *Macromolecules*, **2000**, 33, 1813-1818.

5 Choi, Hak Soo; Ooya, Tooru; Sasaki, Shintaro; Yui, Nobuhiko. Control of Rapid Phase Transition Induced by Supramolecular Complexation of β-Cyclodextrin-Conjugated Poly(ε-Lysine) with a Specific Guest. *Macromolecules,* **2003**, 36, 5342-5347.

6 Bibby, D. C.; Davies, N. M.; Tucker, I. G.. Mechanisms by Which Cyclodextrins Modify Drug Release from Polymeric Drug Delivery Systems. *International Journal of Pharmaceutics,* **2000**, 197, 1-11.

7 Fujita, Hiroaki; Ooya, Tooru; Yui, Nobuhiko. Thermally Induced Localization of Cyclodextrins in a Polyrotaxane Consisting of β-Cyclodextrins and Poly(ethylene

glycol)-Poly(propylene glycol) Triblock Copolymer. *Macromolecules*, **1999**, 32, 2534-2541.

8 Kawaguchi, Yoshinori; Harada, Akira. A Cyclodextrin-Based Molecular Shuttle Containing Energetically Favored and Disfavored Portions in Its Dumbbell Component. *Organic Letters*, **2000**, 2, 1353-1356.

9 Ceccato, Massimo; Lo Nostro, Pierandrea; Baglioni, Piero. α-Cyclodextrin/Polyethylene Glycol Polyrotaxane: A Study of the Threading Process. *Langmuir*, **1997**, 13, 2436-2439.

10 Harada, Akira; Kamachi, Mikiharu. Complex Formation between Poly(ethylene glycol) and α-Cyclodextrin. *Macromolecules,* **1990**, 23, 2821-2823.

11 Lautens, Mark; Abd-El-Aziz, Alaa S.; Schmidt, Gunther. Synthesis and Epoxidation of cis-Enriched Polydeltacyclene. *Macromolecules,* **1990**, 23, 2819-2821.

12 Harada, Akira; Okada, Miyuko; Li, Jun; Kamachi, Mikiharu. Preparation and Characterization of Inclusion Complexes of Poly(propylene glycol) with Cyclodextrins. *Macromolecules*, **1995**, 28, 8406-8411.

13 Jiao, Hua; Goh, S. H.; Valiyaveettil, S.. Inclusion Complexes of Single-C60-End-Capped Poly(ethylene oxide) with Cyclodextrins. *Macromolecules*, **2002**, 35, 1399-1402.

14 Harada, Akira; Nishiyama, Toshiyuki; Kawaguchi, Yoshinori; Okada, Miyuko; Kamachi, Mikiharu. Preparation and Characterization of Inclusion Complexes of Aliphatic Polyesters with Cyclodextrins. *Macromolecules*, **1997**, 30, 7115-7118.

15 Kawaguchi, Yoshinori; Nishiyama, Toshiyuki; Okada, Miyuko; Kamachi, Mikiharu; Harada, Akira. Complex Formation of Poly(ε-caprolactone) with Cyclodextrins. *Macromolecules*, **2000**, 33, 4472-4477.

16 Harada, Akira; Suzuki, Syukuko; Okada, Miyuko; Kamachi, Mikiharu. Preparation and Characterization of Inclusion Complexes of Polyisobutylene with Cyclodextrins. *Macromolecules*, **1996**, 29, 5611-5614.

17 Huh, Kang Moo; Ooya, Tooru; Lee, Won Kyu; Sasaki, Shintaro; Kwon, Ick Chan; Jeong, Seo Young; Yui, Nobuhiko. Supramolecular-Structured Hydrogels Showing a Reversible Phase Transition by Inclusion Complexation between Poly(ethylene glycol) Grafted Dextran and α-Cyclodextrin. *Macromolecules*, **2001**, 34, 8657-8662.

18 Okumura, Yasushi; Ito, Kohzo. Design and Properties of Topological Gels. *Polymer Preprints (American Chemical Society, Division of Polymer Chemistry)*, **2003**, 44, 614-615.

19 Ritter, Helmut; Sadowski, Oleg; Tepper, Elmar. Influence of Cyclodextrin Molecules on the Synthesis and the Thermo-Responsive Solution Behavior of N-Isopropylacrylamide Copolymers with Adamantyl Groups in the Side-Chains. *Angewandte Chemie, International Edition*, **2003**, 42, 3171-3173.

20 Ogoshi, Tomoki; Chujo, Yoshiki. Synthesis of Organic-Inorganic Polymer Hybrids by Means of Host-Guest Interaction Utilizing Cyclodextrin. *Macromolecules*, **2003**, 36, 654-660.

21 Fischer, Peter; Koetse, Marc; Laschewsky, Andre; Wischerhoff, Erik; Jullien, Ludovic; Persoons, Andre; Verbiest, Thierry. Orientation of Nonlinear Optical

Active Dyes in Electrostatically Self-Assembled Polymer Films Containing Cyclodextrins. *Macromolecules*, **2000**, 33, 9471-9473.

22 Liu, Yu; Fan, Zhi; Zhang, Heng-Yi; Diao, Chun-Hua. Binding Ability and Self-Assembly Behavior of Linear Polymeric Supramolecules Formed by Modified β-Cyclodextrin. *Organic Letters,* **2003**, 5, 251-254.

23Hamasaki, Keita; Ikeda, Hiroshi; Nakamura, Asao; Ueno, Akihiko; Toda, Fujio; Suzuki, Iwao; Osa, Tetsuo. Fluorescent Sensors of Molecular Recognition. Modified Cyclodextrins Capable of Exhibiting Guest-Responsive Twisted Intramolecular Charge Transfer Fluorescence. *Journal of the American Chemical Society*, **1993**, 115, 5035-5040.

24 Kuwabara, Tetsuo; Aoyagi, Taiyo; Takamura, Makoto; Matsushita, Akiko; Nakamura, Asao; Ueno, Akihiko. Heterodimerization of Dye-Modified Cyclodextrins with Native Cyclodextrins. *The Journal of Organic Chemistry*, **2002**, 67, 720-725.

25 Mcalpine, Shelli R.; Garcia-Garibay, Miguel A. Studies of Naphthyl-Substituted β-Cyclodextrins. Self-Aggregation and Inclusion of External Guests. *Journal of the American Chemical Society*, **1998**, 120, 4269-4275.

26 Hoshino, Taiki; Miyauchi, Masahiko; Kawaguchi, Yoshinori; Yamaguchi, Hiroyasu; Harada, Akira. Daisy Chain Necklace: Tri[2]Rotaxane Containing Cyclodextrins. *Journal of the American Chemical Society,* **2000**, 122, 9876-9877.

27 Liu, Yu; Chen, Guo-Song; Li, Li; Zhang, Heng-Yi; Cao, Dong-Xu; Yuan, Ying-Jin. Inclusion Complexation and Solubilization of Paclitaxel by Bridged Bis(β-

cyclodextrin)s Containing a Tetraethylenepentaamino Spacer. *Journal of Medicinal Chemistry,* **2003**, 46, 4634-4637.

28 Rapoport, Natalya; Pitt, William G; Sun, Hao; Nelson, Jared L. Drug Delivery in Polymeric Micelles: From in Vitro to in Vivo. *Journal of Controlled Release: Official Journal of the Controlled Release Society,* **2003**, 91, 85-95.

29 Mi, Fwu-Long; Lin, Yi-Mei; Wu, Yu-Bey; Shyu, Shin-Shing; Tsai, Yi-Hung. Chitin/PLGA Blend Microspheres as a Biodegradable Drug-Delivery System: Phase-Separation, Degradation and Release Behavior. *Biomaterials,* **2002**, 23, 3257-3267.

30 Ichi, T; Watanabe J; Ooya, T; Yui, N. Controllable Erosion Time and Profile in Poly(ethylene glycol) Hydrogels by Supramolecular Structure of Hydrolyzable Polyrotaxane. *Biomacromolecules*, **2001**, 2, 204-210.

31 Koros, W. J. Barrier Polymers and Structures: Overview. In Barrier Polymers and Structures; Koros, W. J., Eds.; American Chemical Society: Washington, D. C., **1990**, Chapter 1, pp 1-21.

32 Lin, J.; Shenogin, S.; Nazarenko, S. Oxygen Solubility and Specific Volume of Rigid Amorphous Fraction in Semicrystalline Poly(ethylene terephthalate). *Polymer*, **2002**, 43, 4733-4743.

33 Joly, C.; Smaihi, M.; Porcar, L.; Noble, R. D. Polyimide-Silica Composite Materials: How Does Silica Influence Their Microstructure and Gas Permeation Properties? *Chemistry of Materials,* **1999**, 11, 2331-2338.

34 Teshima, Katsuya; Inoue, Yasushi; Sugimura, Hiroyuki; Takai, Osamu. Growth and Structure of Silica Films Deposited on a Polymeric Material by

Plasma-Enhanced Chemical Vapor Deposition. *Thin Solid Films,* **2002**, 420-421, 324-329.

35 Teshima, Katsuya; Sugimura, Hiroyuki; Inoue, Yasushi; Takai, Osamu. Gas Barrier Performance of Surface-Modified Silica Films with Grafted Organosilane Molecules. *Langmuir*, **2003**, 19, 8331-8334.

36 Kit, Kevin M.; Schultz, Jerold M.; Gohil, Ramesh M.. Morphology and Barrier Properties of Oriented Blends of Poly(ethylene terephthalate) and Poly(ethylene 2,6-naphthalate) with Poly(ethylene-co-vinyl alcohol). *Polymer Engineering and Science*, **1995**, 35, 680-692.

37 Motta, O.; Di Maio, L.; Incarnato, L.; Acierno, D.. Transport and Mechanical Properties of PET/Rodrun 3000 Blown Films. *Polymer*, **1996**, 37, 2373-2377.

38 Hu, Y. S.; Prattipati, V.; Hiltner, A.; Baer, E.; Mehta, S.. Improving Transparency of Stretched PET/MXD6 Blends by Modifying PET with Isophthalate. *Polymer*, **2005**, 46, 5202-5210.

39 Hu, Y. S.; Prattipati, V.; Mehta, S.; Schiraldi, D. A.; Hiltner, A.; Baer, E. Improving Gas Barrier of PET by Blending with Aromatic Polyamides. *Polymer,* **2005**, 46, 2685-2698.

40 Polyakova, A.; Liu, R. Y. F.; Schiraldi, D. A.; Hiltner, A.; Baer, E. Oxygen-Barrier Properties of Copolymers Based on Ethylene Terephthalate. *J. Polym. Sci.: Part B: Polym. Phys.,* **2001**, 39, 1889-1899.

41 Yano, Kazuhisa; Usuki, Arimitsu; Okada, Akane; Kurauchi, Toshio; Kamigaito, Osami. Synthesis and Properties of Polyimide-Clay Hybrid. *J. Polym. Sci.: Part A: Polym. Chem.,* **1993**, 31, 2493-2498.

42 Lan, Tie; Kaviratna, Padmananda D.; Pinnavaia, Thomas J.. On the Nature of Polyimide-Clay Hybrid Composites. *Chemistry of Materials*, **1994**, 6, 573-575.

43 Ke, Zeng; Bai, Yongping. Improve the Gas Barrier Property of PET Film with Montmorillonite by in Situ Interlayer Polymerization. *Materials Letters,* **2005**, 59, 3348-3351.

44 Choi, Won Joon; Kim, Hee-Joon; Yoon, Kwan Han; Kwon, Oh Hyeong; Hwang, Chang Ik. Preparation and Barrier Property of Poly(ethylene terephthalate)/Clay Nanocomposite Using Clay-Supported Catalyst. *J. Appl. Polym. Sci.*, **2006**,100, 4875-4879.

45 Labuschagne, Philip W.; Germishuizen, W. Andre; Verryn, Sabine M. C.; Moolman, F. Sean. Improved Oxygen Barrier Performance of Poly(vinyl alcohol) Films through Hydrogen Bond Complex with Poly(methyl vinyl ether-co-maleic acid). *Eur. Polym. J.,* **2008**, 44, 2146-2152.

46 Bennett, Carl; Mathias, Lon J.. Synthesis and Characterization of Polyamides Containing Octadecanedioic Acid: Nylon 2 18, Nylon 3 18, Nylon 4 18, Nylon 6 18, Nylon 8 18, Nylon 9 18,and Nylon 12 18. *J. Polym. Sci.: Part A: Polym. Chem.,* **2005**, 43, 936-945.

47 Ehrenstein, M.; Dellsperger, S.; Kocher, C.; Stutzmann, N.; Weder, C.; Smith, P. New Polyamides with Long Alkane Segments: Nylon 6 24 and 6 34. *Polymer*, **2000**, 41, 3531-3539.

48 Bennett, Carl; Mathias, Lon J.. Linear Unsaturated Polyamides: Nylons 6 U18 and 18 U18. *Macromol. Chem. Phys.*, **2004**, 205, 2438-2442.

49 Cui, Xiaowen; Li, Weihua; Yan, Deyue; Yuan, Cuiming; Di Silvestro, Giuseppe. Synthesis and Characterization of Polyamides X 18. *J. Appl. Polym. Sci.*, **2005**, 98, 1565-1571.

50 Ehrenstein, Moritz; Smith, Paul; Weder, Christoph. Polyamides X 34: A New Class of Polyamides with Long Alkane Segments. *Macromol. Chem. Phys.*, **2003**, 204, 1599-1606.

51 Jones, Nathan A.; Atkins, Edward D. T.; Hill, Mary J. Comparison of Structures and Behavior on Heating of Solution-Grown, Chain-Folded Lamellar Crystals of 31 Even-Even Nylons. *Macromolecules*, **2000**, 33, 2642-2650.

52 Shimomura, Yasushi; White, James L.; Spruiell, Joseph E.. A Comparative Study of Stress-Induced Crystallization of Guayule, Hevea, and Synthetic Polyisoprenes. *J. Appl. Polym. Sci.*, **1982**, 27, 3553-3567.

53 Murthy, N. Sanjeeva. Hydrogen Bonding, Mobility, and Structural Transitions in Aliphatic Polyamides. *J. Polym. Sci.: Part B: Polym. Phys.*, **2006**, 44, 1763-1782.

54 Mathias, Lon J.; Davis, Rick D.; Jarrett, William L. Observation of α and γ Crystal Forms and Amorphous Regions of Nylon 6-Clay Nanocomposites Using Solid-State ^{15}N Nuclear Magnetic Resonance. *Macromolecules,* **1999**, 32, 7958-7960.

55 Johnson, C. Gregory; Cypcar, Christopher C.; Mathias, Lon J.. ^{13}C and ^{15}N Solid-State NMR of Copolymers of Nylons 6 and 7: Observation of a Stable Pseudohexagonal Phase. *Macromolecules,* **1995**, 28, 8535-8540.

56 Powell, Douglas G.; Sikes, Allison M.; Mathias, Lon J. Natural-Abundance Nitrogen-15 CPMAS NMR of Solid Polyamides: A Technique Sensitive to Composition and Conformation in the Solid State. *Polymer,* **1991**, 32, 2523-2533.

57 Song, Jianbin; Zhang, Huiliang; Ren, Minqiao; Chen, Qingyong; Sun, Xiaohong; Wang, Shuyun; Zhang, Hongfang; Mo, Zhishen. Crystal Transition of Nylon 12 12 under Drawing and Annealing. *Macromolecular Rapid Communications,* **2005**, 26, 487-490.

58 Ehrenstein, Moritz; Sikorski, Pawel; Atkins, Edward; Smith, Paul. Structures of X 34-Nylons in Chain-Folded Lamellae and Gel-Spun Fibers. *J. Polym. Sci.: Part B: Polym. Phys.,* **2002**, 40, 2685-2692.

59 Cui, Xiaowen; Li, Weihua; Yan, Deyue. A Study of the Crystalline Transitions of Polyamides X 18. *Polymer International*, **2004**, 53, 2031-2037.

60 Li, Weihua; Yan, Deyue. Crystal Structures of Polyamides X 18 Made from Long Alkyl Dicarboxylic Acid. *Cryst. Growth Des.*, **2006**, 6, 2182-2185.

61 Peng, Puping; Hodge, Philip. Cyclic Oligo(undecanamide)s (Nylon 11s) and Cyclic Alternating Oligo(undecanamide-undecanoate)s: Their Synthesis Using High Dilution Conditions and Their Analysis. *Polymer*, **1998**, 39, 981-990.

62 Glans, J. H.; Akkapeddi, M. K.. Synthesis and Polymerization of 2,15-Diaza-1,16-dioxo[16]paracyclophane. *Macromolecules,* **1992**, 25, 5526-5527.

63 Gong, Wei-Tao; Hiratani, Kazuhisa; Oba, Toru; Ito, Satoshi. A Convenient and Efficient Route for the Synthesis of Amide Crownophanes via 1:1 Macrocyclization of Di(acid chloride) with Diamine Derivatives. *Tetrahedron Letters,* **2007**, 48, 3073-3076.

64 Kagiya, Tsutomu; Izu, Masatsugu; Matsuda, Takehisa; Fukui, Kenichi. Synthesis of Polyamides by the Polyaddition of Bis-Succinimides with Diamines. *J. of Poly. Sci.: Part A-1: Polym. Chem.*, **1967**, 5, 15-20.

65 Cote, Pierre; Brisson, Josee. Miscibility of Polyamide Blends.2. Thermal Study of Poly(hexamethylene isophthalamide)/Nylon-N,M Blends. *Macromolecules*, **1994**, 27, 7329-7338.

66 Jones, N. A.; Atkins, E. D. T.; Hill, M. J.; Cooper, S. J.; Franco, L. Chain-Folded Lamellar Crystals of Aliphatic Polyamides. Comparisons between Nylons 4 4, 6 4, 8 4, 10 4, and 12 4. *Macromolecules*, **1996**, 29, 6011-6018.

CHAPTER II

SYNTHESIS AND CHARACTERIZATION OF PHYSICAL CROSSLINKING SYSTEMS BASED ON CYCLODEXTRIN INCLUSION/HOST-GUEST COMPLEXATION

Abstract

New supramolecular assemblies based on cyclodextrin and adamantane were prepared. Two methacrylate monomers bearing cyclodextrin and adamantane were synthesized, and copolymerized with poly(ethylene glycol) methyl ether methacrylate,(PEGMA, 300 g/mol), by free radical polymerization. Copolymers bearing pendent cyclodextrin and adamantane were characterized by NMR, FTIR, TGA, SEC, DSC, and UV–visible spectrophotometer. All copolymers showed two distinct glass transitions. The specific interaction between pendent adamantyl and cyclodextrin was examined by ^{1}H NMR. The viscoelastic properties of supramolecular assemblies were investigated with frequency and temperature sweep experiments. The specific host-guest interaction between pendent adamantyl and cyclodextrin lead to large increases of the viscosity; and depending on the concentration of these groups, also to gel formation.

Introduction

Cyclodextrins (CDs) have been extensively used for industrial applications in many fields from laundry soap to food and pharmaceuticals. They also have been investigated as building blocks for supramolecular chemistry because they can form complexes with a number of different molecules and polymers through host-guest interaction.[1,2] The most widely used CDs are α-CD, β-CD, and γ-CD, which respectively consist of six, seven, or eight D-glucopyranose units. They possess truncated, cone-shaped hydrophobic cavities in which the narrow end has primary and the wide end secondary hydroxyl groups. Since the inner cavity does not have any hydroxyl groups,[3] it can bind a number of different hydrophobic moieties. The driving forces for complex formation are the expulsion of high energy water from the hydrophobic cyclodextrin cavity, the release of ring strain, van der Waals interactions, and hydrogen bonding.[4]

Several physical crosslinking systems have been reported utilizing cyclodextrins. Yui, et al.,[5] reported supramolecular hydrogels based on inclusion complexation between α-cylodextrin and poly(ethylene glycol)-grafted dextran. α-Cyclodextrin threaded PEG chains come together to form channel-type crystalline micro-domains. These crystalline microphases create physical junctions between dextran main chains. The sol-gel transition is based on physical threading-dethreading of α-CDs with the polymeric guests. The process is strongly affected by temperature changes, making gelation thermo-reversible. The transition temperature can be varied by changing the solution concentrations,

the PEG content in the graft polymer, and the stoichiometric ratio between guest and host molecules.

Yui, et al.,[3] used both ionic and hydrophobic interactions to obtain sol-gel systems with rapid phase transitions. They modified poly(ε-lysine) (PL) with β-CD to give biocompatible and biodegradable polymeric hosts (β-CDPL). The guest, 3-trimethylsilylpropionic acid (TPA), containing both hydrophobic and ionic groups, was chosen specifically to provide dual interactions with the polymeric host and each other. In this system, TPA is included into the CD cavity by host-guest interaction to create physical crosslinks through co-operative hydrophobic and ionic interactions. The system showed a very rapid phase transition with small change in temperature across the upper critical solution region. Because of the ionic character, these systems are profoundly affected by pH changes.

A variety of hydrophobic groups interact strongly with CD's. The interaction between adamantane and β-cyclodextrin was reported to be very strong compared to other bulky groups as studied by AFM.[6] In recent years, there have been a number of reports published utilizing these strong host-guest interactions.[7,8,9,10] Harada, et al., reported a use of these host-guest interactions to obtain high molecular weight (M_n=100000) supramolecular polymers formed from a β-cyclodextrin dimer and a guest dimer having adamantyl groups linked by poly(ethylene glycol).[11]

Polymers consisting of poly(ethylene glycol) methyl ether methacrylate (PEGMA) have been investigated extensively for biomedical applications due to PEG biocompatibility and nonadhesive interactions to proteins.[12] These polymers

also exhibit a lower critical solution temperature (LCST) which may be useful for nanotechnology and biotechnology applications.[13] Currently, several derivatives of PEGMA macromonomers with different molecular weights and chain ends such as methoxy or hydroxyl are commercially available. They have been copolymerized with a variety of monomers using several different methods including atom transfer radical polymerization (ATRP)[14,15], reversible addition-fragmentation chain transfer (RAFT)[16,17], and conventional free radical methods.[18,19,20] Most of these copolymer systems have been studied for synergistic effects of two different units; for instance, to form pH and temperature sensitive copolymers.[16,12]

Here we report the synthesis of two novel monomers and their polymers bearing adamantane and cyclodextrin pendant groups, respectively. These monomers were copolymerized with PEGMA at three different compositions (5, 10, 15 mol-% feed ratio) by conventional free radical polymerization techniques. The characterization of these copolymers has been done using NMR, FTIR, TGA, SEC, and DSC. In addition, the effect of the comonomers on the LSCT of PEGMA copolymers was also studied. Finally, the host-guest interactions between PEG and adamantane units with pendent cyclodextrin units were examined, and the viscoelastic properties of these new physical network-forming systems were investigated with both frequency and temperature sweep rheology experiments.

Experimental

Materials. β-Cylcodextrin (β-CD) was purchased from TCI and used without purification. Poly(ethylene glycol) methyl ether methacrylate (PEGMA, 300 g/mol), *p*-toluenesulfonyl chloride (*p*-TsCl) and 1,6-hexanediamine (HDA), were purchased from Aldrich Chemical Co. and used as received. Azobisisobutyronitrile(AIBN) was purchased from Aldrich Chemical Co., and recrystallized from methanol three times before use. 6-*O*-Monotosyl-6-deoxy-β-cyclodextrin (mono-6-OTs-β-CD) was synthesized based on a literature procedure.[21] 4-(1-Adamantyl)phenyl methacrylate (APM) was previously synthesized in our laboratory, and this procedure was followed to obtain APM as a white powder.[22]

6-(6-Aminohexyl)amino-6-deoxy-β-cyclodextrin[23] (β-CD-HDA). A 250 mL three-necked round-bottom flask was charged with 5.0 g (3.8 mmol) of mono-6-OTs-β-CD and excess HDA (20 g, 172 mmol) in 25 ml DMF. The reaction was carried out overnight at 80 °C. After completion of the reaction, the mixture was allowed to cool down to room temperature and the product precipitated into excess acetone. After filtration, the product was dissolved in DMF and reprecipitated in acetone. After several reprecipitation cycles, the crude product was washed with diethyl ether and kept in vacuum oven at room temperature for 24 h. β-CD-HDA (2.3068 g) was obtained as white powder in 43% yield. ^{1}H NMR (300 MHz, DMSO-d_6): 7.98, 5.75, 4.84, 4.49, 3.63, 3.4, 3.32, 3-3.1, 2.8-2.92, 2.64-2.74, 2.1, 1.35, 1.26 ppm. ^{13}C NMR (300 MHz, DMSO-d_6): 102, 81.5, 73, 72.4, 72, 60, 49.5, 37, 29.5, 29, 26.5, 26.3 ppm.

(1-Methacrylamidohexyl)amino-6-deoxy-β-cyclodextrin (MCD). A 100 mL three-necked round-bottom flask was charged with methacrylic anhydride (10 g, 64 mmol) and 20 ml DMF. To this solution, β-CD-HDA (7.73 g, 6.3 mmol) in 20 ml DMF was added dropwise under nitrogen atmosphere. The solution was stirred overnight. The product was precipitated into excess acetone. The solid powder was dissolved in DMF and reprecipitated into acetone several times. The final product was obtained as a white powder which was dried in a vacuum oven at 70 °C overnight. The yield was quantitative. ^{1}H NMR (300 MHz, DMSO-d_6): 5.7, 5.6, 5.3, 4.8, 4.5, 4.2, 3.2-3.7, 3, 2, 1.6-1.9, 1.37, 1.15 ppm. ^{13}C NMR (300 MHz, DMSO-d_6): 167.9, 140.2, 119.1, 102, 81.7, 73, 72.4, 72, 60, 30.8, 28.9, 26.1, 25.9, 19.1 ppm.

Synthesis of copolymer (PEGMA-co-MCD). A typical copolymerization is given for (PEGMA-15-MCD). MCD (3.84 g, 2.9 mmol) , PEGMA (4.9 g, 16 mmol), AIBN (0.079 g, 0.49 mmol), and 32 mL DMF were charged to a 50 mL three-necked round bottom flask. Nitrogen was bubbled through the solution for 15 min before heating at 50 °C for 24 h. The mixture was then precipitated into ethyl ether. After three reprecipitation cycles, the product was dried in a vacuum oven for 12 h at 40 °C. For further purification, the polymer was dissolved in deionized water, placed in Spectra Por dialysis tubing with a molecular cutoff of 12000-14000 and dialyzed against deionized water for 7 days. The final polymer was freeze-dried to obtain a fiber-like, slightly yellowish solid in ca. 77% yield.

Synthesis of copolymer (PEGMA-co-APM). A typical copolymerization is given for (PEGMA-15-APM).. APM (1.33 g, 4.5 mmol), PEGMA (7.65 g, 25.5

mmol), AIBN (0.098 g, 0.6 mmol), and 62 mL DMF were charged to a 100 mL three-necked round bottom flask, and bubbled with nitrogen for 15 min before heating. The reaction was carried out at 50 °C for 24 h, and the mixture was then precipitated into ethyl ether. After three reprecipitation cycles, the product was dried in a vacuum oven for 12 h at 40 °C. The copolymer was then dissolved in deionized water, placed in Spectra Por dialysis tubing with a molecular cutoff of 12000-14000 and dialyzed against deionized water for 7 days. The final polymer was freeze-dried to obtain the final product as a transparent solid in ca. 55% yield. Only the copolymer with 5 mol-% APM (PEGMA-5-APM) was sticky; all others were non-sticky materials.

Instrumental Analysis

NMR measurements were conducted on a Varian 300 MHz NMR using DMSO-d_6 and D_2O as solvents. FTIR spectra were obtained on a Nicholet 5DX using pressed KBr pellets. SEC was performed on a system using a HP 1037A RI detector with a constaMetric pump flowing THF at 100 ml/min through five American Polymer Standards separation columns with porosities ranging from 100 to 1,000,000 A. The SEC runs were calibrated using polystyrene standards.

Differential scanning calorimetry (DSC) experiments were performed on a TA Instruments 2920 using pierced-lid crimped aluminum pans at a ramp rate of 10.0 °C/min for both heating and cooling. Temperature and heat capacity were calibrated with indium and sapphire standards, respectively. Thermogravimetric analysis was conducted on a TA instrument 2960 at a heating rate of 10 °C/min under nitrogen.

The optical transmittances of polymer solutions were recorded as a function of temperature on a UV–visible spectrophotometer (Shimadzu, UV-1601PC). A 2.5 wt-% solution of each polymer was prepared and the samples were heated at 2 °C/min while transmittances were recorded. All polymers showed a sharp transition for the LCST, which was defined as the temperature on heating at which the solution gave almost no transmittance.

Rheological measurements

Viscoelastic characterization was conducted with an Advanced Rheometerics Expansion System (ARES, Rheometrics Inc.) equipped with two 25 and 40 mm diameter parallel plates. A thin layer of low-viscosity silicone oil was applied to the air/sample interface to inhibit water loss. Frequency sweep experiments were conducted at two different temperatures (20 and 30 °C) to obtain complex viscosity, storage and loss moduli over a wide range of frequencies. Temperature sweep experiments were conducted with a stress controlled rheometer (TA Instruments AR-G2) in a 40 mm double gap concentric cylinder system.

Results and Discussion

The copolymers bearing cyclodextrin and adamantane pendent groups were synthesized by free radical polymerization as described in the experimental section. The general routes for the synthesis of monomers and polymers are given in Schemes 1 and 2.

Scheme 2.1. Synthesis of monomers.

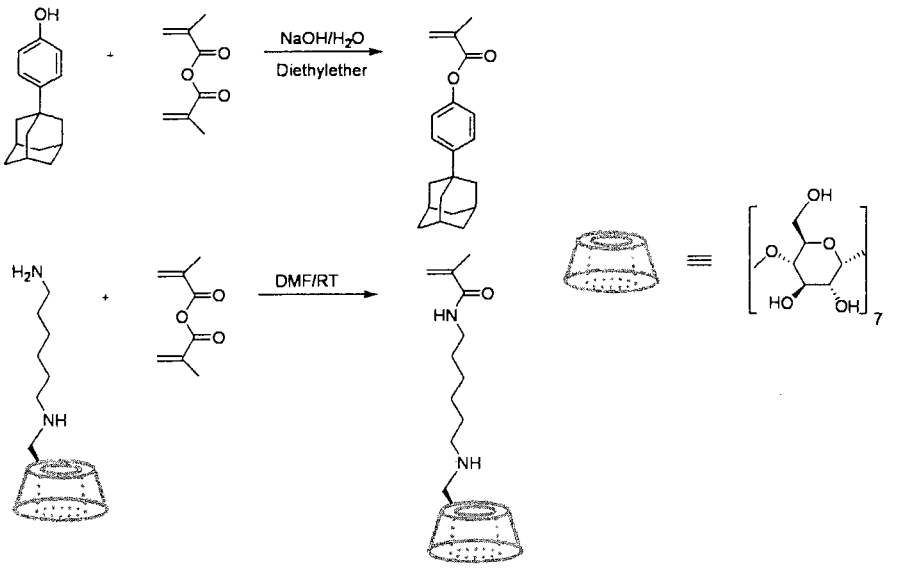

Scheme 2.2. General route for synthesis of copolymers.

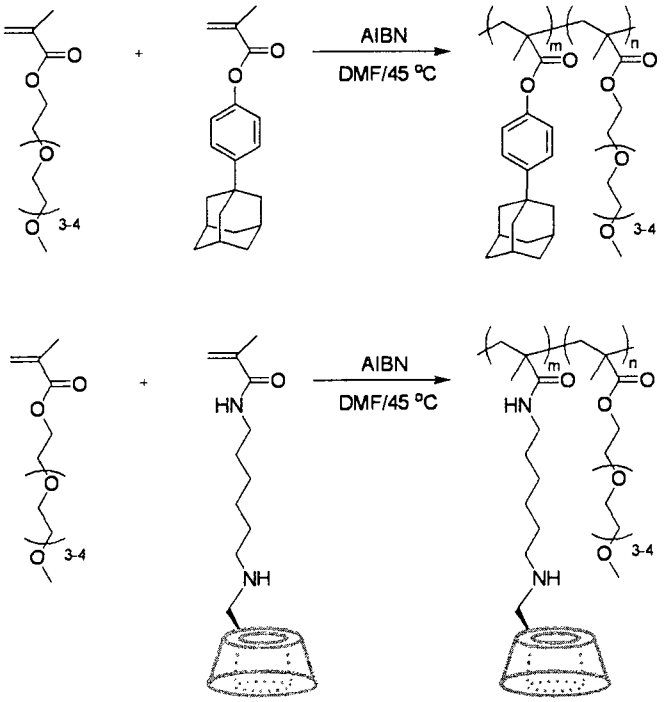

Figure 2.1 shows a typical solution ^{13}C NMR spectrum for a copolymer bearing APM moieties. P(PEGMA-co-15APM) was chosen as an example, and the homopolymer of PEGMA is given for comparison. All peaks are assigned based on the expected structures of the polymers. For PEGMA monomer, the double bond peaks appear at 135.9 and 125.4 ppm and these are absent in the spectra of the homopolymer and copolymers. A broad new peak appears around 44.4 ppm which is associated with the backbone carbons. In addition to PEGMA peaks, those associated with APM units are also observed for the copolymers. The aromatic peaks are located at 125.7 and 120.3 ppm, while the adamantyl peaks (labeled n, o, m and p) appear at 42.8, 36.2, 35.4 and 28.2, respectively. The carbonyl peak of PEGMA monomer is around 166 ppm and shifts to 177 ppm in the homo- and copolymers.

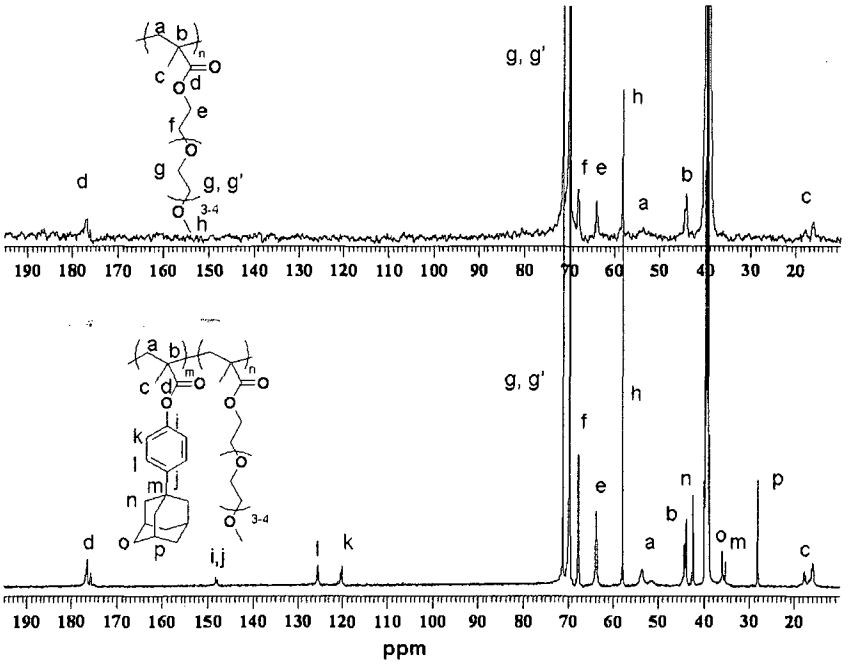

Figure 2.1. ^{13}C solution NMR of P(PEGMA) (top) and P(PEGMA-co-15APM) (bottom) in DMSO-d_6.

The solution ^{1}H NMR spectra of P(PEGMA) and P(PEGMA-co-15APM) are given in Figure 2.2. The double bond peaks of PEGMA at 5.64 and 6.03 ppm, disappear upon polymerization, and the backbone peaks of the homopolymer appear around 1.4-1.9 ppm. The PEG proton chemical shift is observed at 3.5 ppm, while the methylene protons α and β to the ester groups give two distinct peaks at 4.2 and 3.7 ppm, respectively, for PEGMA; these two peaks shift slightly upfield upon polymerization. The methylene protons α to the ester group of PEGMA are at 4 ppm, whereas the methylene protons β to the ester group appear as a shoulder to PEG protons at around 3.6 ppm. In addition to all peaks associated with PEGMA units, new peaks are observed in the ^{1}H NMR spectra of the copolymers due to APM units. The peaks at 7.02 and 7.4 ppm are attributed to the phenyl rings, while three peaks at 1.76, 1.88, and 2.08 ppm due to adamantyl hydrogens overlap the backbone peaks.

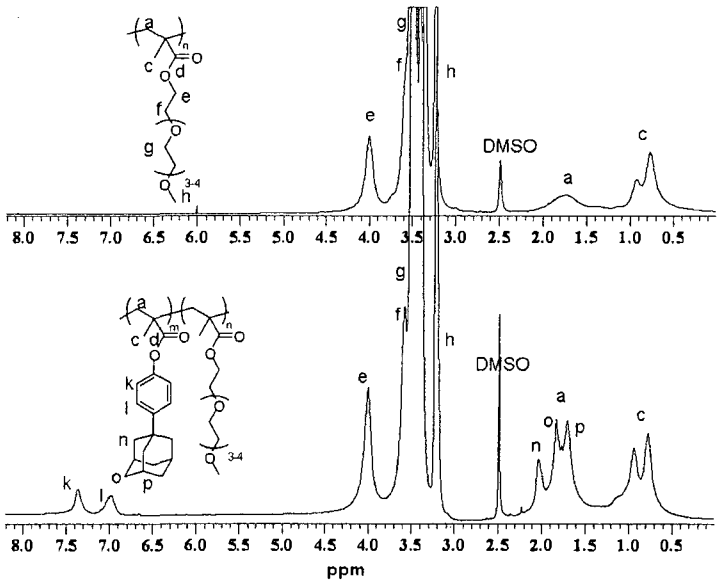

Figure 2.2. ^{1}H solution NMR of P(PEGMA) (top) and P(PEGMA-co-15APM) (bottom) in DMSO-d_6.

The copolymer series bearing MCD moieties was analyzed for copolymer composition by solution ^{13}C NMR. The spectrum of P(PEGMA-co-15MCD) is given in Figure 2.3 as an example. All peaks are assigned based on the expected structure of the copolymers. Upon polymerization, the double bond peaks of MCD observed at 119.1 and 140.2 ppm disappear, while the carbonyl peak shifts from 167.9 ppm to 175.8 ppm. The peaks associated with cyclodextrin units appear at 102.1, 81.4, 73-72, 59.8 ppm, while the peaks attributed to the alkyl spacer between the methacrylamide and cyclodextrin amine appear at 36.7, 28.8, 25.6 ppm. The peaks ascribed to PEGMA units in the copolymer were assigned based on the ^{13}C NMR spectrum of the homopolymer from Figure 2.1.

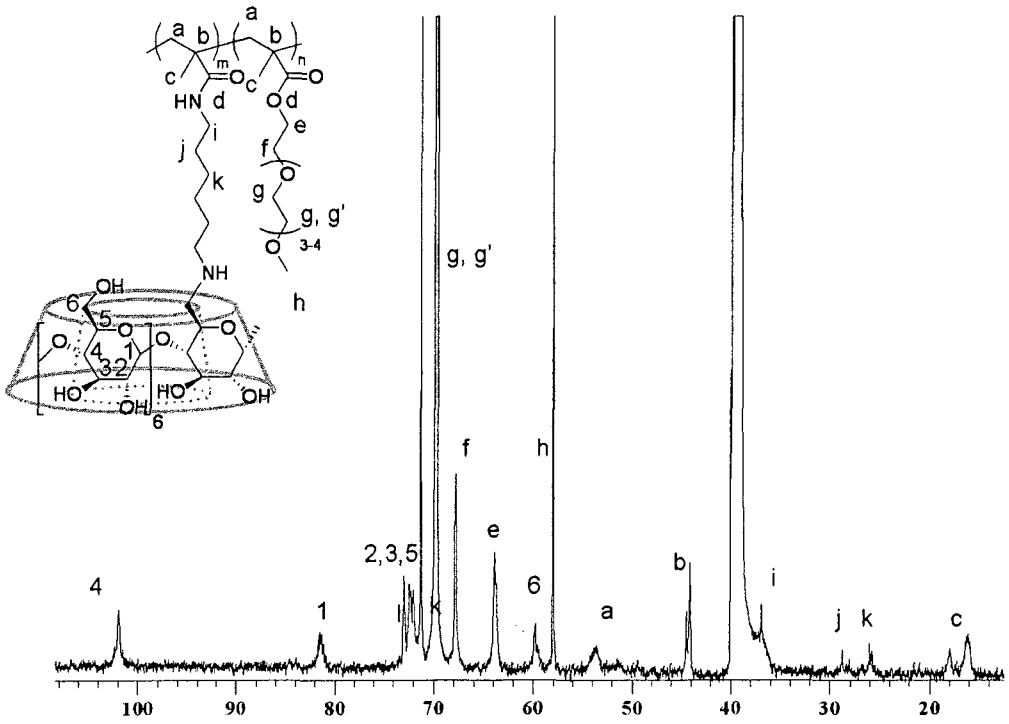

Figure 2.3. ^{13}C solution NMR of P(PEGMA-co-15MCD) in DMSO-d_6.

The solution ^{1}H NMR spectrum of P(PEGMA-co-15MCD) is given in Figure 2.4. The double bond peaks of monomeric PEGMA which appear at 5.64 and 6.03 ppm are under the cyclodextrin peaks (2 and 3), while the double bond peaks of MCD appear at 5.32 ppm and as a shoulder on the cyclodextrin peaks (2 and 3) at 5.6 ppm. Upon polymerization, the double bond peaks disappear. The peaks associated with O(6)H, C(1)H, O(2)H and O(3)H of cyclodextrin units appear at 4.50, 4.85, and 5.73 ppm, respectively. The other peaks attributed to cyclodextrin units are under the proton peaks of PEG units, and can not be seen. The peaks associated with PEGMA units are assigned based on the ^{1}H spectrum of the homopolymer of P(PEGMA) (Figure 2.2).

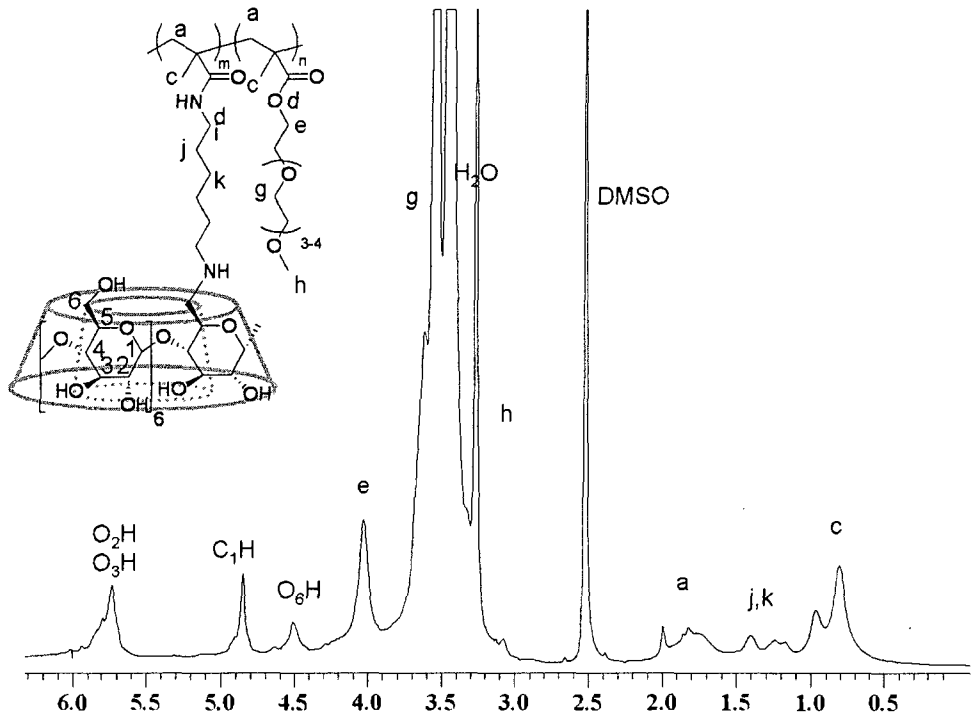

Figure 2.4. ^{1}H solution NMR of P(PEGMA-co-15MCD) in DMSO-d_6.

The molecular weights, Mw and Mn, and polydispersity as estimated by SEC are given in Table 2.1. The copolymer compositions are calculated by the total area ratios of the specific peaks using ^{1}H NMR and are also given in Table 1.The compositions of copolymers bearing APM were calculated from the area ratios of protons in the phenyl-rings (assigned as k and l) and PEGMA protons α to the ester group (assigned as e), using the equation m/n =$(A_1/4)/(A_2/2)$, where A_1 and A_2 are the total area under (k+l) and e, respectively. The composition of copolymers bearing MCD was calculated from the area ratios of C_1H protons of cyclodextrin to PEGMA protons α to the ester group (assigned as e), using the equation, m/n =$(A_1/7)/(A_2/2)$, where A_1 and A_2 are the total area under C_1H and e, respectively.

Table 2.1

Mn, Mw, PDI, compositions, and yield of copolymers.

Sample	feed mol-%[a]	mol-%[b]	M_n[c]	M_w[c]	PDI[c]	Yield %
P(PEGMA-co-5APM)	5	6	20600	128000	6.2	75
P(PEGMA-co-10APM)	10	8	18200	127000	7	80
P(PEGMA-co-15APM)	15	17	55100	278000	5	55
P(PEGMA-co-5MCD)	5	2	42300	165000	3.8	74
P(PEGMA-co-10MCD)	10	3.4	21700	50000	2.3	76
P(PEGMA-co-15MCD)	15	10.2	52800	287000	5.4	77

[a]comonomer feed mol-%
[b]copolymer compositions estimated by ^{1}H NMR
[c]estimated by SEC

The polymers were further characterized by FTIR, and the FTIR spectra of P(PEGMA-co-10APM) and P(PEGMA-co-10MCD) are given as examples of each series of copolymers (Figure 2.5). Since each spectrum is dominated by PEGMA units (90 mol-% in each copolymer), the FTIR spectra of the

homopolymer of PEGMA and the PEGMA monomer are also given for comparison. The band observed at 1640 cm^{-1} due to the double bond of the monomer disappears in the homo- and copolymers which indicates that little or no residual monomer is present.[24] The band associated with stretching of the ester carbonyl group at 1720 cm^{-1} for PEGMA shifts to 1731 cm^{-1} in the polymers. The peak observed around 1133 cm^{-1} is due to C-O-C stretching of ester and ether groups of PEGMA. The FTIR spectrum of P(PEGMA-co-10MCD) shows a broad distinct peak around 3384 cm^{-1} associated with the hydroxyl groups of pendant cyclodextrins and this peak is not observed for the PEGMA monomer, the homopolymer of PEGMA and P(PEGMA-co-10APM).

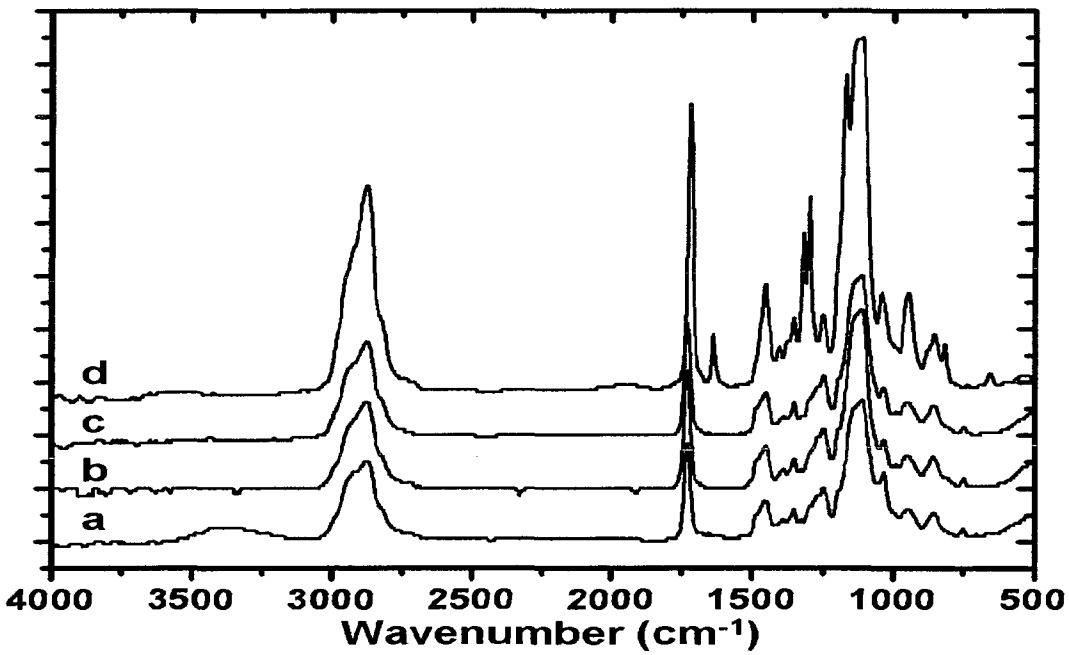

Figure 2.5. FTIR spectra of a) P(PEGMA-co-10MCD), b) P(PEGMA-co-10APM), c) P(PEGMA), and d) PEGMA.

DSC thermograms of selected copolymers are given in Figure 2.6. DSC curves of all copolymers have two distinct T_g transitions, and no observed side chain crystallinity probably due to the PEG side chains not being long enough to form ordered structures. Observation of two T_g's is generally an indication of separate microphases. Similar transitions were observed for various copolymer systems consisting of PEGMA and n-butyl methacrylate.[25] The PEGMA polymers have a limiting T_g corresponding to the glass transition temperature of PEG chains around – 59 °C,[26] and the T_g of P(PEGMA300) previously was given as -57 °C.[27] The T_g1 values, given in Table 2, are slightly higher than the T_g value reported for PEG. However, T_g2 values of P(PEGMA-co-APM) are much lower compared to the homopolymer of APM synthesized in our laboratory which has reported T_g of 253 °C.[28] Therefore, the two glass transitions observed are not due to completely phase separated blocks but to essentially random copolymers with microdomains of pendent PEG groups. The glass transitions of this series of copolymers continuously increase with increasing APM ratio from 5 to 15 mol-%. The T_g values for the copolymer series having MCD units are more or less in the same range of the APM series. The glass transition temperatures of the copolymers are given in Table 2.2.

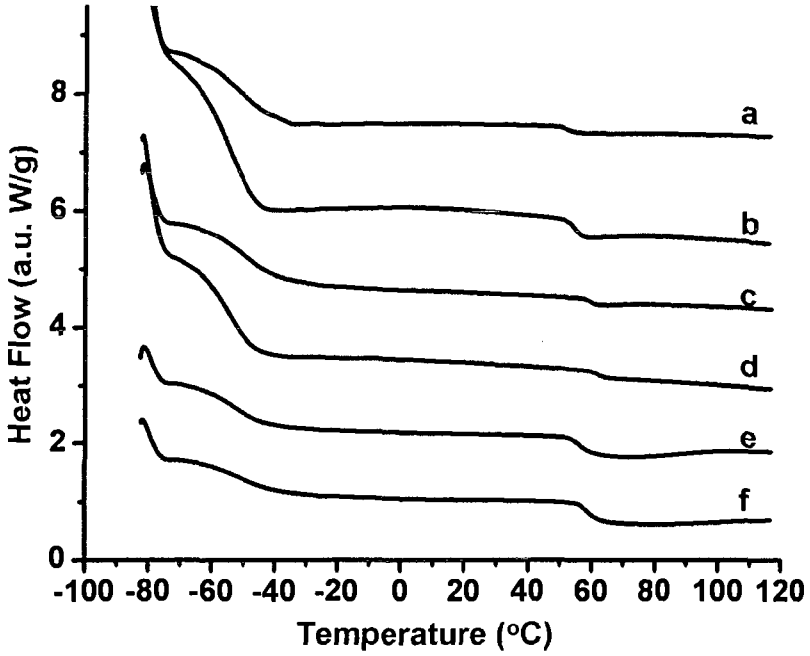

Figure 2.6. DSC thermograms of copolymers a) P(PEGMA-co-5APM), b) P(PEGMA-co-10APM) , c) P(PEGMA-co-15APM), d) P(PEGMA-co-5MCD), e) P(PEGMA-co-10MCD), f) P(PEGMA-co-15MCD).

Table 2.2

T_g1 and T_g2 values of copolymers

Sample	T_g1	T_g2
P(PEGMA-co-5APM)	-51.84	51.81
P(PEGMA-co-10APM)	-54.62	54.34
P(PEGMA-co-15APM)	-48.49	59.27
P(PEGMA-co-5MCD)	-54.53	61.89
P(PEGMA-co-10MCD)	-53.52	55.77
P(PEGMA-co-15MCD)	-48.59	58.46

Thermal stabilities of the copolymers were analyzed by TGA. Figure 2.7 shows TGA thermograms of two copolymers of each series with a heating rate of 10 °C/min in N_2. The copolymers with MCD exhibit a two-step degradation process. The onset of thermal decomposition of P(PEGMA-15MCD) is much

lower compared to other copolymers perhaps due to the thermal degradation of pendant cyclodextrin units seen at lower temperatures. Similar behavior was observed for the copolymers having the highest feed ratio of MCD. The temperature at 10 wt-% loss for this polymer is 250 °C. The copolymers with 5 mol-% APM and MCD give almost the same thermograms. The onset of the thermal degradation for the P(PEGMA-co-5MCD) is somewhat earlier because of the less stable cyclodextrin pendant units. However, it is not as pronounced as the onset of the thermal decomposition of the copolymer with 15 mol-% MCD. The temperature at 10 wt-% loss for P(PEGMA-co-15APM) and P(PEGMA-co-5APM) are 290 and 280 °C, respectively. These values are in the same range as the homopolymer of PEGMA.[29] The slight increases may be due to incorporated APM units which have been reported to enhance thermal stabilities in copolymers.[28]

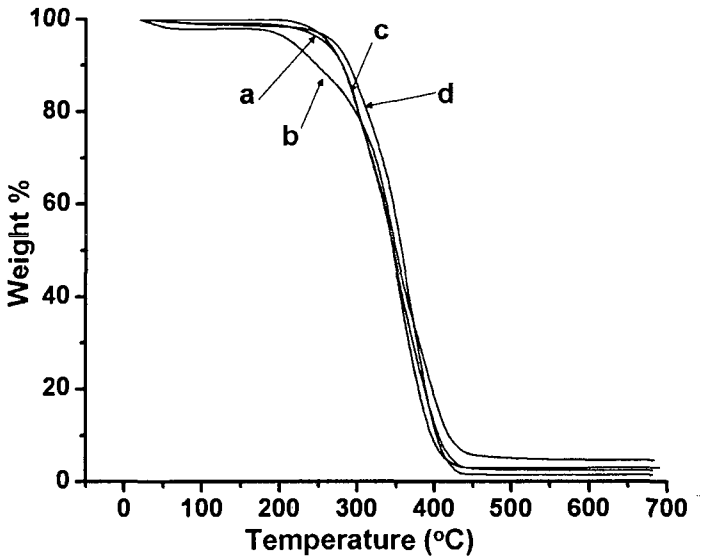

Figure 2.7. TGA thermograms of copolymers a) P(PEGMA-co-5APM), b) P(PEGMA-co-15APM), c) P(PEGMA-co-5MCD), d) P(PEGMA-co-15MCD) in N_2.

The thermosensitive behaviors of solution of the copolymers and the homopolymer of PEGMA were investigated using a UV–visible spectrophotometer. The copolymer composition has a great effect on LCST behavior of the polymers, since the hydorphobicity-hydrophilicity balance changes with composition. In general, hydrophobic comonomers decrease the LCST, while hydrophilic comonomers increase it.[16] It was expected that the copolymers with hydrophobic APM moieties and hydrophilic MCD would show different thermoresponsive behaviors. The effect of these hydrophobic or hydrophilic comonomers on LCST of P(PEGMA) is summarized in Figure 2.8. All polymers showed a sharp transition at the cloud point. The LCST of the homopolymer of PEGMA was 63 °C which is close to the LCST of 3 wt-% solution of P(PEGMA) reported of 60.8 °C.[28] As expected, the cloud point continuously decreases with increasing content of the hydrophobic APM units in the copolymers. The decrease is as high as 14 °C for the copolymer with 15 mol-% APM. On the other hand, there are slight increases of observed cloud points with increasing MCD ratio in copolymers.

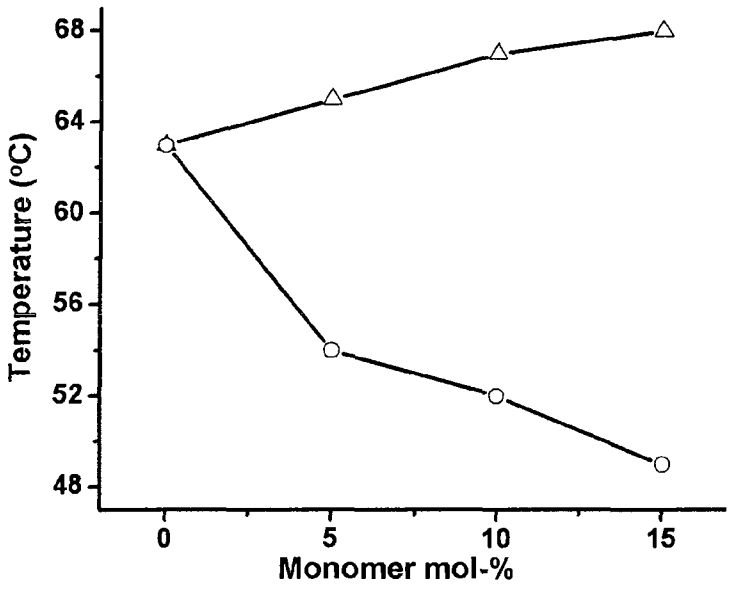

Figure 2.8. Cloud point vs. comonomers feed ratio of copolymer bearing MCD (△), and APM(○).

The copolymers having APM moieties are expected to show amphiphilic properties due to combined hydrophobic and hydrophilic segments. To explore the amphiphilic character of the copolymer, ^{1}H NMR was used and the spectrum of P(PEGMA-co-15APM) is given for two different solvents, DMSO-d_6 and D_2O (Figure 2.9). DMSO-d_6 is a good solvent for the copolymers, and with it, the adamantyl peaks can be easily identified, plus there are two separate peaks associated with the aromatic group of APM. On the other hand, the peaks of the adamantyl groups totally disappear in D_2O or they may not be observed because of overlap with the backbone peaks. The spectrum has very broad peaks with no distinct separation for the aromatic groups of APM consistent with hydrophobic association. The spectral changes due to solvent differences indicate structural rearrangement, and perhaps pendent group association, of the amphiphilic

polymer in D_2O. Similar observation has been reported for the amphiphilic block copolymer of PEG with hydrophobic poly(β-benzyl L-aspartate) and poly [*N*-{*o*-(4-phenyl-4,5-dihydro-1,3-oxazol-2-yl)phenyl}maleimide].[30,31] In D_2O, the hydrophobic groups tend to aggregate and may form a micelle-like structure. Mobility decreases in micelle structures, which would cause broadening of the APM peaks, as can easily be seen for the peaks associated with the aromatic groups, and disappearance of peaks associated with adamantane.

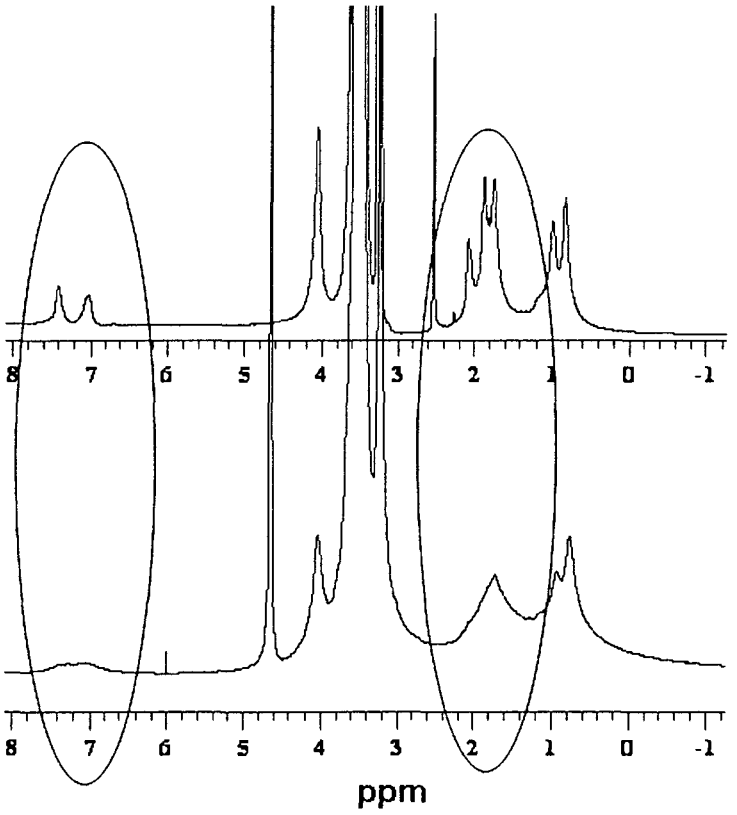

Figure 2.9. ^1H NMR analysis of P(PEGMA-co-15APM) in D_2O (bottom) and DMSO-d_6 (top).

It is generally accepted that, unlike α-cyclodextrin which has been reported to form polyrotaxane type complexes with PEG, β-cyclodextrin cannot form such stable complex as with PEG.[32,33,34] However, Ripmeester, et al.,[35] did

report stable binding between PEG and β-cyclodextrin and this complexation was further investigated by Cosgrove, et al.,[36] In both cases, complexation of linear PEG with free β-cyclodextrin was investigated. Here, on the other hand, the mobilities of PEG and β-cyclodextrin units are restricted by the main polymer chain. Therefore, the binding and interactions of these groups would be expected to be different. Considering expected compositions of copolymers with adamantane and PEG units, three possibilities should be considered: 1) PEG units of the polymers can form stable complexes with cyclodextrin; 2) PEG units do not form stable complexes but inhibit interactions of adamantyl moieties with cyclodextrin; and 3) only adamantane and cyclodextrin groups form stable complexes. Another important factor which will influence the host-guest interaction between adamantyl and cyclodextrin groups may be the inter- and intramolecular self-association of bulky adamantyl moieties which may lead to inhibition of the host-guest complex formation between adamantyl groups and cyclodextrins.

^{1}H NMR analysis has been extensively used to probe inclusion formation in similar complexes.[37,38,39] The formation of inclusion complexes between free cyclodextrin and adamantyl moieties of P(PEGMA-co-10APM) was investigated here using ^{1}H NMR. Figure 2.10 shows variation of the ^{1}H NMR spectra with increasing free cyclodextrins in solution. The top spectrum is the ^{1}H NMR spectrum of P(PEGMA-co-10APM) given for comparison. The shifts of specific peaks in the polymer spectrum result from the inclusion complexation between adamantyl moieties and PEG units with added cyclodextrin.

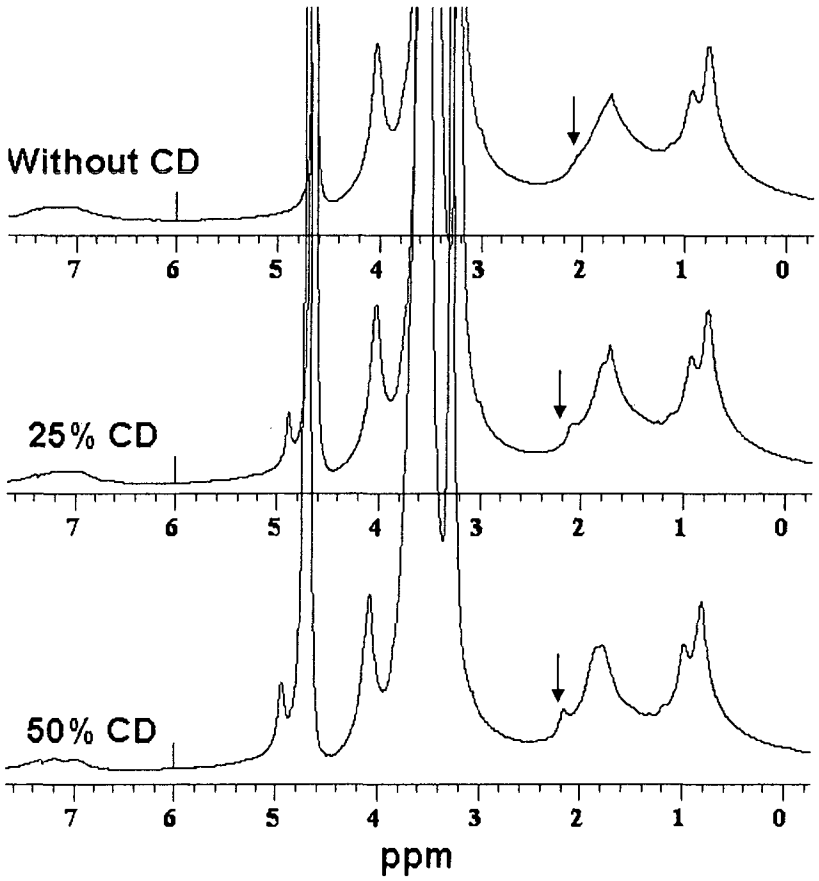

Figure 2.10. ^{1}H NMR analysis of inclusion complex formation between P(PEGMA-co-10APM) with various concentrations of free cyclodextrin.

The downfield shift indicates that there is indeed host-guest complex formation between pendant adamantane and cyclodextrin, this confirms that self-association of the amphiphilic polymer does not inhibit specific complexation between the two groups. In fact, the interaction between these two groups is so strong that the self-association of hydrophobic adamantyl moieties may be disturbed upon addition of the cyclodextrin. Figure 2.11 shows a schematic representation and photograph of the gel formation. This gel was obtained with the 30 wt-% of the P(PEGMA-co-15APM)/P(PEGMA-co-15MCD) mixture. Initially, both solutions of 30 wt-% of P(PEGMA-co-15APM) and 30 wt-% of P(PEGMA-

co-15MCD) were prepared; these solutions were viscous liquids at these concentration. After mixing, gel formation occurs rapidly, as demonstrated by the test tube inversion method.

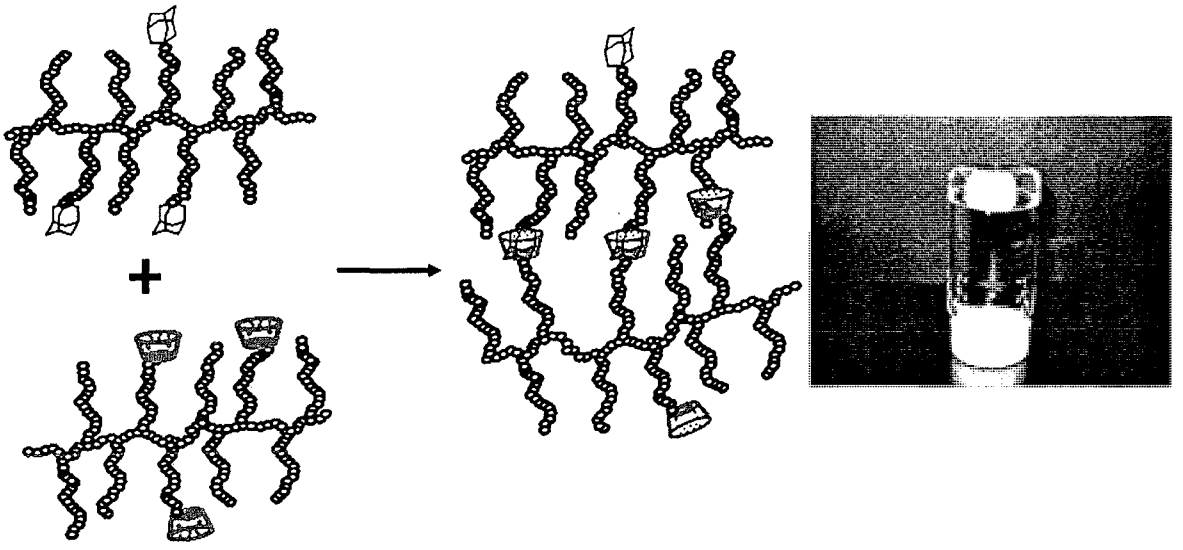

Figure 2.11. Photograph and schematic representation of gel formation as a result of inclusion complexation between adamantyl and cyclodextrin pendent groups of copolymers.

To investigate viscoelastic properties of supramolecular assemblies, four aqueous solution mixtures were prepared: P(PEGMA-co-15APM)/P(PEGMA-co-15MCD), P(PEGMA-co-10APM)/P(PEGMA-co-10MCD), P(PEGMA-co-5APM)/ P(PEGMA-co-5MCD). Each pair was mixed together to explore the effect of increasing associative group contents on viscosity. An aqueous solution of P(PEGMA)/P(PEGMA-co-10MCD) was used as the control to probe the interaction between PEG units of P(PEGMA) and the pendent cyclodextrins groups of P(PEGMA-co-10MCD). For consistency, all samples were prepared as 10 wt-% solutions in water, and the complex viscosity, storage and loss moduli as a function of angular frequency were determined in frequency sweep

measurements. The viscosities were measured for two different temperatures, 20 and 30 °C.

The complex viscosities of the mixtures of viscous liquids as a function of angular frequency are given Figure 2.12. The complex viscosities are almost independent of frequency for all four samples for both temperatures. The viscosity values are dramatically higher for those samples with higher ratios of associative groups in the copolymers. The 1:1 mixtures of P(PEGMA-co-15APM)/P(PEGMA-co-15MCD), and P(PEGMA-co-10APM)/P(PEGMA-co-10MCD) show the highest viscosities which indicates that the solution properties of P(PEGMA) are tunable by changing the associating comonomer content. It is worth noting that the temperature dependence of viscosity is stronger for the samples with higher comonomer loading. Therefore, it can be concluded that the decrease in viscosity with temperature must be related to the supramolecular association of adamantyl and cyclodextrin groups rather than the interaction between PEG units and cyclodextrins. Another interesting finding is the fact that the viscosity increases for the samples bearing 5 mol-% associative groups to 10 mol-% associative groups is significant, whereas there is no further increase for the mixture of copolymers bearing 15 mol-% associative groups. Since P(PEGMA-co-15APM) possesses more hydrophobic groups which enhance micelle formation and hydrophobic associations, and this may limit or decrease the inclusion complexation once the adamantyl group reaches a certain concentration.

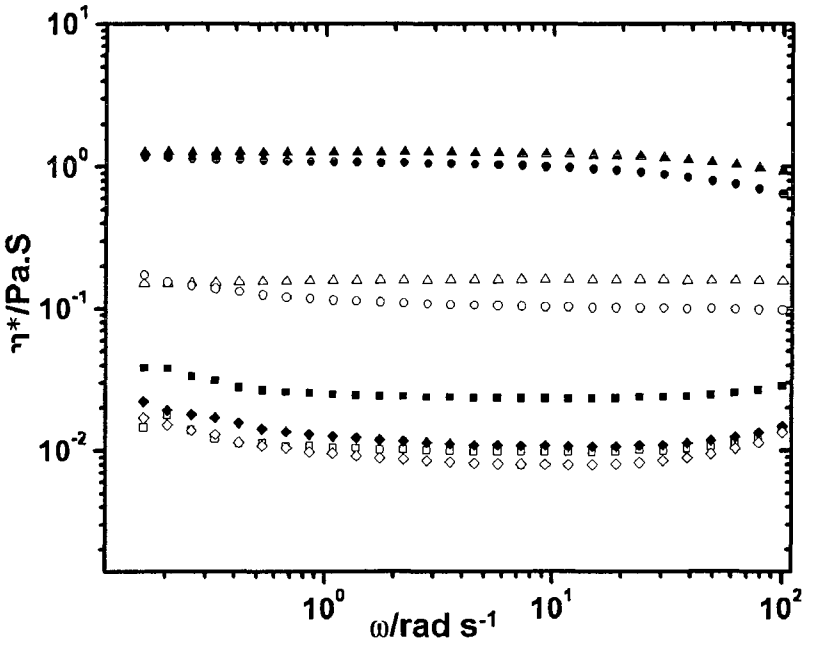

Figure 2.12. Angular frequency dependence on complex viscosity for the mixture of 10 wt-% P(PEGMA-co-5APM)/P(PEGMA-co-5MCD) (■,□), P(PEGMA-co-10APM)/P(PEGMA-co-10MCD) (▲,△), P(PEGMA-co-15APM)/P(PEGMA-co-15MCD) (●,○), and P(PEGMA)/P(PEGMA-co-10MCD) (◆,◇) at 20 (filled symbols) and 30 °C (open symbols).

The storage modulus, G', and the loss modulus, G", of the four samples in 10 wt-% solutions are given in Figure 2.13. The values of both G' and G" increase with increasing associative groups in the copolymer compositions, and the magnitudes of G" is higher than that of G' for all sample which means viscous flow dominates elastic response over the range of angular frequencies monitored. However, at low frequency, G" is almost equal to G' for the samples bearing the highest associative groups, P(PEGMA-co-15APM)/P(PEGMA-co-15MCD), and the difference between G" and G' increases with angular frequency. The data at Figure 2.13 indicates that P(PEGMA-co-

15APM)/P(PEGMA-co-15MCD) is at the gel boundry, and the inclusion complexes are dissociated as viscous flow dominates the elastic response with increasing angular frequency. This observation is not surprising considering adamantyl/cyclodextrin inclusion complexation is in dynamic equilibrium and the fast exchange between free and complexed adamantyl moieties may not maintain long-range connectivity.[40] The data indicates that both G' and G" are frequency dependent, and that they increase with increasing applied frequency. Similar observations were reported for G' and G" of cyclodextrin and adamantyl-grafted chitosan, and the decrease of G' and G" with decreasing frequency was explained by network relaxation as a result of breaking and reforming of the crosslink points.[36]

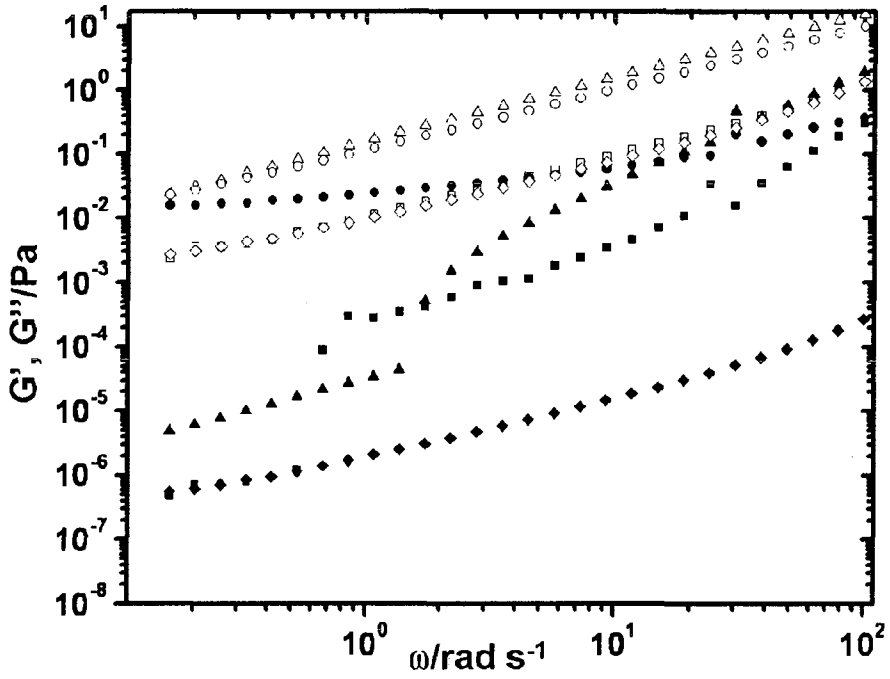

Figure 2.13. Frequency dependence on storage (filled symbols) and loss moduli (open symbols) for the mixture of 10 wt-% P(PEGMA-co-5APM)/P(PEGMA-co-5MCD) (■,□), P(PEGMA-co-10APM)/P(PEGMA-co-10MCD) (▲,△), P(PEGMA-

co-15APM)/P(PEGMA-co-15MCD) (●,○), and P(PEGMA)/P(PEGMA-co-10MCD) (♦,◇) at 30 °C.

Temperature effects on host-guest complex formation were further investigated for the 5 wt-% aqueous solution of P(PEGMA-co-10APM)/ P(PEGMA-co-10MCD) via temperature sweep measurement. The variation in viscosity as a function of temperature is given in Figure 2.14. The viscosity change of the 5 wt-% aqueous solution of P(PEGMA-co-10MCD) with temperature is also included in the same plot for comparison. As expected, the initial viscosity is significantly higher for the P(PEGMA-co-10APM)/P(PEGMA-co-10MCD) mixture due to host-guest inclusion complexation between adamantyl and cyclodextrin pendent groups. However, the viscosity constantly and drastically decreases with increasing temperature since the inclusion complexation is enthalpy driven. That is, temperature increases leads to decreases in the number of inclusion complexes which in turn result in lower apparent molecular weight and decreased viscosity.[40,41,42] This may result in a thermoreversible gel system such as has been reported by Hennick, et al., for a star-shaped 8-arm poly(ethylene glycol) (PEG) which was end-modified with β-cyclodextrin and cholesterol moieties. The storage (G') and loss moduli (G'') of the hydrogel system formed by the mixture of β-cyclodextrin end-capped PEG and cholesterol end-capped PEG decreased with increasing temperature from 4 to 37 °C and reverted back to original values with cooling.[43] Another important factor which leads to decreased viscosity may be increasing phase separation

with temperature; this may explain the slight decrease of the viscosity seen even for P(PEGMA-co-10MCD).

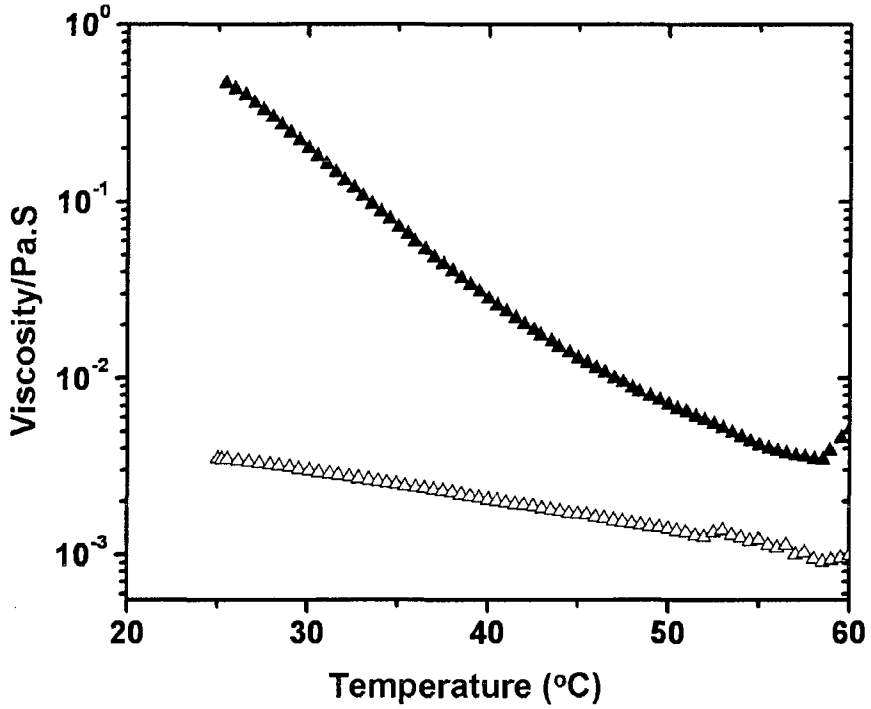

Figure 2.14. Viscosity dependence on temperature for the mixture of P(PEGMA-co-10APM)/P(PEGMA-co-10MCD) (▲) and P(PEGMA-co-10MCD) (△) alone.

Conclusion

Methacrylate monomers bearing cyclodextrin and adamantane pendent groups were synthesized, and copolymerized with poly(ethylene glycol) methyl ether methacrylate by free radical polymerization. Both ^{13}C and ^{1}H solution NMR showed peaks associated with adamantyl and cyclodextrin units besides PEGMA units. Although micelle formation (hydrophobic interaction of adamantyl groups) was observed for the copolymer bearing APM moieties examined by ^{1}H NMR, these associations did not inhibit the host-guest complex formation between pendent adamantyls with free cyclodextrins. The viscoelastic properties of

supramolecular assemblies were investigated with frequency and temperature sweep experiments. It was shown that PEG units did not form stable complexes with pendent CD groups, while the specific host-guest interaction between pendent adamantyl and cyclodextrin moieties lead to large increases in viscosity. It has thus been shown that the viscosity of these systems is tunable by varying the concentration of these groups in water-soluble copolymers.

References

1 Wenz, Gerhard. Cyclodextrins as Synthons for Supramolecular Structures and Functional Units. *Angewandte Chemie*, **1994**, 106, 851-70 (See also *Angew. Chem., Int. Ed. Engl.*, **1994**, 33, 803-22).

2 Rusa, Cristian C.; Tonelli, Alan E. Separation of Polymers by Molecular Weight through Inclusion Compound Formation with Urea and α-Cyclodextrin Hosts. *Macromolecules*, **2000**, 33, 1813-1818.

3 Choi, Hak Soo; Ooya, Tooru; Sasaki, Shintaro; Yui, Nobuhiko. Control of Rapid Phase Transition Induced by Supramolecular Complexation of β-Cyclodextrin-Conjugated Poly(ε-lysine) with a Specific Guest. *Macromolecules*, **2003**, 36, 5342-5347.

4 Bibby, D. C.; Davies, N. M.; Tucker, I. G. Mechanisms by which Cyclodextrins Modify Drug Release from Polymeric Drug Delivery Systems. *International Journal of Pharmaceutics,* **2000**, 197, 1-11.

5 Huh, Kang Moo; Ooya, Tooru; Lee, Won Kyu; Sasaki, Shintaro; Kwon, Ick Chan; Jeong, Seo Young; Yui, Nobuhiko. Supramolecular-Structured Hydrogels Showing a Reversible Phase Transition by Inclusion Complexation between Poly(ethylene glycol) Grafted Dextran and α-Cyclodextrin. *Macromolecules*, **2001**, 34, 8657-8662.

6 Auletta, Tommaso; De Jong, Menno R.; Mulder, Alart; Van Veggel, Frank C. J. M.; Huskens, Jurriaan; Reinhoudt, David N.; Zou, Shan; Zapotoczny, Szczepan; Schoenherr, Holger; Vancso, G. Julius; Kuipers, Laurens. β-Cyclodextrin Host-Guest Complexes Probed under Thermodynamic Equilibrium: Thermodynamics

and AFM Force Spectroscopy. *Journal of the American Chemical Society*, **2004**, 126, 1577-1584.

7 Guo, Mingyu; Jiang, Ming; Pispas, Stergios; Yu, Wei; Zhou, Chixing. Supramolecular Hydrogels Made of End-Functionalized Low-Molecular-Weight PEG and α-Cyclodextrin and Their Hybridization with SiO_2 Nanoparticles through Host-Guest Interaction. *Macromolecules*, **2008**, 41, 9744-9749.

8 Li, Li; Guo, Xuhong; Wang, Jie; Liu, Peng; Prud'homme, Robert K.; May, Bruce L.; Lincoln, Stephen F. Polymer Networks Assembled by Host-Guest Inclusion between Adamantyl and β-Cyclodextrin Substituents on Poly(acrylic acid) in Aqueous Solution. *Macromolecules,* **2008**, 41, 8677-8681.

9 Koopmans, Carsten; Ritter, Helmut. Formation of Physical Hydrogels via Host-Guest Interactions of β-Cyclodextrin Polymers and Copolymers Bearing Adamantyl Groups. *Macromolecules*, **2008**, 41, 7418-7422.

10 Charlot, Aurelia; Auzely-Velty, Rachel. Synthesis of Novel Supramolecular Assemblies Based on Hyaluronic Acid Derivatives Bearing Bivalent β-Cyclodextrin and Adamantane Moieties. *Macromolecules*, **2007**, 40, 1147-1158.

11 Hasegawa, Yasushi; Miyauchi, Masahiko; Takashima, Yoshinori; Yamaguchi, Hiroyasu; Harada, Akira. Supramolecular Polymers Formed from β -Cyclodextrins Dimer Linked by Poly(ethylene Glycol) and Guest Dimers. *Macromolecules*, **2005**, 38, 3724-3730.

12 Cheng, Zhenping; Zhu, Xiulin; Kang, E. T.; Neoh, K. G. Brush-type Amphiphilic Diblock Copolymers from Living/Controlled Radical

Polymerizations and Their Aggregation Behavior. *Langmuir,* **2005**, 21, 7180-7185.

13 Yamamoto, Shin-ichi; Pietrasik, Joanna; Matyjaszewski, Krzysztof. Temperature- and Ph- Responsive Dense Copolymer Brushes Prepared by ATRP. *Macromolecules*, **2008**, 41, 7013-7020.

14 Magnusson, Johannes Pall; Khan, Adnan; Pasparakis, George; Saeed, Aram Omer; Wang, Wenxin; Alexander, Cameron. Ion-Sensitive Isothermal Responsive Polymers Prepared in Water. *Journal of the American Chemical Society,* **2008**, 130, 10852-10853.

15 Xu, F. J.; Li, Y. L.; Kang, E. T.; Neoh, K. G. Heparin-Coupled Poly(poly(ethylene glycol) monomethacrylate)-Si(111) Hybrids and Their Blood Compatible Surfaces. *Biomacromolecules*, **2005**, 6, 1759-1768.

16 Fournier, David; Hoogenboom, Richard; Thijs, Hanneke M. L.; Paulus, Renzo M.; Schubert, Ulrich S. Tunable pH- and Temperature- Sensitive Copolymer Libraries by Reversible Addition-Fragmentation Chain Transfer Copolymerizations of Methacrylates. *Macromolecules,* **2007**, 40, 915-920.

17 Hang, Xiwen; Lian, Xueming; Liu, Li; Zhang, Jian; Zhao, Hanying. Synthesis of Comb Copolymers with Pendant Chromophore Groups Based on RAFT Polymerization and Click Chemistry and Formation of Electron Donor-Acceptor Supramolecules. *Macromolecules,* **2008**, 41, 7863-7869.

18 Lee, Haerim; Lee, Eunhye; Kim, Do Kyung; Jang, Nam Kyu; Jeong, Yong Yeon; Jon, Sangyong. Antibiofouling Polymer-Coated Superparamagnetic Iron Oxide Nanoparticles as Potential Magnetic Resonance Contrast Agents for in

Vivo Cancer Imaging. *Journal of the American Chemical Society,* **2006,** 128, 7383-7389.

19 Kalra, Bhanu; Kumar, Ajay; Gross, Richard A.; Baiardo, Massimo; Scandola, Mariastella. Chemoenzymatic Synthesis of New Brush Copolymers Comprising Poly(ω -pentadecalactone) with Unusual Thermal and Crystalline Properties. *Macromolecules,* **2004**, 37, 1243-1250.

20 Janata, Miroslav; Toman, Ludek; Spevacek, Jiri; Brus, Jiri; Sikora, Antonin; Latalova, Petra; Vlcek, Petr; Michalek, Jiri; Dvorankova, Barbora. Amphiphilic Conetworks. III. Poly(2,3-dihydroxypropyl methacrylate)-Polyisobutylene and Poly(ethylene glycol) methacrylate-Polyisobutylene Based Hydrogels Prepared by Two-Step Polymer Procedure. *J. Polym. Sci.: Part A: Polym. Chem.*, **2007**, 45, 4074-4081.

21 McNaughton Michael; Engman Lars; Birmingham Anne; Powis Garth. A Cyclodextrin-Derived Diorganyl Tellurides as Glutathione Peroxidase Mimics and Inhibitors of Thioredoxin Reductase and Cancer Cell Growth. *Journal of Medicinal Chemistry*, **2004**, 47, 233-239.

22 Acar, Havva Y.; Jensen, Jennifer J.; Thigpen, Kevin; McGowen, John A.; Mathias, Lon J. Evaluation of the Spacer Effect on Adamantane-Containing Vinyl Polymer Tg's. *Macromolecules*, **2000**, 33, 3855-3859.

23 Liu, Yu-yang; Fan, Xiao-dong; Gao, Lei. Synthesis and Characterization of β -Cyclodextrin Based Functional Monomers and its Copolymers with N-Isopropylacrylamide. *Macromolecular Bioscience,* **2003**, 3, 715-719.

24 Feng, Li-Bang; Zhou, Shu-Xue; You, Bo; Wu, Li-Min. Synthesis and Surface Properties of Polystyrene-Graft-Poly(ethylene glycol) Copolymers. *J. Appl. Polym. Sci.*, **2007**, 103, 1458-1465.

25 Kreutzer, Georg; Ternat, Celine; Nguyen, Tuan Q.; Plummer, Christopher J. G.; Mnson, Jan-Anders E.; Castelletto, Valeria; Hamley, Ian W.; Sun, Frank; Sheiko, Sergei S.; Herrmann, Andreas; Ouali, Lahoussine; Sommer, Horst; Fieber, Wolfgang; Velazco, Maria Ines; Klok, Harm-Anton. Water-Soluble Unimolecular Containers Based on Amphiphilic Multiarm Star Block Copolymers. *Macromolecules*, **2006**, 39, 4507-4516.

26 Bo, Gao; Wesslen, Bengt; Wesslen, K. Bodil. Amphiphilic Comb-Shaped Polymers from Poly(ethylene glycol) Macromonomers. *J. Polym. Sci.: Part A: Polym. Chem.*, **1992**, 30, 1799-1808.

27Jones, Janevieve A.; Novo, Noel; Flagler, Kendra; Pagnucco, Christina D.; Carew, Steve; Cheong, Charles; Kong, Xiang Z.; Burke, Nicholas A. D.; Stover, Harald D. H. Thermoresponsive Copolymers of Methacrylic Acid and Poly(ethylene glycol) Methyl Ether Methacrylate. *J. Polym. Sci.: Part A: Polym. Chem.*, **2005**, 43, 6095-6104.

28 Mathias, L. J.; Jensen, J.; Thigpen, K.; McGowen, J.; McCormick, D.; Somlai, L. Copolymers of 4-Adamantylphenyl Methacrylate Derivatives with Methyl Methacrylate and Styrene. *Polymer*, **2001**, 42, 6527-6537.

29 Chen, Yiwang; Wang, Wencai; Yu, Weihong; Yuan, Zeliang; Kang, En-Tang; Neoh, Koon-Gee; Krauter, Berit; Greiner, Andreas. Nanoporous low -κ Polyimide Films via Poly(amic acid)s with Grafted Poly(ethylene glycol) Side Chains From a

Reversible Addition-fragmentation Chain-Transfer-Mediated Process. *Advanced Functional Materials,* **2004**, 14, 471-478

30 Kwon, G.; Naito, M.; Yokoyama, M.; Okano, T.; Sakurai, Y.; Kataoka, K. Micelles Based on AB Block Copolymers of Poly(ethylene oxide) and Poly(β -benzyl L-aspartate). *Langmuir*, **1993**, 9, 945-949.

31 Lou, Liping; Jiang, Liming; Sun, Weilin; Shen, Zhiquan. A Novel Optically Active Diblock Copolymer Composed of Poly(ethylene glycol) and Poly[*N*-{*o*-(4-phenyl-4,5-dihydro-1,3-oxazol-2-yl)phenyl}maleimide]: Synthesis, Micellization Behavior, and Chiroptical Property. *J. Polym. Sci.: Part A: Polym. Chem.,* **2008**, 46, 1025-1033.

32 Harada, Akira; Kamachi, Mikiharu. Complex Formation between Poly(ethylene glycol) and α-Cyclodextrin. *Macromolecules,* **1990**, 23, 2821-2823.

33 Harada, Akira; Li, Jun; Suzuki, Syukuko; Kamachi, Mikiharu. Complex Formation between Polyisobutylene and Cyclodextrins: Inversion of Chain-Length Selectivity between β-Cyclodextrin and γ-Cyclodextrin. *Macromolecules,* **1993**, 26, 5267-5268.

34 Harada, Akira; Nishiyama, Toshiyuki; Kawaguchi, Yoshinori; Okada, Miyuko; Kamachi, Mikiharu. Preparation and Characterization of Inclusion Complexes of Aliphatic Polyesters with Cyclodextrins. *Macromolecules*, **1997**, 30, 7115-7118.

35 Udachin, Konstantin A.; Wilson, Lee D.; Ripmeester, John A. Solid Polyrotaxanes of Poly(ethylene glycol) and Cyclodextrins: The Single Crystal X-Ray Structure of PEG-β-cyclodextrin. *Journal of the American Chemical Society,* **2000**, 122, 12375-12376.

36 Joseph, Julie; Dreiss, Cecile A.; Cosgrove, Terence. Stretching a Polymer Brush by Making in Situ Cyclodextrin Inclusion Complexes. *Langmuir*, **2008**, 24, 10005-10010.

37 Auzely-Velty, Rachel; Rinaudo, Marguerite. New Supramolecular Assemblies of a Cyclodextrin-Grafted Chitosan through Specific Complexation. *Macromolecules,* **2002**, 35, 7955-7962.

38 Newkome, George R.; Kim, Hyung Jin; Choi, Kyung Ho; Moorefield, Charles N. Synthesis of Neutral Metallodendrimers Possessing Adamantane Termini: Supramolecular Assembly with β -Cyclodextrin. *Macromolecules,* **2004**, 37, 6268-6274.

39 Ohga, Kahori; Takashima, Yoshinori; Takahashi, Hirokazu; Kawaguchi, Yoshinori; Yamaguchi, Hiroyasu; Harada, Akira. Preparation of Supramolecular Polymers from a Cyclodextrin Dimer and Ditopic Guest Molecules: Control of Structure by Linker Flexibility. *Macromolecules,* **2005**, 38, 5897-5904.

40 Charlot, Aurelia; Auzely-Velty, Rachel. Novel Hyaluronic Acid Based Supramolecular Assemblies Stabilized by Multivalent Specific Interactions: Rheological Behavior in Aqueous Solution. *Macromolecules*, **2007**, 40, 9555-9563.

41 Charlot, Aurelia; Auzely-Velty, Rachel; Rinaudo, Marguerite. Specific Interactions in Model Charged Polysaccharide Systems. *Journal of Physical Chemistry B,* **2003**, 107, 8248-8254.

42 Li, Li; Guo, Xuhong; Wang, Jie; Liu, Peng; Prud'homme, Robert K.; May, Bruce L.; Lincoln, Stephen F. Polymer Networks Assembled by Host-Guest

Inclusion between Adamantyl and β-Cyclodextrin Substituents on Poly(acrylic acid) in Aqueous Solution. *Macromolecules*, **2008**, 41, 8677-8681.

43 van de Manakker, Frank; van der Pot, Martin; Vermonden, Tina; van Nostrum, Cornelus F.; Hennink, Wim E. Self-Assembling Hydrogels Based on β-Cyclodextrin /Cholesterol Inclusion Complexes. Macromolecules, **2008**, 41, 1766-1773.

CHAPTER III

UV CURABLE COATINGS FOR IMPROVED GAS BARRIER PROPERTIES OF POLY(ETHYLENE TEREPHTHALATE)

Abstract

A new high-barrier coating based on methyl (α-hydroxymethyl)acrylate (MHMA) for poly(ethylene terephthalate) (PET) was developed along with the process for preform dipping and cure prior to blow molding into bottles. The UV curable coating gives excellent barrier improvement to PET biaxially oriented thin films and bottle sidewalls. The affect of photoinitiator concentration, initiator types, and temperature on photopolymerization kinetics of MHMA was investigated. Once the photoinitiator, Irgacure 819®, concentration became larger than 1 mol-%, a decrease in rate of propagation was observed. The conversion also decreased with high initiator concentration. Irgacure 819® reduced the autoacceleration peak and induced maximum rates of polymerization much faster than Irgacure 651®. It gave a slightly higher conversion, but overall conversion for combinations of these photoinitiators were all high and above 80%. Real-time FTIR (RT-FTIR) studies of copolymerization of MHMA and methyl methacrylate (MMA) showed that conversion is fairly high up to 25 mol-% MMA. However, once MMA feed ratio exceeded 10 mol-%, a decrease in barrier performance was observed. A series of coated PET films based on two additional monomers synthesized in our research group with MHMA/MMA (50/50) were prepared, and these coated PET showed oxygen

permeability reduced by 1.4-2.5 times that of the uncoated PET control. Finally, only MHMA coated preforms were blown into bottles using conventional methods, and blown bottle side walls from these coated preforms showed 2-3 times barrier improvement over uncoated side walls.

Introduction

Gas barrier is the ability of a material to limit permeation of certain gases and is a key factor in the design of food and beverage packaging. Poly(ethylene terephthalate) (PET) is increasingly used for packaging applications due to its transparency, ease of processing, and low cost, plus its semi-crystalline nature inherently gives rise to moderate gas barrier properties. However, a three- to five-fold decrease in permeability is needed for new applications such as packaging for beer, fruit juices, and hot-fill baby foods. For this reason, increasing emphasis has been put on investigating methods to decrease the solubility and diffusivity of gasses in PET.

Impermeable inorganic materials have been used as fillers for PET,[1, 2] as coatings,[3, 4] and in hybrid organic-inorganic coatings.[5] Improvements in barrier are generally related to a decrease in diffusivity by formation of a torturous pathway in the case of inorganic fillers, or by high density in the case of inorganic coatings. Generally, inorganic coatings are brittle, and cracking or hole formation quickly deteriorates barrier properties.

In polymers, free volume must be reduced or excluded to form high barrier materials.[6] Thus, polymers with high degrees of hydrogen bonding, tight chain packing, and/or high degrees of molecular order in the amorphous phase

exhibit the best gas barrier properties. Ethylene/vinyl alcohol (EVOH) copolymers have excellent barrier properties under dry conditions, and have been widely investigated as barrier coatings,[7-10] although properties suffer nearly a hundred fold when exposed to moisture. Moisture plasticizes EVOH and can irreversibly change the EVOH morphology, resulting in increased free volume.[11]

Tiemblo, et al.,[12] correlated fractional free volume to gas diffusivity of methacrylic ester copolymers with varying side chain lengths. Fractional free volume was calculated based on the specific volume of the polymer and the specific van der Waals volume. Additional methylenes in the side chain increased the fractional free volume, which in turn increased diffusion of gas molecules. Varying the size of the gas penetrant did not significantly affect the diffusivity, implying that the high flexibility of the side chains allows kinetic transport.

The influence of molecular packing was exhibited in the high oxygen barrier of self-assembled melamine coatings. Melamine was vapor deposited onto PET films to form a transparent coating with high barrier to oxygen.[13] Although melamine is a small molecule, it assembled into regular arrays due to the presence of symmetrical hydrogen bond donor and acceptor sites (Figure 3.1).

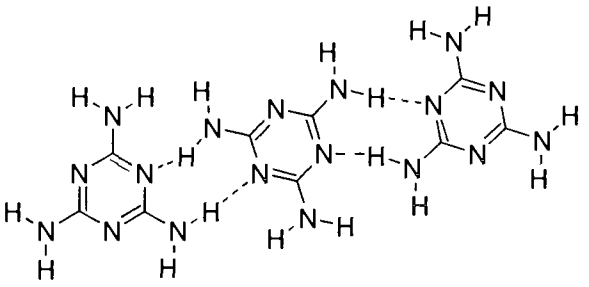

Figure 3.1. Structure of the supramolecular assembly of melamine.

Coatings of hyperbranched polyesters based on bis(hydroxymethyl)propionic acid improved oxygen barrier of PET and polypropylene,[14] although the coatings were moisture sensitive. The hyperbranched polyester had an average of 64 hydroxyl end-groups per molecule. Hyperbranched polymers with 15-30% methacrylate groups included for crosslinking showed the best barrier properties compared to uncrosslinked or lightly crosslinked systems. Unexpectedly, addition of semi-crystalline poly(ε-caprolactone) to the shell of hyperbranched polyesters decreased barrier properties. Moisture sorption in these systems was comparable to amorphous EVOH, and depended greatly on the concentration of hydroxyl groups.[15]

A number of epoxy-amine derivatives have demonstrated excellent barrier properties.[16, 17] Brennan,et al.,[18, 19] synthesized new high-barrier thermoplastics based on bisphenol-A diglycidyl ether and bisphenols with an amide linkage. Lower oxygen permeabilities were obtained by either reducing the number of methylene units or increasing the population density of amide groups, which increased hydrogen-bonding interactions. Interestingly, the barrier properties of poly(hydroxy amide ethers) improved in the presence of moisture. A detailed investigation into the effect of polymer structure showed

that replacing methylene units with meta-linked phenylene units decreased permeability.[20] Also, barrier properties improved as the aromatic backbone unit became planar (improving chain packing) or had a strongly polar pendent functional group that strengthened hydrogen bonding.[21]

In this work, a functionalized methacrylate, methyl (α-hydroxymethyl)acrylate (MHMA), was applied to PET film, then photopolymerized to produce a coated structure possessing three times the oxygen barrier of the biaxially-oriented PET substrate alone. In addition, a series of coatings based on MHMA with various MMA concentrations were prepared on biaxially-oriented PET samples. The samples containing less than 10 mol-% MMA showed no substantial decrease in barrier properties of PET. Coatings based on two additional comonomers synthesized in our research group with MHMA/MMA (50/50) showed excellent barrier improvement. Finally, PET preforms were dipped in just MHMA solution and the obtained thin coating photopolymerized to produce a coated preform that could be blown into a bottle possessing at least two times the oxygen barrier of uncoated bottles

Results and Discussion

MHMA is a unique monomer in that it is an α-substituted methacrylate (Figure 3.2). It shows very fast photopolymerization rates and high conversions. Poly(MHMA) is completely amorphous, and offers cost saving advantages (estimated 1.5-3.5 times lower) over current commercially available barrier coatings. When polymerized, MHMA is completely transparent with optical clarity rivaling polycarbonate.

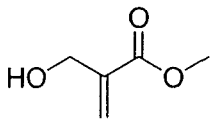

MHMA

Figure 3.2. Structure of methyl (α-hydroxymethyl)acrylate (MHMA).

Another unique property of poly(MHMA) is its very high density (Table 2.1).[22] This high density leads to excellent solvent resistance and extremely low moisture absorption. Poly(MHMA) is completely insoluble in acetone, methanol, ether and water, and only partially soluble in *N*-*N*-dimethylformamide, dimethyl sulfoxide, and hexafluoroisopropanol. These properties combine to give poly(MHMA) excellent barrier properties.

Table 3.1

Density comparison for methacrylate monomers.[22]

Polymer	Density (g/cm^3)
MHMA	1.388
HEMA	1.07
MMA	1.19

Coating Experiments on PET Biaxially Oriented Thin Films

Initial coating experiments involved application of thin monomer films to biaxially oriented PET films. The substrates were not washed prior to coating. An MHMA solution was prepared containing 1 mol-% Irgacure 651® photoinitiator. Approximately 0.5 mL of the MHMA solution was placed in the middle of a 90 mm diameter film. The solution was brushed outward using a small paintbrush, and samples were placed in a chamber with a nitrogen atmosphere. After purging the chamber, the samples were irradiated with UV

light from an external hand-held UV source through a UV transparent cover of polypropylene. Some samples were coated twice in order to cover coating defects such as small pin holes.

Surprisingly, these crude MHMA photocured coatings resulted in excellent oxygen (Table 3.2) and carbon dioxide barrier properties (Table 3.3). Film thicknesses ranged from 0.8-1.8 mils, which showed oxygen permeability reduced 2.5-3.7 times that of the uncoated substrate. Carbon dioxide permeability also showed marked decreases compared to the uncoated substrate (3-4 x lower).

Table 3.2

Oxygen permeation results for PET thin films coated with MHMA and photocured.

Sample #	Cure Time (h)	Total Thickness (mils)	Coat (mils)	P	D	S	P_0/P
1	0	4.3	0	0.133	2.0	0.075	--
2	1	5.2	0.9	0.049	1.1	0.052	2.7
3[a]	1	5.6	1.3	0.042	0.9	0.054	3.2
4[a]	1	6.1	1.8	0.036	0.82	0.051	3.7
5	1	5.1	0.8	0.053	1.2	0.045	2.5

[a] Two coats photocured

P – cc(STP) cm m^{-2} atm^{-1} day^{-1}; D – $x10^{-13}$ m^2 sec^{-1}; S – cc(STP) cm^{-3} atm^{-1}

Table 3.3

Carbon dioxide permeation results for PET thin films coated with MHMA and photocured.

Sample	Cure Time (h)	Total Thickness (mils)	Coat (mils)	P	D	S	P_0/P
1	0	4.3	0	0.863	0.6	1.66	--
2	1	5.2	0.9	0.240	0.26	1.07	3.5
3[a]	1	5.6	1.3	0.235	0.25	1.09	3.7
4[a]	1	6.1	1.8	0.220	0.24	1.06	4
5	1	5.1	0.8	0.283	0.3	1.09	3

[a] Two coats photocured

P – cc(STP) cm m^{-2} atm^{-1} day^{-1}; D – $x10^{-13}$ m^2 sec^{-1}; S – cc(STP) cm^{-3} atm^{-1}

An important factor in altering the nature of PET is the effect a coating has on recycling. During the recycling process, PET bottles are subject to washing in hot caustic solutions. The poly(MHMA) coating was completely removed from PET thin films by a 2 wt-% solution of sodium hydroxide at 80 °C in the absence of agitation. Therefore, PET recycling will not be hindered by MHMA barrier coatings.

Scotch® tape adhesion testing of MHMA-treated PET films was conducted on samples that had been UV cured for 60 minutes. The coated surface was not affected by the adhesion test. Furthermore, bending the coated film did not cause cracking or breaking of the coating layer. However, when the coated PET was folded over and creased, cracking of the coating was observed.

In order to probe the importance of the MHMA hydroxyl group to adhesion, methyl methacrylate (MMA) monomer was coated onto PET thin films using the same method as was employed with MHMA. The obtained coatings of MMA were not homogeneous. Cracks formed during the photochemical cure, and the Scotch® Tape adhesion test caused significant loss of the coating. Adhesion of poly(MHMA) on aluminum surface was strong while the poly(MMA) could be removed easily. Both polymers adhered to glass substrates well.

UV Photopolymerization and PhotoDSC

We have been pursuing the chemistry of alkyl α-hydroxymethylacrylate (RHMA) for several years. This family of monomers shows very fast photopolymerization rates with high conversions. One of the main objectives in the UV curing of coatings is to obtain a high degree of conversion at the surface

and throughout the coating layer. The concentration of initiator, on the other hand, significantly effects overall conversion and rate of polymerization. In order to obtain good through-cure of coating, the light has to penetrate throughout the coating. The use of a high concentration of photoinitiator may lead to screening, resulting in a gradient of the conversion and lower overall conversion.[23] This is especially important for barrier properties of the coating since any residual monomers will act as plasticizers of the matrix, increasing the free volume and leading to lower barrier. Therefore, it is important to determine the optimal photoinitiator concentration that leads to fast polymerization with high conversion.

Figure 3.3 shows the effect of cure time and initiator concentration on the rate and polymerization conversion of MHMA. The data given are for Irgacure 819® up to 3 mol-% of the photoinitiator. The solubility of photoinitiator became an issue over 3 mol-% Irgacure 819®, whereas up to 5 mol-% Irgacure 651® easily dissolved in MHMA. Once the photoinitiator, Irgacure 819®, concentration became higher than 1 mol-%, a decrease in rate of propagation was observed. This may be due to screening of UV light as the photoinitiator concentration increases. The higher levels of photoinitiator absorb more UV light, preventing it from penetrating throughout the sample. This also effects overall conversion, and conversions decreased at initiator concentrations above 1 mol-%. The overall conversions for 0.5 and 1 mol-% initiator concentration were above 80%, whereas with initiator concentration higher than 1 mol-%, conversions were around 60%. Another interesting observation is that the decrease in rate of

photopolymerization was very sharp for 0.5 and1 mol-% initiator concentration once the polymerization rate reached the maximum. These sharp decreases were not observed for higher photoinitiator concentrations. The autoacceleration peak was not observable for any of these systems except with 0.1 mol-% photoinitator concentration, as shown below.

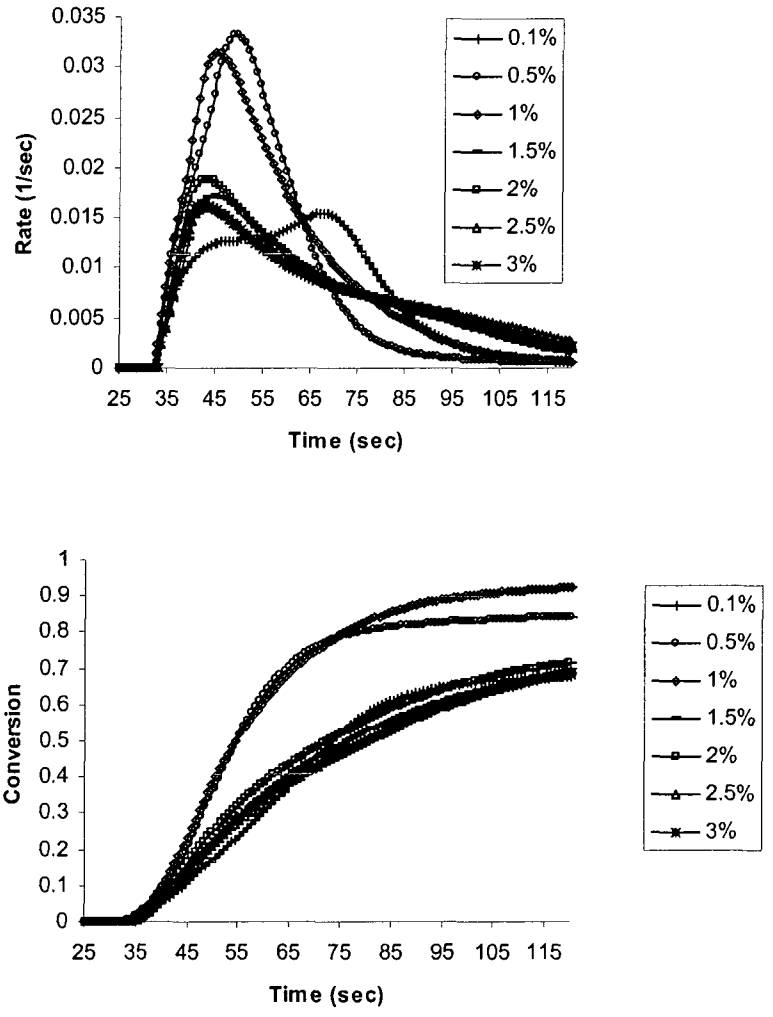

Figure 3.3. A) Rate versus time, and B) conversion versus time plots for MHMA with various Irgacure 819® initiator concentrations at 30 °C.

It was also one of our objectives to evaluate the temperature effect on photopolymerization of MHMA with various initiator concentrations. Elevated rates of photopolymerization are usually observed when the reactions are performed at higher temperatures. Figure 3.4 shows the rate and the conversion of MHMA with various concentrations of Irgacure 819® initiator at 50 °C. Contrary to our expectation, no significant change of overall rate and conversion was observed. A slight decrease was seen for systems with 0.5 and 1 mol-% Irgacure 819®, while no change occurred with higher photoinitiator concentrations. The slight decrease of the systems with 0.5 and 1 mol-% Irgacure 819® may be related to the reduction of the extent of the hydrogen bonding at higher temperatures; i.e., the rate increase due to increasing temperature may not compensate for the decrease in hydrogen bonding. Jansen, et al., reported similar result for photopolymerization of undecyl amide N-ethyl acrylate.[24] Even though the rate of photopolymerization at 50 °C was higher than at 30 °C, the rate was showing a decreasing trend when the temperature was over 40 °C.

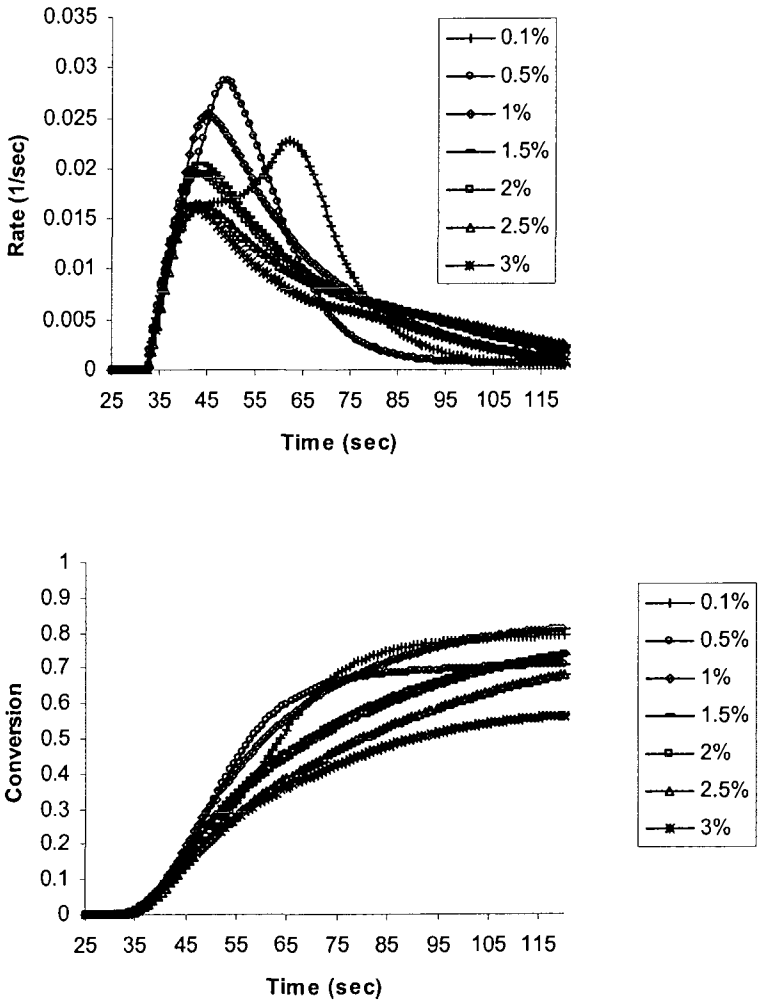

Figure 3.4. A) Rate versus time, and B) conversion versus time plots for MHMA with various Irgacure 819® initiator concentrations at 50 °C.

The effect of initiator type, dimethoxy phenylacetophenone (Irgacure 651®) or phenyl bis(trimethylbenzoyl)phosphine oxide (Irgacure 819®) on photopolymerization (chemical structures given in Figure 3.5) rates and conversions was investigated with respect to various ratios of these two photoinitators. The total concentration of photoinitiators was kept constant at 1 mol-%, while the Irgacure 651® ratio was changed from 0 to 100%. Irgacure 819® is able to generate four initiating radicals per photoinitiator molecule,

whereas Irgacure 651® is only able to create two radicals with photoinitation.[25, 26] It is expected that the number of formed radicals plus absorbance difference of these two photoinitiators will have a dramatic effect on photopolymerization of MHMA. The initial monomer-initiator solutions for Irgacure 819® are yellow, whereas they are clear for Irgacure 651®. However, the initial yellowness of the solution disappears with curing. Figure 3.6 shows rate and conversion versus time plots for various ratios of the two different types of initiators. Irgacure 819® reduced the autoacceleration peak and reached maximum rates of polymerization much faster than Irgacure 651®. It gave a slightly higher conversion, but overall conversion for combinations of these photoinitiators were all high and above 80%. The peak maximum shifted to the right on the time scale with increasing Irgacure 651® concentration.

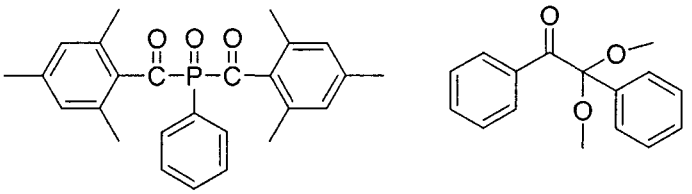

Irgacure 819 Irgacure 651

Figure 3.5. Chemical structures of Irgacure 651® and Irgacure 819® photoinitiators.

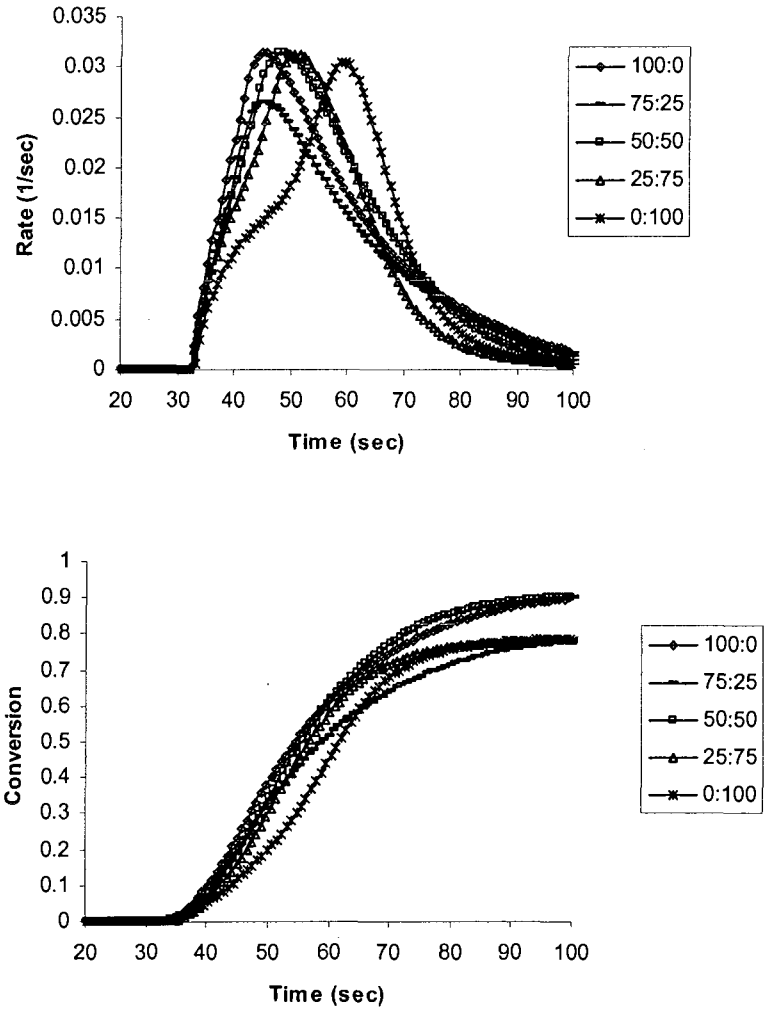

Figure 3.6. Rate versus time plots for MHMA with Irgacure 819® vs. 651® initiator at 30°C.

Effect of Cure Time and Initiator Concentration on Barrier

Barrier measurements were performed on selected samples to determine what affect the cure time and initiator concentration had on oxygen (Table 3.4) and carbon dioxide (Table 3.5) barrier properties. Irgacure 651® was used as photoinitiator. Barrier improvement over uncoated PET thin films was somewhat smaller than for previous systems. Once photoinitiatior concentrations became

larger than 2.5 mol-%, a further decrease in barrier performance was observed. This may be due to screening of UV light as film thickness increases leading to higher residual monomer concentration that acts as a plasticizer.

Table 3.4

Oxygen barrier of MHMA on PET thin films UV cured with varied initiator concentration and cure times.

[I] (mol-%)	Cure Time (min)	Total Thickness (mils)	Coat (mils)	P	D	S	P_0/P
1.5	15	5.3	1.0	0.083	1.4	0.070	1.6
2.0	5	5.5	1.2	0.086	1.5	0.067	1.5
2.5	5	5.5	1.2	0.081	1.5	0.063	1.6
3.0	3	5.8	1.5	0.092	1.8	0.061	1.4
5.0	2	5.4	1.1	0.107	1.7	0.091	1.2

P – cc(STP) cm m^{-2} atm^{-1} day^{-1}; D – x10^{-13} m^2 sec^{-1}; S – cc(STP) cm^{-3} atm^{-1}

Table 3.5

Carbon dioxide barrier of MHMA on PET thin films UV cured with varied initiator concentration and cure times.

[I] (mol-%)	Cure Time (min)	Total Thickness (mils)	Coat (mils)	P	D	S	P_0/P
1.5	15	5.3	1.0	0.484	0.38	1.49	1.8
2.0	5	5.5	1.2	0.537	0.39	1.58	1.6
2.5	5	5.5	1.2	0.472	0.40	1.38	1.8
3.0	3	5.8	1.5	0.586	0.46	1.48	1.5
5.0	2	5.4	1.1	0.670	0.49	1.59	1.3

P – cc(STP) cm m^{-2} atm^{-1} day^{-1}; D – x10^{-13} m^2 sec^{-1}; S – cc(STP) cm^{-3} atm^{-1}

Effect of Coating Thickness and Humidity on Barrier

After initial work to coat PET substrates, draw-down rods with different effect numbers were used instead of brushing. An MHMA solution containing 1 mol-% Irgacure 819 photoinitiator was applied on the PET substrate and the coating made more uniform using the draw-down rods. The coated samples were placed in a handmade sealed metal chamber with a quartz window, and

then the samples were irradiated with an external hand-held UV source (Blak-Ray Long Wave Ultraviolet, Model B 100 AP).

In order to understand the effect of thickness of the MHMA coating on PET permeability, three different the draw-down rods (3, 6, and 13) were used to obtain PET coated samples with various coating thicknesses. From Table 3.6, it can be seen the MHMA coating gave marked improvement in oxygen barrier properties on PET. The improvement was up to a factor 2.1 for the thicker sample MHMA-13 compared to the neat PET substrate. The barrier performance of coatings improved with increasing hydroxyl content in the coating for dry conditions due to hydrogen bonding giving a denser network. However, the barrier performance of the polymer matrix is complicated under humid conditions. Lange, et al., [14] investigated the correlation between humidity and hydroxyl content for hydroxy-functional hyperbranched polyester resin. It was reported that up to a certain hydroxyl content fraction, permeability is lower for the polyester resin compared to permeability of the same polyester in dry conditions.[14] Hydroxyl content fraction of poly(MHMA) is very high, and it is expected that MHMA coatings will be susceptible to humidity. The permeability data is given in Table 3.7 at 85% relative humidity (RH) for the samples. As expected, the coated samples showed reduced improvement over PET at 85% relative humidity due to high water uptake of MHMA coating, and plasticizing effect of water.

Table 3.6

Effect of thickness of MHMA coating on PET permeability at 0 % RH

ID	Thickness (mil)	Coating thickness (mil)	P	D	S	P_o/P	Estimated $P_{coating}$
3Mcontrol	4.2 ± 0.1	-	0.160	2.1	0.089	-	-
MHMA-3[a]	4.6 ± 0.1	0.4 ± 0.2	0.106	2.0	0.060	-	-
MHMA-6	4.7 ± 0.1	0.5 ± 0.2	0.091	1.9	0.054	-	-
MHMA-13	5.5 ± 0.1	1.3 ± 0.2	0.068	1.7	0.047	-	-

[a] rod number

P – cc(STP) cm m^{-2} atm^{-1} day^{-1}; D – x10^{-13} m^2 sec^{-1}; S – cc(STP) cm^{-3} atm^{-1}

Table 3.7

Effect of thickness of MHMA coating on PET permeability at 85 % RH

ID	Thickness (mil)	Coating thickness (mil)	P	D	S	P_o/P	Estimated $P_{coating}$[a]
3Mcontrol	4.1 ± 0.2	-	0.134	2.7	0.059	-	-
MHMA-3	4.6 ± 0.1	0.4 ± 0.1	0.143	3.0	0.055	-	-
MHMA-6	4.7 ± 0.1	0.5 ± 0.1	0137	3.3	0.048	-	-
MHMA-13	5.5 ± 0.1	delaminated during conditioning					

P – cc(STP) cm m^{-2} atm^{-1} day^{-1}; D – x10^{-13} m^2 sec^{-1}; S – cc(STP) cm^{-3} atm^{-1}

Considering possible applications of MHMA coating, water uptake and transmittance will be important criteria. Investigation of the water absorption was conducted for various stand-alone films based on MHMA, MMA, and MHMA/MMA (50/50). For comparison, two other samples consisting of copolymers of MHMA with butyl acrylate (BA), and MHMA with methacrylic acid (MA) were prepared. The samples were soaked in water, and the weight change and transmittance were determined. The results are given in Table 3.8. Water uptake of the homopolymer of MMA is the least at 0.4 wt-%, whereas poly(MHMA-co-MA) (50/50) is the most at 27 wt-% gain in 24 hours.

Interestingly, water absorbance of poly(MHMA-co-MMA) (50/50) is very low 3.6 wt-% in 24 hours, and no transmittance changes were observed.

Table 3.8

Water absorption and transmittance changes

Film Composition	Wt-% Gain	Transmittance
P(MHMA / MA*) (50 / 50)	27	Changed in 24 h
P(MHMA / BA*) (50 / 50)	4.7	Changed in 48 h
P(MHMA)	19.8	Changed in 24 h
P(MHMA / MMA) (50 / 50	3.6	same
P(MMA)	0.4	same

Copolymerization with MMA

To investigate copolymerization kinetics, thermal and barrier properties, a series of copolymers of MHMA with various mol fractions of MMA was prepared. The photopolymerization of MHMA/MMA (50/50) mixture was followed by FTIR at various time intervals. The mixture was applied between two salt plates and exposed to hand-held UV source for given times. Unfortunately, the absorbance spectra of MMA and MHMA almost completely overlap which makes it impossible to evaluate the effect of hydrogen bonding on copolymerization of MHMA and MMA. The broad O-H stretching band around 3475 cm^{-1} observed in Figure 3.7 is due to various hydrogen bonding structures in this systems. Absorptions at 821 cm^{-1} and 1639 cm^{-1} are due to vinyl groups. The intensity of these two peaks decreased with time, and there were no spectral changes after 300 sec, although residual double bonds were still observed. The copolymers showed expected characteristic peaks. The bands at 2956 and 3000 cm^{-1} were ascribed to CH_3 vibration, and the sharp peak around 1727 cm^{-1} to C=O vibration.

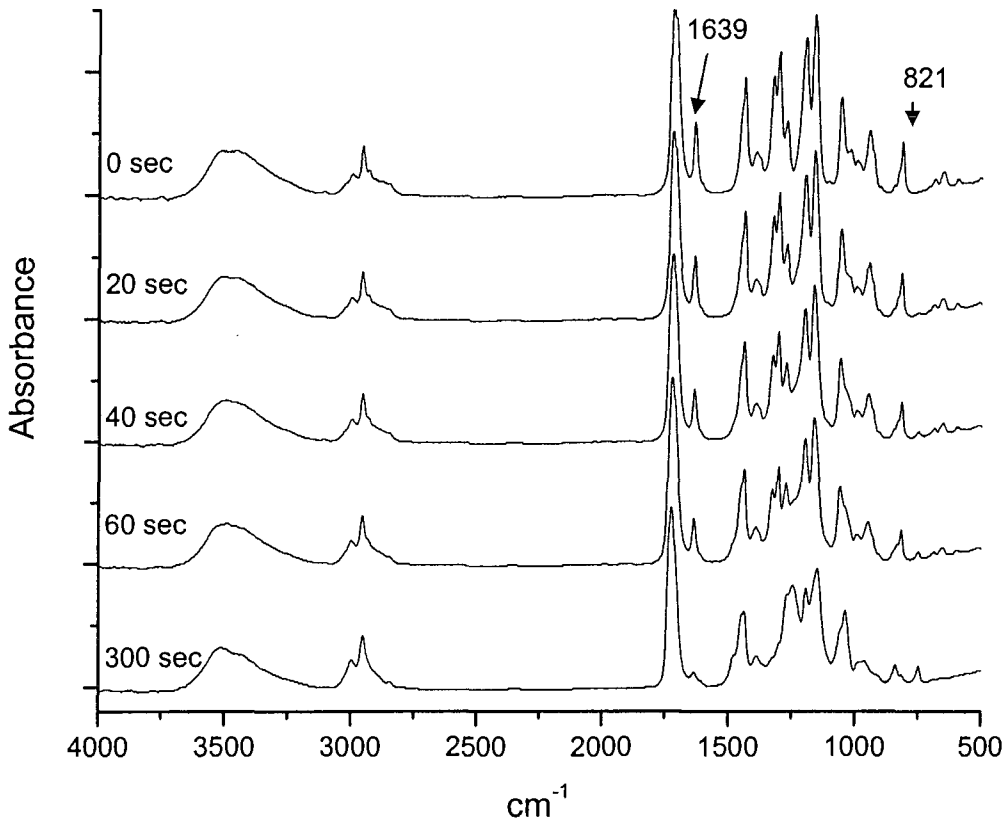

Figure 3.7. FTIR spectra of MHMA/MMA (50/50) mixture exposed to UV for various time intervals.

Figure 3.8 is a plot of % conversion versus irradiation time and shows the effect of methyl methacrylate (MMA) concentration on MHMA polymerization rate and conversion. Jansen, et al., indicate that acrylate monomers capable of hydrogen bonding have very high rates compared with non-hydrogen bonding analogues with the same secondary functionality.[24] The enhanced rate of photopolymerization was attributed to hydrogen bonding resulting in preorganization of the monomers. Viscosity differences may also play a significant role. Because MHMA has a hydroxyl group at the β position which is

capable of hydrogen bonding with carbonyl groups or hydroxyl groups of other MHMA monomers, it is expected that MHMA will have a much higher rate of polymerization than MMA. The RT-FTIR plot (Figure 3.8) supports the importance of hydrogen bonding to the rate of polymerization of MHMA. The rate is given by the initial slope of the plots, and MHMA shows a significantly higher rate of polymerization and greatly increased final conversion (around 75 % in 10 sec) than does MMA.

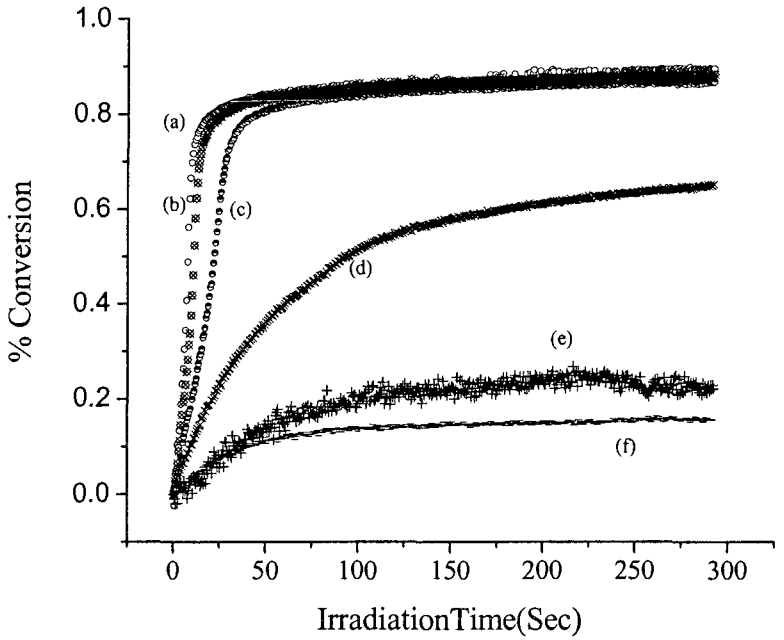

Figure 3.8. RT-FTIR plot of % conversion as a function of irradiation time for (a) MHMA, (b) MHMA:MMA with a ratio of (90:10), (c) MHMA:MMA (75:25), (d) MHMA:MMA (50:50), (e) MHMA:MMA (10:90), and (f) MMA.

Figure 3.9 shows the DSC thermograms of pure poly(MHMA), pure poly(MMA), and several copolymers with various ratios of MHMA/MMA under nitrogen with a heating rate of 10 °C/min. The samples were dried at 110 °C before DSC runs to remove water and residual monomers. All copolymers have a single T_g which shifted to lower temperature with increasing MMA concentration in copolymer compositions. The feed ratios and glass transitions are given in Table 3.9. The pure poly(MHMA) and pure poly(MMA) have T_g of 154 and 98 °C, respectively. Intermolecular interaction leads to closer packing of amorphous regions that results in reduced free volume.[10] Thus, high T_g plus hydrogen bonding are two important factors that lead to high barrier properties of poly(MHMA). It must be noted that even the copolymer with 75/25 monomer ratios gave a T_g of 138 °C which may relate to the high barrier properties of this copolymer. The thermal stability of these polymers and the 50/50 copolymers were investigated by TGA under nitrogen with a heating rate of 10 °C/min. These three polymers gave very different decomposition patterns as shown in Figure 3.13. The two-step decomposition of poly(MHMA) must be due to methanol loss in the first stage and random scission of polymer chains in the second stage.

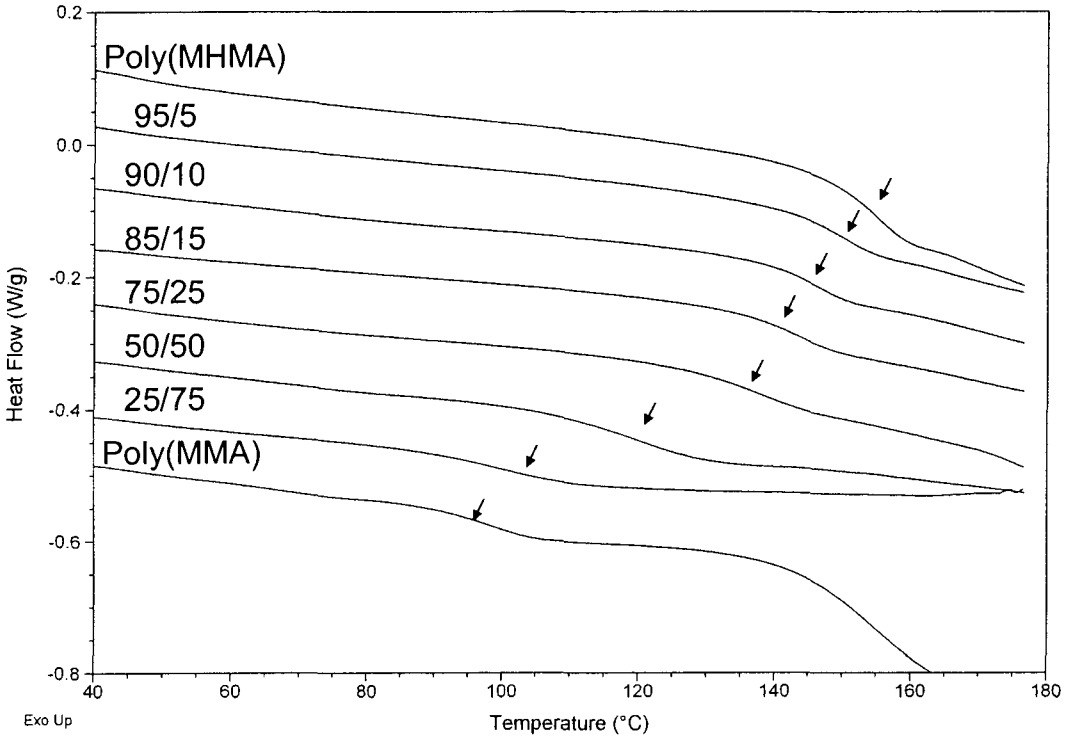

Figure 3.9. DSC thermograms of homopolymers and copolymers.

Table 3.9.

Compositions and T_g values of homopolymers and copolymers.

Composition	MHMA (mol-%)	MMA (mol-%)	T_g
MHMA	100	0	154
MHMA/MMA	95	5	150
MHMA/MMA	90	10	146
MHMA/MMA	85	15	143
MHMA/MMA	75	25	138
MHMA/MMA	50	50	119
MHMA/MMA	25	75	101
MMA	0	100	98

To understand effect of MMA concentrations on barrier properties of MHMA coating, several MHMA-MMA copolymer coated PET samples were

prepared. Both number 6 and 10 rods were used to obtain two series of samples with two different coating thicknesses. MMA fractions were from 1 mol-% to 25 mol-%. Both series showed a similar trend with increasing MMA mol fraction in poly(MHMA-co-MMA) increasing oxygen permeability. The results are given for thicker and thinner coating samples in Table 3.10.

Table 3.10

Oxygen barrier of MHMA with various MMA concentrations ranging from 1 mol-% to 25 mol-%.

ID	Thickness (mils)	Coating thickness (mils)	P	D	S	P_o/P	Estimated $P_{coating}$
3M Control	4.2 ± 0.1	-	0.160	2.1	0.089	1.0X	-
MHMA	4.7 ± 0.1	0.5 ± 0.2	0.091	1.9	0.054	1.8X	0.0197
MHMA/MMA 1%[a]	4.6 ± 0.1	0.4 ± 0.2	0.115	1.7	0.078	1.4X	0.0291
MHMA/MMA 5%[a]	4.5 ± 0.1	0.3 ± 0.2	0.120	1.6	0.086	1.3X	0.0267
MHMA/MMA 5%[b]	4.8 ± 0.1	0.6 ± 0.2	0.085	1.6	0.063	1.9X	0.0199
MHMA/MMA10%[c]	4.6 ± 0.1	0.4 ± 0.2	0.116	1.5	0.089	1.4X	0.0298
MHMA/MMA10%[t]	5.0 ± 0.2	0.8 ± 0.3	0.079	1.6	0.057	2.0X	0.0216
MHMA/MMA15%[c]	4.8 ± 0.1	0.6 ± 0.2	0.124	1.7	0.085	1.3X	0.0481
MHMA/MMA25%[c]	4.7 ± 0.1	0.5 ± 0.2	0.127	1.7	0.084	1.3X	0.0465
MHMA/MMA25%[t]	5.1 ± 0.1	0.9 ± 0.2	0.094	1.8	0.059	1.7X	0.0321

[a] rod number 6
[b] rod number 10
P – cc(STP) cm m^{-2} atm^{-1} day^{-1}; D – x10^{-13} m^2 sec^{-1}; S – cc(STP) cm^{-3} atm^{-1}

For a better comparison, estimated coating permeability for each sample were calculated using the following equation[3]:

Equation 3.1

$$\frac{h}{P} = \frac{h_c}{P_c} + \frac{h_s}{P_s}$$

where h, h_c, and h_s represent the coated film, coating, and substrate thickness, respectively. P is apparent oxygen permeability of coated film, and P_c and P_s are the oxygen permeabilities of the coating and substrate, respectively. Estimated P_c data are given in Table 10 in the last column. Poly(MHMA-co-MMA) coatings with low MMA concentration showed comparable oxygen barrier, although, once the MMA concentration exceeded 10 mol-%, a further decrease in barrier performance was observed.

Hardness of the coatings. The hardness of MHMA and MMA coatings were measured using the pencil hardness test. The value for all coatings was determined to be 6H. The coatings were homogenous and transparent. For comparison, the Persoz hardness test was also used. The basic principle of this test is that the amplitude of the pendulum's oscillation will decrease more quickly when supported on a softer surface. The results of pencil hardness test are in agreement with pendulum hardness, and there was no significant change of hardness for copolymer films up to 25 mol-% MMA. All films gave almost the same result, ranging from 71 to 77 sec.

Copolymerization with MF and DF

Recently a new monomer and a crosslinking agent were synthesized in our research group. The synthesis routes and structures are given in Figure 3.10. Michael addition reaction of equimolar amounts of AHM and EA gave 3-(*N*-propionate ethylene glycol amino)-2-hydroxypropyl methacrylate (MF), while two equivalents of AHM gave a difunctional crosslinking agent 3-(*N,N*-bis(propionate) ethylene glycol amino)-2-hydroxypropyl methacrylate (DF).

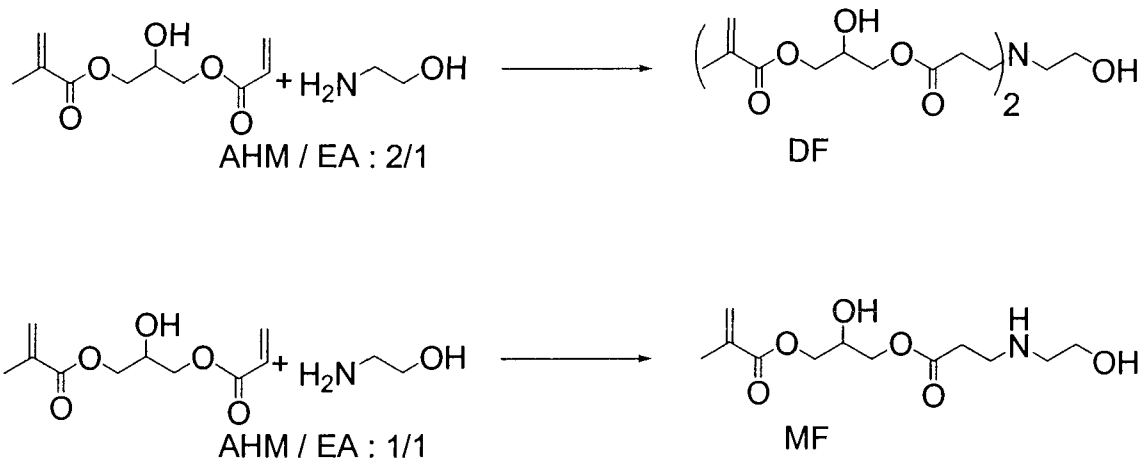

Figure 3.10. The synthesis routes for DF and MF monomers.

To investigate the effect these mono- and difunctional monomers had on rates and conversions of MHMA photopolymerizations, photo-DSC experiments were conducted for two different mol-ratios of each of these two monomers with MHMA. MHMA was mixed with either 5 or 10 mol-% of DF or MF momomers plus 1 mol-% photoinititor (Irgacure 819). No significant change was observed with either type of monomer; however, the peak maximum shifted to the right with MF monomer for both concentrations. The rate quickly decreased for MHMA/DF systems due to faster gelation. The conversions were high for both monomers at both concentrations. However, MHMA/DF systems showed slightly lower conversion compared to MHMA/MF solution systems. This might be due to rapid gelation and network formation leading to trapped double bonds and residual monomers in this network that limited the overall conversions.

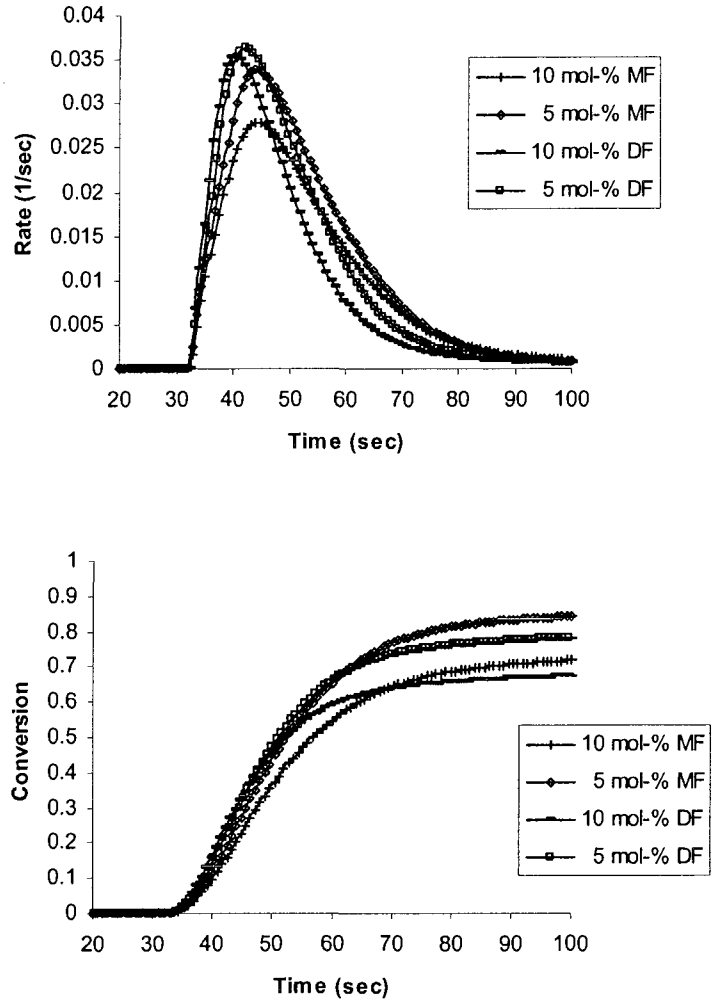

Figure 3.11. Rate versus time plots for MHMA with MF and DF using 1 mol-% Irgacure 819® at 30 °C.

A series of coated PET samples were prepared based on reaction between MF and DF with MHMA/MMA (50/50) mixture. The mol ratios of MF and DF for each series ranged from 1 to 10. These combinations gave excellent barrier improvement (Table 3.11). The coatings were drawn-down by number 6 rods and showed oxygen permeability reduced 1.4-2.5 times that of uncoated substrate. Estimated $P_{coating}$ of poly(MHMA-co-MMA) with 10 mol-% MF were

calculated to be 0.0139. This marked improved of oxygen barrier is presumably due to increasing hydroxyl group content capable of hydrogen bonding.

Table 3.11

Oxygen barrier of poly(MHMA-co-MMA) with varied concentrations of MF and DF.

ID	Thickness (mils)	Coating thickness (mils)	P	D	S	P_o/P	Estimated $P_{coating}$
3M Control	4.2 ± 0.1	-	0.160	2.1	0.089	1.0X	-
1 mol-% DF+ MHMA:MMA(1:1)	4.9 ± 0.1	0.7±0.2	0.092	1.8	0.060	1.7X	0.0259
5 mol-% DF+ MHMA:MMA(1:1)	4.8 ± 0.1	0.6±0.2	0.094	2.0	0.055	1.7X	0.0242
10 mol-% DF+ MHMA:MMA(1:1)	4.9 ± 0.1	0.7±0.2	0.087	7.8	0.056	1.8X	0.0233
1 mol-% MF+ MHMA:MMA(1:1)	4.7 ± 0.1	0.5±0.2	0.117	2.1	0.064	1.4X	0.0359
5 mol-% MF+ MHMA:MMA(1:1)	4.6 ± 0.1	0.4±0.2	0.114	2.0	0.065	1.4X	0.0284
10 mol-% MF+ MHMA:MMA(1:1)	4.9 ± 0.2	0.7±0.3	0.064	1.3	0.056	2.5X	0.0139

P – cc(STP) cm m^{-2} atm^{-1} day^{-1}; D – x10^{-13} m^2 sec^{-1}; S – cc(STP) cm^{-3} atm^{-1}

Figure 3.12 shows the DSC thermograms of MHMA/MMA (50/50) polymers with various mol-% of either DF or MF monomers. The samples were dried at 110 °C before DSC runs and were run under nitrogen with a heating rate of 10 °C/min. The T_g values, mol and weight percent of monomers are given in Table 3.12. The T_g values were higher for copolymers with MF compared to those of the copolymers with DF. These results were in accordance with the photodsc results where the conversions with MF were higher than those with DF. The trapped double bonds and residual monomers in DF systems might act as a plasticizer for this polymer network, leading to lower T_g. Another indication

of plasticizing effect of the DF monomers was the wide T_g transitions, especially with 5 and 10 mol-% DF systems. Flexibility of these momomers as well as the trapped double bonds, may be the reason for lower T_g.

TGA was used to evaluate the thermal stability of these polymers under nitrogen with a heating rate of 10 °C/min. Figure 3.13 shows TGA thermograms of copolymers with 10 mol-% DF or MF. Char residue for these systems was about 7%. The copolymers showed slight increases in thermal stability probably due to higher crosslinking density.

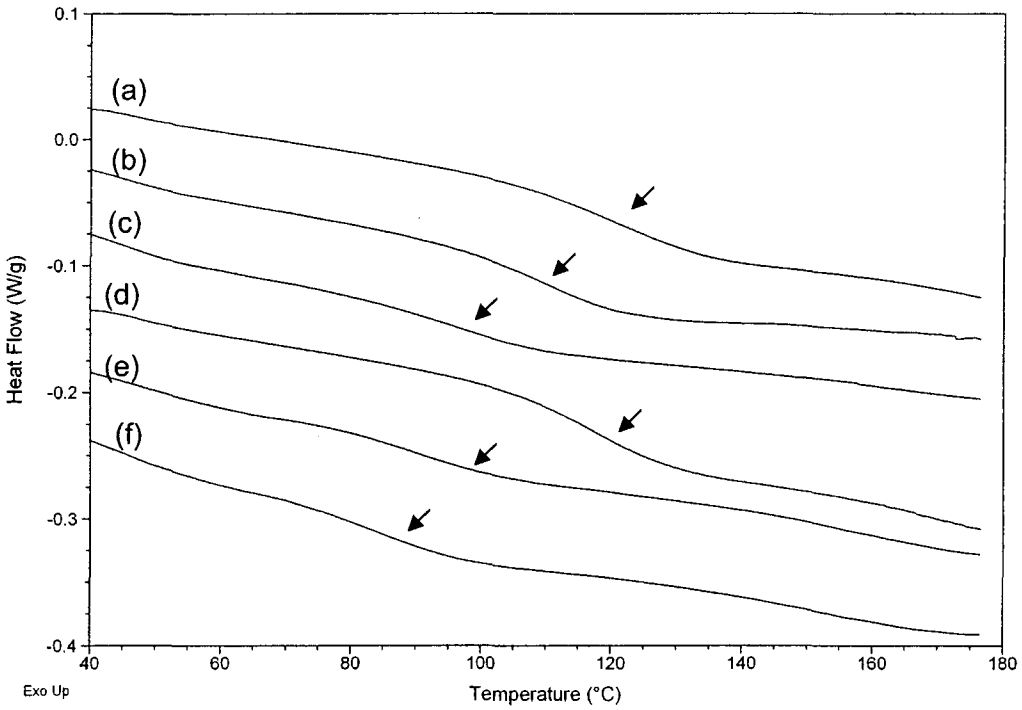

Figure 3.12. DSC thermograms for poly(MHMA-co-MMA) (50/50) with a)1 mol-% MF, b) 5 mol-% MF, c) 10 mol-% MF, d) 1 mol-% DF, e) 5 mol-% DF, and f) 10 mol-% DF.

Table 3.12

T_g values for copolymers with MF and DF

MHMA/MMA (50/50)	mol-%	wt-%	T_g
MF	1	2.5	120
MF	5	13	110
MF	10	25	95
DF	1	4	117
DF	5	22	88
DF	10	45	81

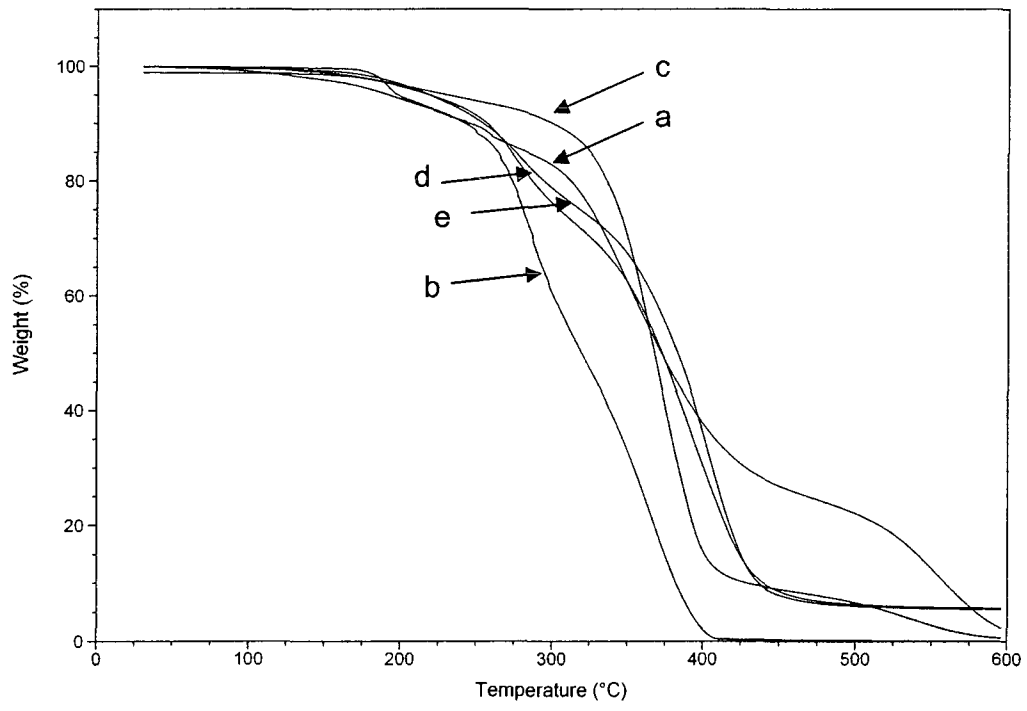

Figure 3.13. TGA for homo- and copolymers of a) poly(MHMA), b) poly(MMA), c) poly(MHMA-co-MMA) (50/50), d) poly(MHMA-co-MMA) (50/50) with 10 mol-% MF, and e) poly(MHMA-co-MMA) (50/50) with 10 mol-% DF.

Preform Dipping Experiments

Currently, barrier coatings for drink bottles are applied after the bottle has been blown, or are formed in situ as sandwiched laminate layers in preforms. These processing approaches have the disadvantage of requiring coating processes at the blow molding sites, or producing the entire bottle (preform and bottle) at the same site. Because preforms are injection molded in only a few locations worldwide, barrier coated bottles would be ideally processed by coating preforms prior to blow molding. This would lower the number of manufacturing sites that require the additional processing step (coating procedure).

It was important to tailor viscosity in the coating formulations because MHMA monomer was not viscous enough by itself for dip coating PET preforms. Attempts to dip and quickly photocure gave little if any barrier coating on the preform. Therefore, viscosity needed to be increased without using additives that could diminish barrier properties. In order to circumvent this problem, MHMA was thermally polymerized, and quenched at low conversion (~ 8%). This resulted in a viscous solution of poly(MHMA) dissolved in MHMA monomer. Photoinitiator was then dissolved in the viscous solution, and preforms dipped and photocured to give transparent coatings on PET preforms.

^{1}H NMR of the thermally polymerized viscous solution showed multiple peaks for the pendent hydroxyls (Figure 3.14 A). After curing, residual monomer was detected by ^{1}H NMR (Figure 3.14 B). Apparently, in the viscous solution there is monomer-monomer and monomer-polymer hydrogen bonding,

and this causes two broad peaks of equal intensity (one the monomer –OH and one an average of the monomer and polymer –OH). The appearance of multiple broad peaks for the hydroxyl proton in UV cured films indicates a variety of hydrogen bonded environments. Cured samples are partially soluble in DMSO-d_6. Highly swollen viscous gels can be observed after cure, which may also contribute to differences in hydrogen bonding environments.

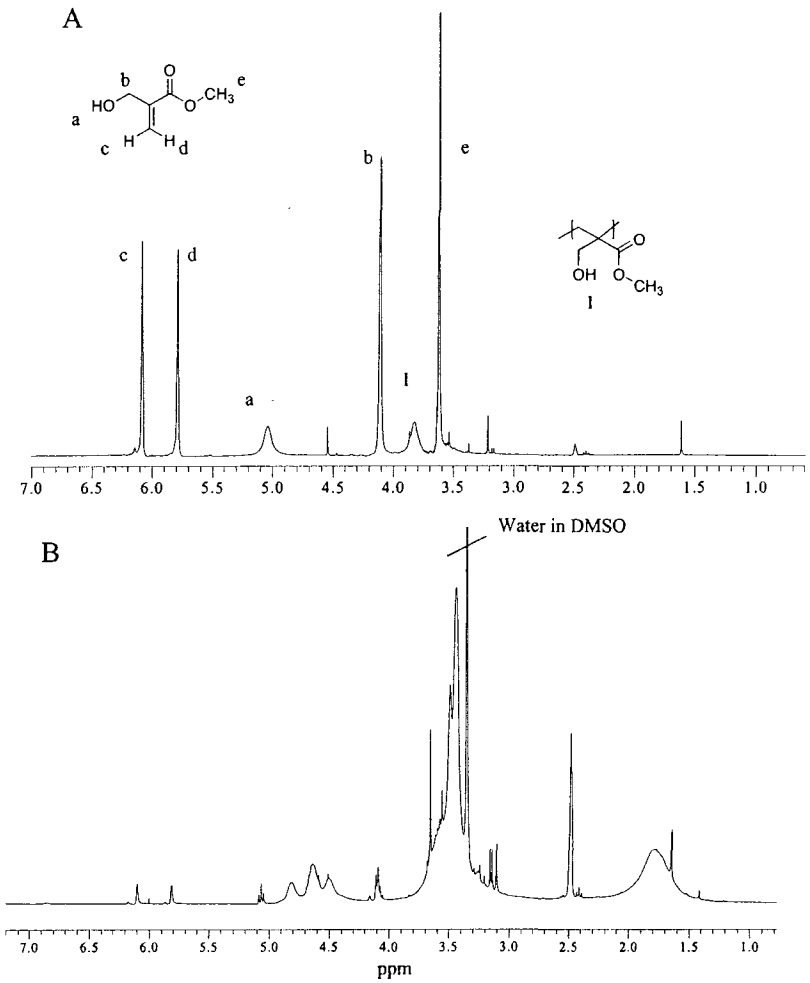

Figure 3.14. ^{1}H NMR spectra in DMSO-d_6 of (A) thermally polymerized viscous solution and (B) UV cured coating removed from a preform.

Table 3.13 gives the oxygen barrier of the blown bottle sidewalls. Entries 1-6 showed little improvement over the uncoated PET sidewall control. However, these coatings are an order of magnitude thinner than previous brush coatings. The viscosity of the dipping solution was increased in order to increase the thickness of preform coatings. Entries 7-10 show some improvement, while entries 11 and 12 exhibited marked improvement over PET control. Dipping solutions for entries 11 and 12 were deoxygenated with nitrogen bubbling prior to dip coating which most likely increased the degree of cure.

Table 3.13

Oxygen barrier results of blown bottle sidewalls

Sample	Average Total Thickness (mils)	Estimated Coating Thickness (mils)	P	D	S	P_0/P
Control	8.9	0	0.178	2.50	0.081	--
1	8.8	0.18	0.155	1.82	0.099	1.1
2	10.7	0.12	0.165	2.15	0.089	1.1
3	10.7	0.20	0.156	2.11	0.086	1.1
4	8.2	0.12	0.160	1.78	0.104	1.1
5	9.6	0.23	0.151	1.86	0.094	1.2
6	9.4	0.13	0.161	2.08	0.090	1.1
Control 2	8.2	0	0.183	2.84	0.075	--
7	12.0	NC	0.122	2.08	0.068	1.5
8	14.7	NC	0.166	2.16	0.062	1.1
9	13.7	NC	0.102	1.86	0.063	1.8
10	13.4	NC	0.100	1.69	0.069	1.8
11	**14.9**	**NC**	**0.064**	**1.5**	**0.048**	**2.9**
12	**14.5**	**NC**	**0.088**	**1.4**	**0.071**	**2.1**

P – cc(STP) cm m^{-2} atm^{-1} day^{-1}; D – x10^{-13} m^2 sec^{-1}; S – cc(STP) cm^{-3} atm^{-1}
NC indicates thickness was not calculated

The results in Table 3.13 demonstrate that a number of variables can influence gas barrier for even a one-component coating. Increasing thickness

increased the barrier slightly, although decreasing the amount of residual monomer made a significant improvement in barrier properties.

Inherent Barrier Properties of UV Cured MHMA

In order to determine the inherent barrier properties of photocured MHMA films, monomer thin films were cured on aluminum foil substrates. The thin aluminum substrate could be peeled from the back of the UV cured films. This gave stand-alone poly(MHMA) films, synthesized following an analogous procedure to PET thin film coatings and preform dip coatings. MHMA stand-alone films showed outstanding barrier to oxygen (P = 0.0071 for 20 mil thick sample). This demonstrates that optimizing curing conditions, coating thickness, and conversion will lead to packaging materials with even lower gas permeabilities.

Conclusions

MHMA is a viable material for use in solvent-free barrier coatings on PET. The hydroxyl group serves as an anchor, or compatibilizing agent, to enhance adhesion to the surface of the polyester. The strong hydrogen bonding interactions in the polymer lead to its high density, high solvent resistance, and high barrier properties. Barrier improvements of nearly four times that of uncoated PET thin films were obtained for both oxygen and carbon dioxide. Although MHMA film has excellent barrier properties under dry conditions, the barrier is very sensitive to humidity. Copolymerization of MHMA with MMA can be utilized to address this problem. Films obtained by reaction of MHMA/MMA (50/50) with 10 mol-% MF gave a barrier improvement 2.5 times that of neat

PET substrate. Coated preforms that were blown into bottles showed nearly a three-fold decrease in oxygen permeability. Recycle process testing suggests that hot caustic solution, such is can be found in commercial recycling facilities, will remove the barrier coating. A unique pre-polymerization approach to increased viscosity without additives proved effective for controlling coating amounts deposited by dip coating.

Acknowledgments

The work presented here reflects collaborations with KoSa, Spartanburg, SC and Case Western Reserve University, Cleveland, OH. Preforms and thin films were coated at the University of Southern Mississippi, bottles were blown at KoSa, and gas barrier was measured at Case Western Reserve University.

The author gratefully acknowledges Dr. David A. Schiraldi, Case Western Reserve University (formerly of KoSa), and Dr. Sanjay Mehta, KoSa, for valuable discussions; Tai Yeon Lee and Dr. Charles Hoyle, University of Southern Mississippi, for real-time FT-IR studies; and Richard Liu, Yushan Hu, and Vamsi Prattipati, along with Dr. Anne Hiltner, and Dr. Eric Baer, for carrying out gas barrier measurements at Case Western Reserve University.

Experimental

Materials. MHMA was purchased from Nippon Shokubai, Co., Toyko, Japan, and passed through a short column of dry silica gel to remove inhibitor. Photoinitiators, 2,2-dimethoxy-1,2-diphenylethan-1-one (Irgacure 651®) and phenyl bis(trimethylbenzoyl)phosphine oxide (Irgacure 819®) were donated by Ciba Specialty Chemicals, Basel, Switzerland. All other chemicals were

purchased from Aldrich Chemical Company and used as received. Biaxially oriented PET thin films were purchased from 3M, Minneapolis, MN, and used as received. Amorphous PET preforms were provided by KoSa, Spartanburg, SC.

Synthesis of 3-(N-propionate ethylene glycol amino)-2-hydroxypropyl methacrylate (MF). MF was synthesized by Michael addition reaction of ethanol amine (EA) with one equivalent of 3-(acryloyloxy)-2-hydroxypropyl methacrylate (AHM). AHM (10 g, 46 mmol) and EA (2.9 g, 46 mmol) were charged into a 50 ml round bottom flask in an ice bath. Since the reaction was extremely exothermic, the mixture was stirred in the ice bath for couple hours to prevent formation of bis-adduct. The mixture was stirred overnight which gave the final product as viscous clear liquid. The yield was quantitative based on the NMR analysis.

Synthesis of 3-(N,N-bis(propionate) ethylene glycol amino)-2-hydroxypropyl methacrylate (DF). DF was synthesized by Michael addition reaction of ethanol amine (EA) with two equivalents of 3-(acryloyloxy)-2-hydroxypropyl methacrylate (AHM). AHM (21 g, 98 mmol) and EA (3 g, 49 mmol) mixture were charged into a 50 ml round bottom flask at ambient temperature and stirred overnight. The temperature was increased to 45 oC and the reaction was carried out at this temperature for another 2 h. The final product was very viscous clear liquid. The yield was quantitative based on the NMR analysis.

Instrumentation. Fourier transform infrared spectra were obtained with a Mattson 5000 spectrometer. Thermal analyses were performed using a TA

instrument 2960 controlled by a thermal analyst 2100, under nitrogen with a heating rate of 10 °C/min. Differential scanning calorimetry (DSC) experiments were performed on a TA Instruments 2920 using pierced-lid crimped aluminum pans with heating rates of 10.0 °C/min. Routine solution ^{1}H nuclear magnetic resonance (NMR) was performed on a Varian *Mercury*^{PLUS} 300 MHz spectrometer.

PET film coatings. PET films were coated using the following procedure. Methyl (α-hydroxymethyl)acrylate (MHMA) was passed through a short column of dry silica gel to remove inhibitor. One mol-% 2,2-dimethoxy-1,2-diphenylethan-1-one (Irgacure 651®) was dissolved in the monomer. The resulting solution was spread using a small paint brush on discs of 3M transparency film (biaxially-oriented PET) and placed in a polypropylene chamber. The chamber was purged with nitrogen for 10 minutes and remained under nitrogen throughout the cure process. The samples were then irradiated with an external UV light source (long wave length UV/hand held Blak-Ray model B). Finished samples were tested at Case Western Reserve University for oxygen and carbon dioxide barrier using Mocon oxygen and carbon dioxide analyzers.

Recycle experiments. Samples of PET film coated with MHMA, and photocured (as above) were exposed for 20 minutes to a bath of 2 wt-% caustic soda (NaOH) held at 80° C. The coating was completely removed by this treatment.

Preform dipping experiments. A general procedure for preform dipping follows. MHMA was passed through a short column of dry silica gel to remove inhibitor. 2,2'-Azobisisobutyronitrile (AIBN) was recently recrystallized from methanol. A 50 mL Erylenmeyer flask equipped with a magnetic stir-bar was charged with MHMA (42.2 g, 0.37 mol), 0.5 mol-% AIBN (0.299 g, 0.0018 mol) and sealed with a rubber septa. Nitrogen was bubbled through the monomer-initiator solution for 10 min in order to remove dissolved oxygen. The flask was then placed in a preheated oil bath at 35 °C for 94 min. A substantial increase in viscosity was observed. The viscous solution was immediately exposed to oxygen and 34.4 grams was poured into a flask cooled to 0 °C in order to quench the thermal polymerization. Then, 1 mol-% Irgacure 651® (0.76 g, 0.00296 mol) was dissolved in the viscous solution. The solution was allowed to stand for 24 h at 0 °C. Nitrogen was bubbled through the viscous solution for 10 min. Preforms were weighed and placed in a nitrogen-purged dry-box equipped with the UV lamp source. Each preform was dipped into the solution and irradiated for 9 minutes, rotating a quarter turn every minute. Preforms were removed from the drybox and reweighed to determine the weight gained due to coating.

Alternate procedure. The previous procedure was modified in order to reduce bubbles trapped in the viscous solution prior to dipping. While sealed under nitrogen, the thermal polymerization was quenched by cooling rapidly to 0 °C for 10 minutes. The reaction flask was then introduced into a nitrogen purged dry-box. In the dry-box, Irgacure 651® was carefully dissolved in the

viscous solution with gentle agitation. Approximately 33 mL was transferred to a flask suitable for preform dipping. Preforms were immediately dipped and cured.

Photopolymerizations of various acrylates, MHMA, and MHMA viscous solution. For a typical photopolymerization,1 mol-% Irgacure 819® was dissolved in MHMA. Approximately 2.0 mg of the mixture was placed in a bottom-impressed aluminum DSC pan (approximately 200 μm thickness). A TA Instruments 930 differential photocalorimiter (DPC) was used to measure heats of reaction. The chamber of the DPC was allowed to purge with nitrogen for 5 min before irradiation, and a nitrogen blanket was maintained throughout the reaction. The sample was equilibrated for 30 sec at the desired reaction temperature and irradiated for 5 min, with the light shutter opening set for 30 sec after the beginning of data acquisition. The enthalpy value ΔH_{theor} = 13.1 kcal/mol was used as the theoretical heat evolved for methacrylate double bonds.[27]

Instantaneous rates of polymerization were calculated according to Equation 3.2,[28, 29] where ΔH_{pol} is the heat released per mole of double bonds reacted, *Q/s* is the heat flow per second, *M* the molar mass of the monomer, *n* the number of double bonds per monomer molecule, and *mass* being the mass of monomer in the sample.

Equation 3.2 $\text{Rate} = (Q/s)M/n\Delta H_{pol}\text{mass}$

Real-time FTIR. The polymerisation kinetics of MHMA and MMA were studied by real-time FTIR and the detailed description of the instrument was

given by T.Y. Lee, et al.,[30] A modified Bruker 88 spectrometer which allows light to impinge on a horizontal sample using a fiber-optic cable was used to obtain infrared spectra of samples. The samples were placed between two sodium chloride discs whose edges were sealed by using vacuum grease to prevent both oxygen diffusion into the samples and evaporation of MMA. A 200 W high pressure mercury Xenon lamp (ScienceTech Co.) served as the light source to induce free radical polymerization. Disappearance of methacrylate double bond at 1636 $cm^{-1}$and 750 cm^{-1} was monitored under continuous UV irradiation with a scanning rate of 2 scans/sec. Conversion was calculated according to Equation 3.3, where A_o is the absorbance at t = 0 and At is the absorbance at time = t.

Equation 3.3 $$\% \text{ Conversion} = [(A_o - A_t)/A_o] \times 100$$

Pencil and persoz hardness test. Hardness of coatings were measured according to ASTM designation D3363[31] using a range of pencils from B to 9H. The pencil lead was flattened before using. The pencil was held at a 45° angle from the coating surface and pushed forward on the substrate. The first pencil which could scratch the coating gave the measured pencil hardness. A BYK Gardner pendulum hardness tester was used to determine Persoz pendulum hardness of the coatings. The measurements were conducted at room temperature on polymer coated PET substrates, and repeated at least five times.

References

1 Bissot, T. C. Perfromance of High-Barrier Resins with Platelet-Type Fillers. In Barrier Polymers and Structures; Koros, W. J., Eds.; American Chemical Society: Washington, D. C., **1990**, Chapter 11, pp 225-238.

2 Sekelik, D. J.; Stepanov, E. V.; Nazarenko, S.; Schiraldi, D.; Hiltner, A.; Baer, E. Oxygen Barrier Properties of Crystallized and Talc-Filled Poly(ethylene terephthalate). *J. Polym. Sci.: Part B: Polym. Phys.*, **1999**, 37, 847-857.

3 Leterrier, Y. Durability of Nanosized Oxygen-Barrier Coatings on Polymers. *Prog. Mater. Sci.*, **2003**, 48, 1-55.

4 Agres, L.; Ségui, R.; Raynaud, P. Oxygen Barrier Efficiency of Hexamethyldisiloxane / Oxygen Plasma-Deposited Coating. *J. Appl. Polym. Sci.,* **1996**, 61, 2015-2022.

5 Volpe, R. A.; Lucas, P. C. Hybrid Sol-Gel Barrier Coatings. United States Patent, US 5776565, **1998**.

6 Weinkaup, D. H.; Paul, D. R. Effects of Structural Order on Barrier Properties. In Barrier Polymers and Structures; Koros, W. J., Eds.; American Chemical Society: Washington, D. C., **1990**, Chapter 3, pp 60-91.

7 Deak, G. I. Solution Coating Process for Packaging Film. United States Patent, US 5328724, **1994**.

8 Hata, N.; Osaku, T. Preparation of Storage-Stable Aqueous Ethylene-Vinyl Alcohol Copolymer Dispersions for Gas-Barrier Coatings. Japanese Patent, JP 2001270946, **2001**.

9 Ito, K.; Komiya, Y. Gas-Barrier Containers Having Vinyl Alcohol Polymer-Based Coatings. Japanese Patent, JP 2001270510, **2001**.

10 Labuschagne, Philip W. ; Germishuizen, W. Andre; Verryn, Sabine M. C. ; Moolman, F. S. Improved Oxygen Barrier Performance of Poly(vinyl alcohol) Films through Hydrogen Bond Complex with Poly(methyl vinyl ether-co-maleic acid). *Eur. Polym. J.*, **2008**, 44, 2146-2152.

11 Tsai, B. C.; Wachtel, J. A. Barrier Properties of Ethylene-Vinyl Alcohol Copolymer in Retorted Plastic Food Containers. In Barrier Polymers and Structures; Koros, W. J., Eds.; American Chemical Society: Washington, D. C., **1990**, Chapter 9, pp 192-202.

12 Tiemblo, P.; Fernández-Arizpe, A.; Guzmán, J. Transport of Gases and Vapors in Methacrylic Copolymers of Varying Side Chain Length. *Polymer*, **2003**, 44, 635-641.

13 Jahromi, S.; Moosheimer, U. Oxygen Barrier Coatings Based on Supramolecular Assembly of Melamine. *Macromolecules*, **2000**, 33, 7582-7587.

14 Lange, J.; Stenroos, E.; Johansson, M.; Malmström, E. Barrier Coatings for Flexible Packaging Based on Hyperbranched Resins. *Polymer*, **2001**, 42, 7403-7410.

15 Hedenqvist, M. S.; Yousefi, H.; Malmström, E.; Johansson, M.; Hult, A.; Gedde, U. W.; Trollsås, M.; Hedrick, J. L. Transport Properties of Hyperbranched and Dendrimer-Like Star Polymers. *Polymer,* **2000**, 41, 1827-1840.

16 Carlblom, L. H.; Seiner, J. A.; Niederst, K. W. Multilayer Packaging Material for Oxygen Sensitive Food and Beverage. United States Patent, US 5728439, **1998**.

17 Simic, V.; Boileau, S.; Bouteiller, L.; Gallez, L.; Merlin, P. Gas Barrier and Adhesion of Interpenetrating Polymer Networks Based on Poly(diurethane bismethacrylate) and Different Epoxy-Amine Networks. *Eur. Polym. J.*, **2002**, 38, 2449-2458.

18 Brennan, D. J.; White, J. E.; Haag, A. P.; Kram, S. L.; Mang, M. N.; Pikuin, A.; Brown, C. N. Poly(hydroxyamide ethers): New High-Barrier Thermoplastics. *Macromolecules*, **1996**, 29, 11, 3707-3716.

19 Brennan, D. J.; Silvis, H. C.; White, J. E.; Brown, C. N. Amorphous Phenoxy Thermoplastics with an Extraordinary Barrier to Oxygen. *Macromolecules*, **1995**, 6694-6696.

20 Brennan, D. J.; Haag, A. P.; White, J. E.; Brown, C. N. High-Barrier Poly(hydroxyamide ethers): Effect of Polymer Structure on Oxygen Transmission Rates. 2. *Macromolecules*, **1998**, 31, 2622-2630.

21 Brennan, D. J.; White, J. E.; Brown, C. N. High-Barrier Poly(hydroxyamide ethers): Effect of Polymer Structure on Oxygen Transmission Rates. 3. *Macromolecules*, **1998**, 31, 8281-8290.

22 Nippon Shokubai, Product Literature.

23 Scherzer, T. Depth Profiling of the Conversion During the Photopolymerization of Acrylates Using Real-time FTIR-ATR Spectroscopy. *Vibrational Spectroscopy*, **2002**, 29, 139.

24 Jansen, Johan F. G. A.; Dias,Aylvin A.; Dorschu, Marko; Coussens, Betty;

Fast Monomers: Factors Affecting the Inherent Reactivity of Acrylate Monomers in Photoinitiated Acrylate Polymerization. *Macromolecules*, **2003**, 36, 3861-3873.

25 Crivello, J.V.; Dietliker,K. Volume III: Photoinitiators for Free Radical Cationic& Anionic Photopolymerisation 2nd Edition, J. Wiley & Sons Ltd, Chichester 128-130.

26 Dietliker,K. A Compilation Photoinitiators Commercially Available for UV Today, Sita Technology Limited, Edinburg London UK 96-99.

27 Anseth, K. S.; Wang, C. M.; Bowman C. N. Kinetic Evidence of Reaction Diffusion during the Polymerization of Multi(meth)acrylate Monomers. *Macromolecules,* **1994**, 27, 650-655.

28 Horie, K.; Otagawa, A.; Muraoka, M.; Mita, I. Calorimetric Investigation of Polymerization Reactions. V. Crosslinked Copolymerization of Methyl Methacrylate with Ethylene Dimethacrylate. *J. Polym. Sci.,* **1975**, 13, 445-454.

29 Miyazaki, K.; Horibe, T. Polymerization of Multifunctional Methacrylates and Acrylates. *J. Biomed. Mater. Res.,* **1988**, 22, 1011-1022.

30 Lee, T. Y.; Roper, T. M.; Jonsson, E. S.; Kudyakov, I.; Viswanathan, K.; Nason, C.; Guymon, C. A.; Hoyle, C. E. The Kinetics of Vinyl Acrylate Photopolymerization. *Polymer*, **2003**, 44, 2859-2865.

31 Koleske, J. V. Paint and Coating Testing Manual, 14th Edition of the Gardner-Sward Handbook; Eds.; ASTM Manual Series: MNL 17, ASTM PCN 28-017095-14; ASTM: Philadelphia, PA, **1995**.

CHAPTER IV

SYNTHESIS AND CHRACTERIZATION OF NYLON 18 18 AND NYLON 18 ADAMANTANE

Abstract

Nylon 18 18 and nylon 18 ADA (1,3-adamantanedicarboxylic acid) have been synthesized via melt polycondensation and characterized by thermal and spectroscopic techniques. Good film forming behavior combined with film toughness and flexibility indicate reasonable molecular weights for both. The higher aliphatic content of nylon 18 18 leads to increased resistance to common organic solvents over commercial nylons. Crystallization of nylon 18 18 combines hydrogen bonding of the amide units with a more significant contribution from van der Waals forces than possible for lower aliphatic content nylons due to the greater aliphatic chain lengths. Solid state ^{15}N CP/MAS NMR indicates a mostly amorphous polymer, with crystalline regions comprised of the thermodynamically stable α-form generally adopted by even-even nylons. Nylon 18 ADA as-produced is completely amorphous as determined by DSC. However, solution cast samples of nylon 18 ADA show some ordered structures that can grows into more stable crystals with annealing. These crystals, once melted, do not recrystallize on cooling possibly due to chain rearrangement inhibited by bulky adamantyl groups.

Introduction

Nylons with low amide density and high methylene content are desirable due to improved properties (such as radiation shielding) and applications in thermoplastic processing. These polymers act as "functionalized polyethylene," combining the hydrophobic character of polyethylene with the thermal properties afforded by the hydrogen bonding amide units of polyamides. While there have been previous reports of high aliphatic content AB nylon systems,[1,2] there are only a few reports of high aliphatic content AA-BB nylons with regularly placed amide units, such as nylons *X* 16,[3] nylons *X* 18,[4,5] nylons *X* 20,[6] nylons *X* 22,[7] and nylons *X* 34.[8] Of these, the highest aliphatic content is for nylon 12 34,[8,9] which contains 44 methylene units per two nylon repeat units. While this is an extremely high aliphatic content overall, there is a marked imbalance in the spacing of the amide groups, which are 12 and 32 methylene units apart, a factor that may impact solid phase order and packing.

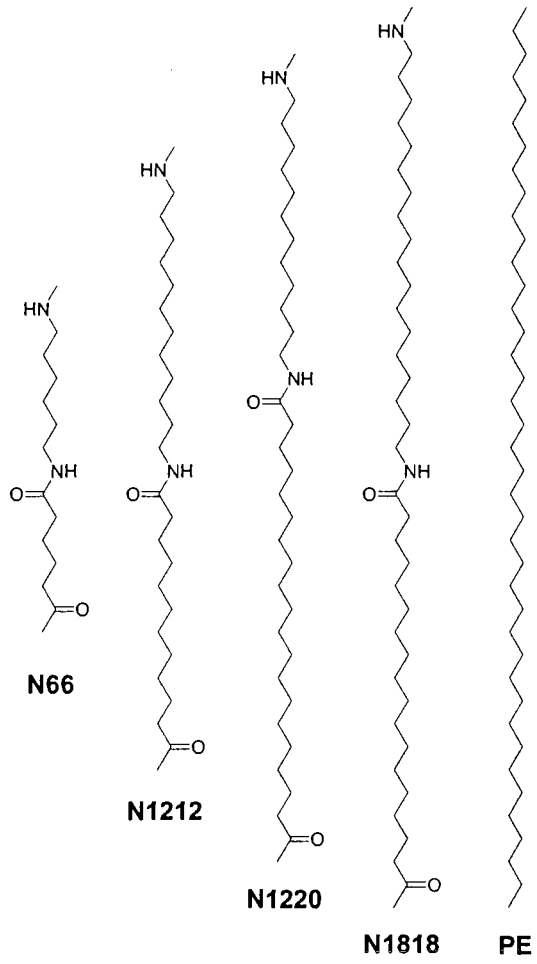

Figure 4.1. Repeat units of nylons with progressively higher aliphatic content. As amide density decreases and the spacing becomes more uniform, the polymer chain more resembles a functionalized polyethylene.

To further evaluate effects of high aliphatic content on nylon properties, there is need for a system with evenly spaced polymethylene segments between amide units. Figure 4.1 represents the progression to higher aliphatic content with regular spacing of the amide units, ranging from nylon 6 6 to nylon 18 18. The highest content reported that retains similar length aliphatic segments are nylons 10 14,[10] 12 12,[11] and 13 13.[12,13] The majority of cases reported in the literature incorporate 1,12-dodecanediamine (as the only commercially available

high aliphatic diamine), combined with higher methylene content in the diacid moiety.

Adamantane, a highly symmetrical tricyclic hydrocarbon, has been incorporated into many polymer structures as a pendant group or directly into the polymer main chain. The incorporation of the adamantane as a pendant group increases solubility, decreases crystallinity, enhances the glass transition temperature, and improves thermal stability.[14,15,16] There have also been a number of reports on incorporation of the adamantane moiety in aromatic polyamides and polyimides.[17,18]

We report here the synthesis and evaluation of nylon 18 18, which contains amide units consistently 16 and 18 methylene units apart. This is the highest degree of spacing reported to date for a regular AA-BB nylon. In addition, we describe a new type of amorphous nylon based on an adamantane segment in the repeat unit. This moiety possesses all sp^3 carbons, a relatively high hydrogen-to-carbon ratio, and a rigid structure that prevents symmetrical packing of the amide groups attached to the adamantane core.

Experimental

Materials. All reagents were used as received. The monomers 1,18-octadecanediamine and 1,18-octadecanedioic acid were supplied by Cognis Corporation. 1,3-Adamantanedicarboxylic acid (ADA) was purchased from Aldrich. All solvents were purchased from Acros, with the exception of 1,1,1,3,3,3-hexafluoroisopropanol (HFIP), which was purchased from Regis Technology. All chemicals were used without further purification.

Synthesis of nylon 18 18. Nylon 18 18 was produced by a melt polycondensation technique. The monomers were mixed together in equalmolar amounts and heated under nitrogen purge using a silicon oil bath at 170-180 °C for 4 hours, then 220-230 °C for 4 hours. At this point, no bubbling was visible in the melt and a vacuum was applied for 0.5 hours. The sample was cooled under vacuum. The resulting material was white in color and translucent.

Synthesis of nylon 18 ADA. Nylon 18 ADA was synthesized in a similar melt polycondensation reaction except the total reaction time was 22-24 hours. This polymer was obtained as a transparent, yellow-brown plug that was very tough and hard to cut or grind.

Characterization. Dilute solution viscometry (DSV) was performed using a Cannon-Ubbelohde 1C C628 viscometer with dichloroacetic acid as the solvent. Efflux times were recorded at a temperature of 35±0.2 °C.

Transmission Infrared measurements were carried out on a Mattson Galaxy Series FTIR 5000 using solution cast films and 256 transients. ATR measurements were made using a Spectra-Tech HATR cell with a ZnSe 45° crystal and melt pressed films in a Nicolet Protégé FTIR.

Thermogravimetric analysis (TGA) was performed on a TA Instruments Q500. The temperature was ramped at a heating rate of 10 °C/min under nitrogen. The temperature at which a 5% loss in weight occurred was recorded as the decomposition onset temperature. In addition, the peak maximum of the derivative of the weight loss curve was recorded as the peak decomposition temperature.

Differential scanning calorimetry (DSC) experiments were performed on a TA Instruments 2920 using pierced-lid crimped aluminum pans. Non-isothermal DSC experiments were recorded at a ramp rate of 10.0 °C/min. Each sequence of scans was recorded twice for reproducibility. The melting temperature was taken as the endotherm maximum, and the crystallization temperature was taken as the exotherm maximum. Annealing was conducted in the DSC. For a typical DSC analyses, small pieces (~4 mg) were cut and placed in aluminum DSC pans. The samples were heated at 10 °C/min to a given temperature and annealed at that temperature for 2 h. They were cooled down to -10 °C with a cooling rate of 10 °C/min, and heated again with a heating rate of 10 °C/min.

Tensile testing of nylons was performed on a MTS Alliance RT/10 according to the standard protocol of ASTM 882. DMA measurements were obtained on a Seiko Instruments SDM 5600 series dynamic mechanical spectrometer (DMS 210).

Wide angle X-ray diffraction (WAXD) measurements were obtained with a Rigaku Ultima III diffractometer operated at 40 kV and 44 mA and run with a scan speed of 0.2° per minute from 2 to 45°. Samples for XRD analysis were placed in a sealed aluminum holder and annealed using a conventional oven.

Routine solution ^{13}C nuclear magnetic resonance (NMR) spectroscopy was performed on a Varian *Mercury*^{PLUS} 300 MHz spectrometer operating at 75.5 MHz for carbon, using a pulse width of 7.8 μsec, acquisition time of 1.8 msec, and no relaxation delay. The sample was prepared in a mixture of 1,1,1,3,3,3-

hexafluoroisopropanol and $CDCl_3$, and referenced to the center peak of the deuterated solvent triplet at δ = 77.23 ppm.

CP/MAS solid state ^{15}N NMR experiments were performed on a Bruker MSL 200 MHz spectrometer operating at 20.28 MHz with a 7.5 mm *Chemagnetics* double resonance probe, with a sample spinning speed of 2.2 kHz. Cross-polarization was conducted using a 3.5 μsec ^{1}H 90° pulse followed by a mixing time of 2 msec. An acquisition time of 42 msec using high powered decoupling was used, with a relaxation delay of 3 sec between scans. Peaks were referenced to the amide nitrogen of ^{15}N labeled glycine at δ=0.0 ppm as an external standard.

Results and Discussion

Nylon 18 18

Nylon 18 18 exhibits similar but enhanced solvent resistance to typical organic solvents seen in the series of nylons *X* 18; i.e., it was insoluble in chloroform, 2,2,2-trifluoroethanol (TFE), or mixtures of TFE with chloroform.[19,20] It was also insoluble in carbon tetrachloride. For the nylon *X* 18 series, *m*-cresol was found to dissolve all but nylons 2 18 and 12 18; it also does not dissolve nylon 18 18. In addition, nylon 18 18 is not soluble in HFIP, which is a good solvent for all other nylons *X* 18 examined to date. Thus, trifluoroacetic acid or an 80-20 mixture of HFIP-$CDCl_3$ was used for solution state NMR characterization. Dichloroacetic acid is also a suitable solvent, and was used in viscosimetric characterization. The intrinsic viscosity was determined to be 0.54 dL/g.

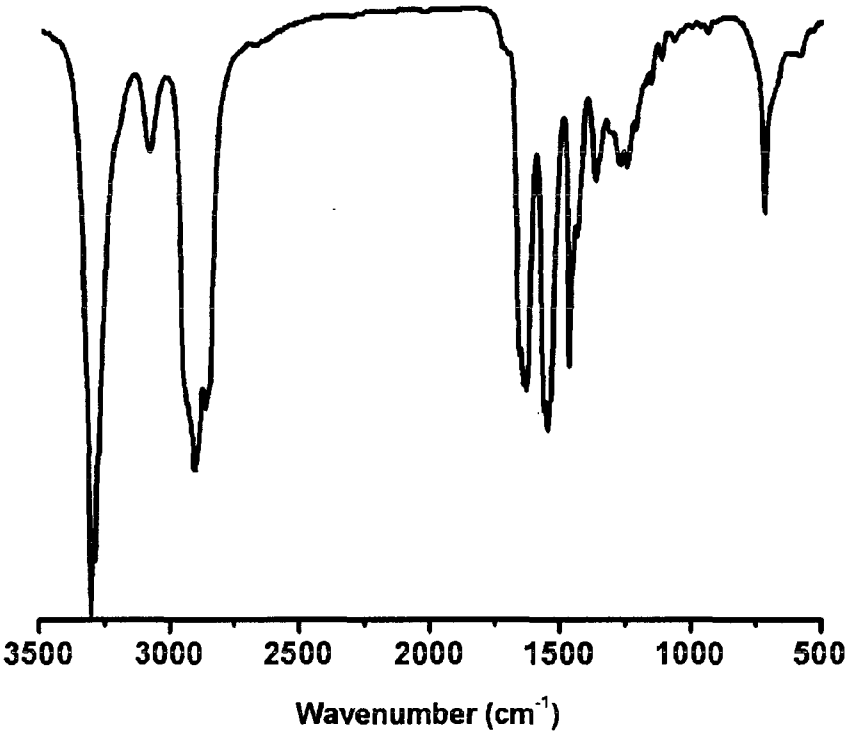

Figure 4.2. FTIR spectrum of nylon 18 18.

Infrared spectra for nylon 18 18 prepared in this study displayed the characteristic peaks of amide groups and methylene groups, as shown in Figure 4.2. The peaks were found at 3324 cm^{-1} (amide A, H-bonded N-H stretching), 3087 cm^{-1} (amide B, overtone of N-H in-plane bending), 2905 cm^{-1} (C-H stretching), 1643 cm^{-1} (amide I, C=O stretch), 1538 cm^{-1} (amide II, C-N stretch and CO-N-H bend), 1273 cm^{-1} (amide III), 943 cm^{-1} (amide IV, C-CO stretch), 721 cm^{-1} (CH_2 rocking), and 591 cm^{-1} (amide VI, C=O out-of-plane bend).

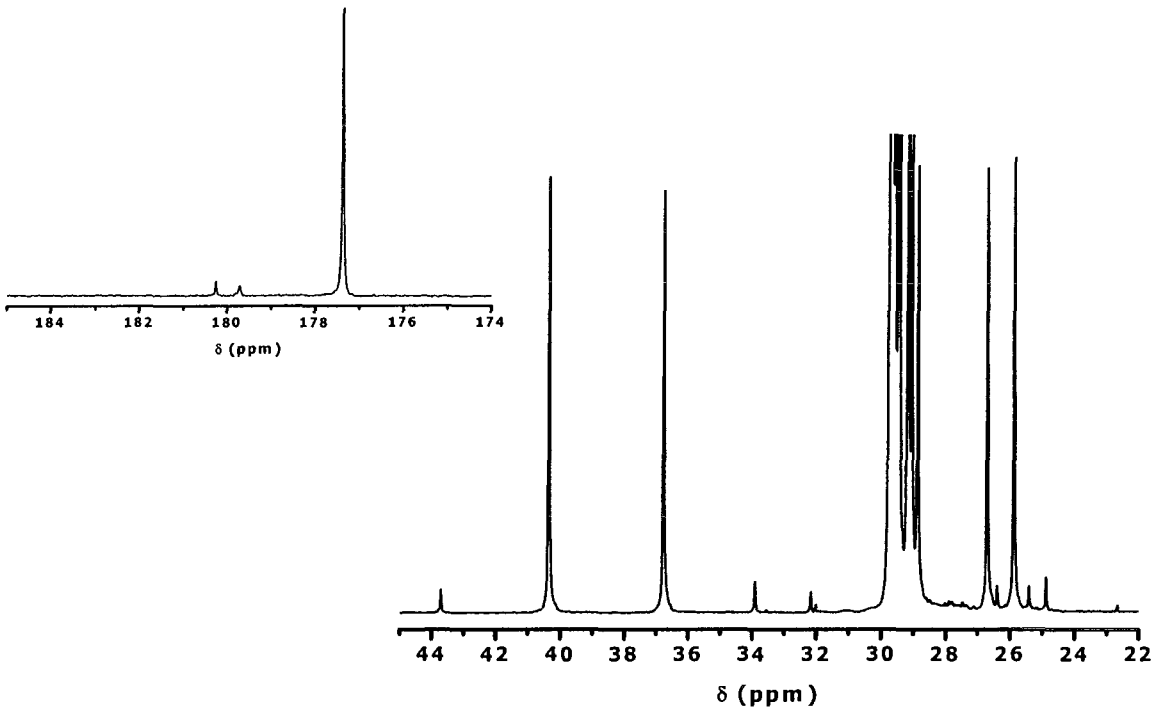

Figure 4.3. ^{13}C solution NMR of the aliphatic and carbonyl (inset) regions of nylon 18 18. Sample was dissolved in a mixture of HFIP:$CDCl_3$.

The solution state ^{13}C NMR spectrum (Figure 4.3) of Nylon 18 18, shows peaks typical of aliphatic nylons, which are summarized in Table 4.1. Previous work in our group[19] has shown the observation of *cis* amide units when the sample is dissolved in a fluorinated alcohol and chloroalkane. It was also shown that the relative population of *cis* amide units (obtained by integration of the *trans* and *cis* carbon peaks α to the amide NH) increases with increasing aliphatic content, from nylon 4 (0.76 %*cis*) to nylon 13 13 (2.70 %*cis*), and this behavior continues to nylon 18 18 (5.18 %*cis*). The 18 carbon diamine contained approximately 1% of the 18 carbon monofunctional amine so that end groups are a combination of carboxylic acid and terminal alkanes, as can be seen by the

small carbonyl carbon peak at δ=180.3 ppm and the terminal methyl group at δ=13.6 ppm (not shown). The peaks associated with amine end groups were not observed, so the tabulated values of end groups include only the acid and alkyl group, with the later denoted by end1, end2, and end3 for the terminal C18 alkane starting from the methyl end group.

Table 4.1. ^{13}C solution NMR chemical shifts for nylon 18 18.

	Nylon 18 18	
	trans	cis
1	40.36	43.77
2	28.88	32.18
3	26.72	---
4	29.19	
5-9	29.46-29.77	---
1'	36.77	33.93
2'	25.88	25.43
3'	29.07	---
4'	29.19	
5'-8'	29.46-29.77	---
9'	177.38	179.73
	end groups	
end1	13.57	---
end2	22.68	---
end3	32.02	---
αCO_2H	33.55	---
βCO_2H	24.90	---
$9'CO_2H$	180.28	---

DSC indicates a T_m of 163 °C and a T_c of 126 °C, taken from the scan obtained at 10 °C/min. Using a procedure based on group additivity values from van Krevelen,[21] the percent crystallinity was calculated from DSC data and theoretical ΔH_f. The equilibrium heat of fusion, ΔH_f, was calculated by adding two amide groups (67.4 J/g) and thirty-four methylene groups (at 270.8 J/g), to

give a combined total of 338.2 J/g. Using a DSC heating rate of 20 °C/min, the experimental enthalpy of fusion after melt crystallization was 68.0 J/g, giving a calculated crystallinity of 20%. This value is lower than for typical commercial polyamides, perhaps owing to conformational and/or librational motion of the polymethylene chains inhibiting crystallization (entropy inhibition).

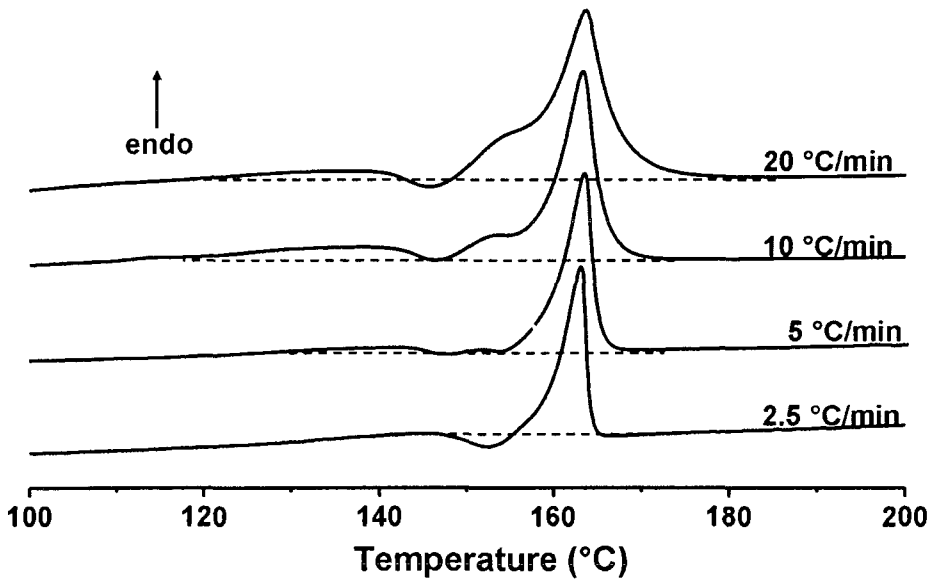

Figure 4.4. Non-isothermal DSC heating traces of nylon 18 18 recorded at different heating rates.

From non-isothermal DSC studies, it can be seen that, as the heating rate increases, a broad melting endotherm develops from 120-140 °C (Figure 4.4), most likely associated with "melting" of aligned polymethylene segments.[22] DSC experiments on polyethylene have shown a similar broadening of the melting endotherm at higher heating rates.[23] This endotherm is not as well-defined at lower heating rates, perhaps because there is sufficient time for reorganization and (re)crystallization as the sample is heated. In addition, as ramp rate

increases, a small crystallization exotherm develops at approximately 148 °C. This behavior is dependent on the cooling rate from above the melt. When the cooling rate increases, the librational mobility of the polymethylene chains precludes high order for the formed crystals, and the recrystallization event reflects a population of less perfect crystallites. Thus, there are three factors leading to a broad population of imperfect crystallites. The first is the random occurrence of gauche configurations in the polymethylene chains. The second is the formation of random switchboard-type lamellae due to the length of the alkane segments involved in the folding process during crystallization. The third is *cis*-amide residues which can not pack into crystal domains.

It has been reported that the predominant mechanism of lamellar formation for nylons is through folding of the alkane segments.[24] As the length of the alkane chain involved in folding increases, these lamellar folds act as impurities because of a more random reentry into the lamellar structure. During heating of the sample, reorganization leads to a higher degree of perfection in the crystallites, demonstrated by the recrystallization event, followed by melting of the more ordered domains. It is not clear how *cis* amide groups influence lamellar packing.

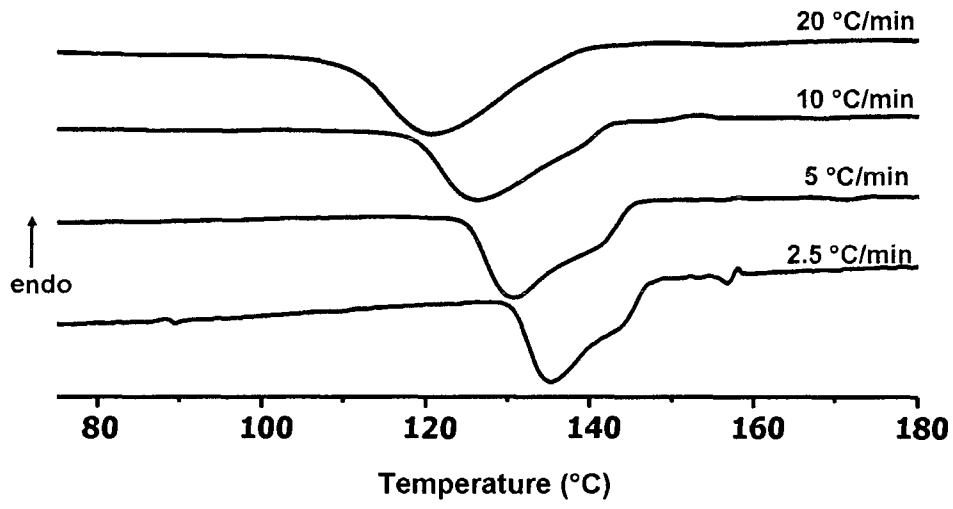

Figure 4.5. Non-isothermal DSC cooling traces of nylon 18 18 at different cooling rates.

When comparing the melting behavior of nylon 18 18 to the even-even series of nylons *X* 18, the broad melting endotherm at 120-140 °C that is present in nylon 18 18 could also be seen in nylon 12 18, but is not observed with lower methylene content diamines, indicating that high aliphatic content in both the diacid and diamine segments is necessary for this transition to be observable. Thus, the broad crystallization and melting curves are considered to be the result of two lesser transitions attributed to two different portions of the chains, the amide linkages and the C16 and C18 polymethylene segments.

Polymethylene segments in polyolefins melt and crystallize at much lower temperatures than those for high-aliphatic nylons. As a result, the broad peaks may involve configurations of amides and CH_2 segments in imperfectly ordered domains in which first, the van der Waals forces of the polymethylene segments are overcome, and at higher temperatures, the hydrogen bonds of the amide

linkages are broken up. In the cooling scans at different cooling rates (Figure 4.5), the crystallization exotherms begin to show two overlapping exotherms at slower cooling rates. The low temperature exotherm is the predominant peak, with a shoulder on the high temperature side. As the cooling rate increases, the two endotherms merge and become indistinguishable. Overall, the T_c shows a significant decrease (~10 °C) as the cooling rate increases. As the sample is cooled from the melt, it would be expected that the hydrogen bonds form first, and act as nucleation sites, or pinning points, for the subsequent crystallization of the polymethylene segments. Thus, unlike traditional nylons, this system appears to resemble a polyethylene backbone with periodic hydrogen bonding that pre-organizes the melt for crystal formation.

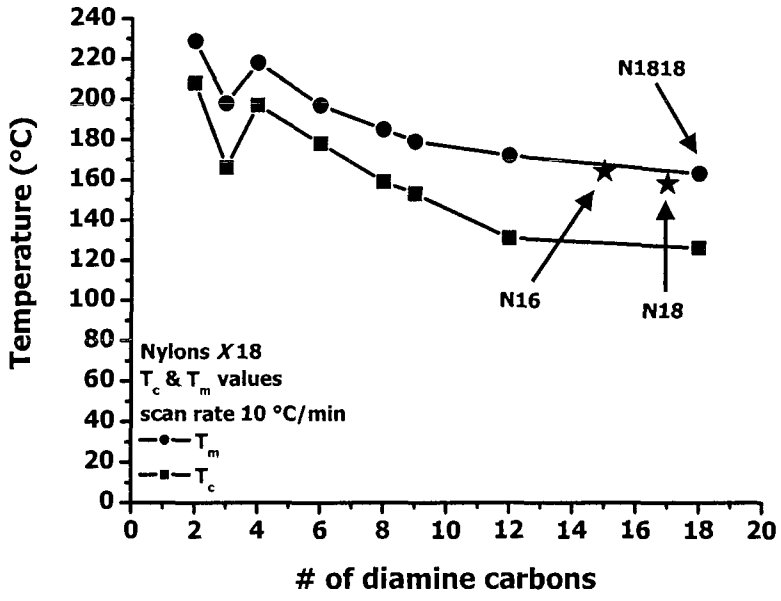

Figure 4.6. Graph of T_m and T_c for nylons X 18.[5] The AB analogs nylon 16[1] and nylon 18[2] are shown for comparison.

Table 4.2. Thermal data for nylons X 18 recorded at a scan rate of 10 °C/min.[5]

Nylon	T_c (°C)	ΔH_c (J/g)	ΔH_m (J/g)	T_m (°C)
2 18	208	37.9	34.4	229
3 18	166	60.5	51.3	198
4 18	197	42.5	40.9	218
6 18	178	50.4	58.3	197
8 18	159	51.2	51.1	185
9 19	153	61.9	57.5	179
12 18	131	48.4	34.9	172
18 18	126	65.8	68.0	163

Further comparison of the melting and crystallization temperatures of nylon 18 18 with the rest of the series nylons *X* 18 shows that these values approach those of polyethylene in a non-linear fashion, as shown in Figure 4.6. Similar trends have been found for both T_c and T_m of nylons *X* 20,[6] as well as the T_m of nylons *X* 34,[8] for which no T_c values were given. The T_m for nylon 6 18 is 197 °C, and for nylon 12 18, with an addition of 6 diamine methylene units, the T_m is 172 °C, a difference of 25 °C. The difference in T_m after another addition of six more diamine methylene units, from nylon 12 18 to 18 18 (T_m=163 °C) is only 9 °C. There comes a point at which the melting point is decreasing in progressively smaller steps as the diamine segment length increases beyond 12 methylene units, and the amide unit spacing becomes more uniform along the backbone.

Typically, AA-BB nylons melt at significantly higher temperatures than their AB analogs with comparable aliphatic content. However, the reported melting temperatures of nylon 16 and nylon 18 are 164 °C[1] and 158 °C,[2] respectively, which are not significantly different from the T_m of nylon 18 18. It is

of note that the enthalpies of both melting and crystallization for nylon 18 18 are significantly higher than those of the rest of the nylons *X* 18 (Table 4.2). This suggests that there is an additional component contributing to the crystallization involving the C16 and C18 polymethylene chains, which augments the observed enthalpy values related mainly to behavior of the amide ordered units.

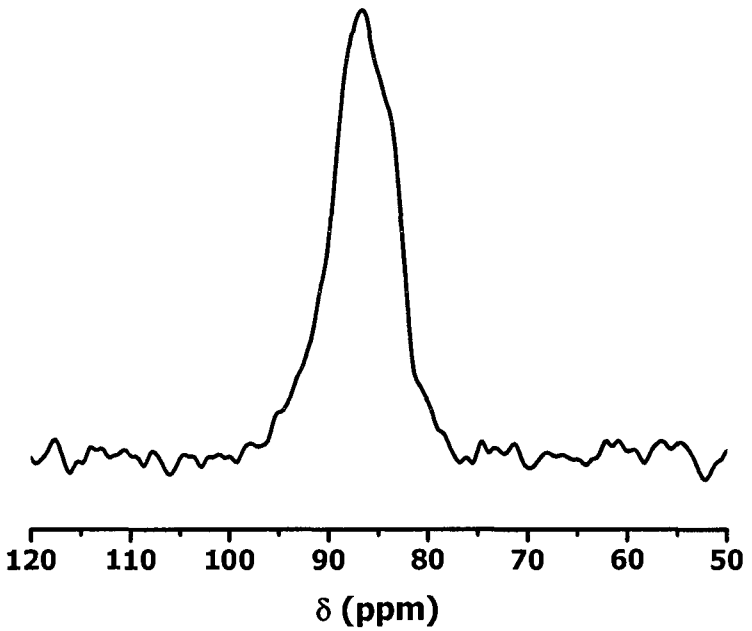

Figure 4.7. Solid state ^{15}N CP/MAS NMR of nylon 18 18.

The solid state ^{15}N CP/MAS NMR spectrum, shown in Figure 4.7, contains a broad peak resulting from a highly amorphous system, observed at 87 ppm. A significant shoulder to this amorphous peak is found at 84 ppm, associated with the α crystalline structure, the thermodynamically stable form for even-even nylons.[5] The even-even nylons *X* 18 previously reported show a trend toward higher amorphous content as the aliphatic content increases. This can be attributed to the librational motion of the polymethylene segments in both the

diacid and diamine moieties, which affects both the kinetics and thermodynamics of crystallization. It is most likely also related to the higher cis-amide content of higher aliphatic nylons which also inhibits crystalline packing.

Nylon 18 ADA

Nylon 18 ADA was readily soluble in $CHCl_3$, HFIP and m-cresol. It is partially soluble in methylene chloride, 2,2,2-trifluoroethanol (TFE), and trifluoroacetic acid leading to a cloudy suspension. It is also partially soluble in a 80-20 mixture of TFE-$CDCl_3$. Films cast from solution were clear and tough. Infrared spectra of nylon 18 ADA showed characteristic absorption bands of amide groups and methylene segments as seen in Figure 4.8. Peaks were found at 3345 cm^{-1} (N-H stretching), 2921-23 cm^{-1} (C-H stretching), 1633-35 cm^{-1} (amide I, C=O stretch), 1535 cm^{-1} (amide II, C-N stretch and CO-N-H bend), 1284 cm^{-1} (amide III), and 736 cm^{-1} (CH_2 rocking).

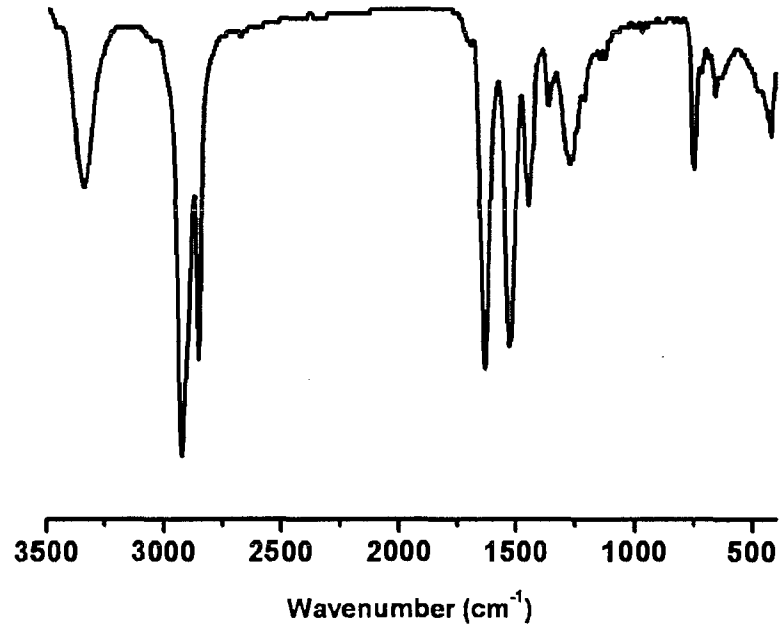

Figure 4.8. FTIR spectrum of nylon 18 ADA.

Based on the Coleman's previous work[25] on nylon 11, N-H stretching bands can be divided into three parts. The band at 3456 cm^{-1} is due to free N-H, the band at 3362 cm^{-1} is due to disordered hydrogen bonded N-H in the amorphous phase, and the band at 3320 cm^{-1} is due to ordered hydrogen bonded N-H in the crystalline phase. The frequency of hydrogen bonded N-H indicates the strength, while the breadth of this band results from the conformational distribution of hydrogen bonded groups. The N-H stretching band of nylon 18 18 is broad, from 3146 to 3480 cm^{-1}, while the band for nylon 18 ADA is more narrow from 3256 to 3480 cm^{-1}. The peak positions and the breadth of the peaks suggests that nylon 18 18 is mostly amorphous with some ordered structures, whereas nylon 18 ADA is almost totally amorphous. Its interesting to note that the amide II overtone band at 3084 cm^{-1} (nylon 18 18, Figure 4.2) is not observed for nylon 18 ADA.

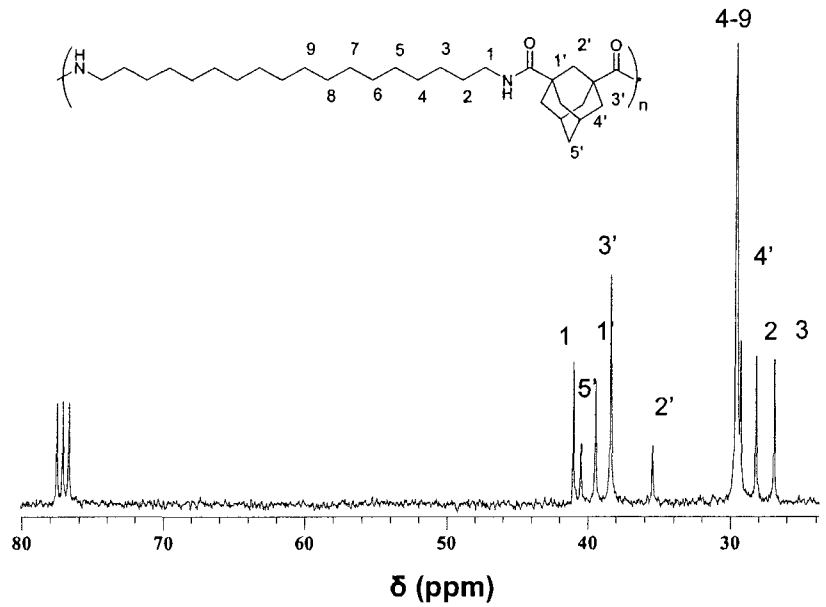

Figure 4.9. ^{13}C solution NMR of Nylon 18 ADA. Sample was dissolved in $CDCl_3$.

Figure 4.9 shows solution ^{13}C spectra for Nylon 18 ADA. All peaks are assigned based on the structure of the polymer except the carbonyl carbon which shows up at 176.92 ppm. The adamantane carbons next to the carbonyl carbon are seen at 39.48 ppm (2C), while the carbon atom between these two carbons is observed at 35.45 ppm (1C). The other adamantyl carbons show up at 29.29 (2C), 38.42 (4C), and 40.48 ppm (1C). Peaks associated with amine end groups were not observed. Like nylon 18 18, only terminal carboxylic acid and alkanes were assigned for nylon 18 ADA. The carbonyl carbon peak of the end groups appears at 178.71 ppm. The other peaks associated with adamantane end groups were observed at 40.78, 40.19, 37.98, 27.95 ppm. End1 and end2 of terminal alkanes were observed at 13.98 and 22.58 ppm, respectively, due to the

presence of previously mentioned C18 monoamine. The molecular weight of nylon 18 ADA was calculated from NMR data using the following equation:[20]

$$M_n\ (g/mol) = M_0\ (I_1/2)/[(I_{\beta COOH} + I_{end2})/2]$$

where M_0 is the molecular weight of the repeating unit for nylon 18 ADA (472.75 g/mol), I_1 is the intensity of the methylene carbons α to the nitrogen atom, while $I_{\beta COOH}$ and I_{end2} are the intensities of the methylene carbon β to acid end groups and the terminal methyl group donated as end2, respectively. The intensity of the methylene carbon β to acid end groups was calculated based on the assumption that the ratio of the intensities of carbonyl end groups to carbonyl main chain peaks will be the same as the ratio of the intensities of the methylene carbon β to acid end groups to the methylene carbons α to nitrogen. The number-average molecular weight of nylon 18 ADA was then calculated to be 21 000 g/mol.

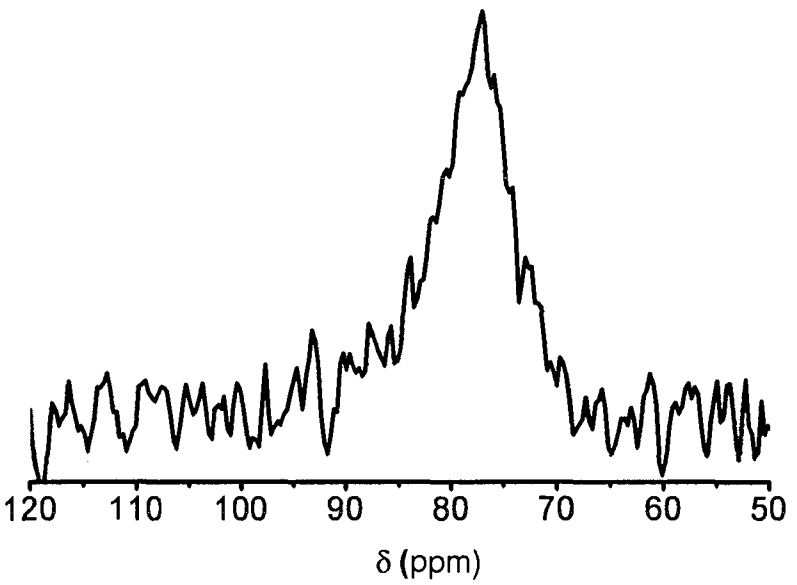

Figure 4.10. Solid state ^{15}N CP/MAS NMR of nylon 18 ADA.

It has been shown that the chemical shift of amide nitrogens in ^{15}N CP/MAS NMR spectra indicates the crystalline form of the nylon samples. The solid state ^{15}N CP/MAS NMR spectrum of nylon 18 ADA is shown in Figure 4.10 and contains only a broad peak resulting from a highly amorphous system, with a peak value at 77 ppm.

Annealing of Nylon 18 ADA

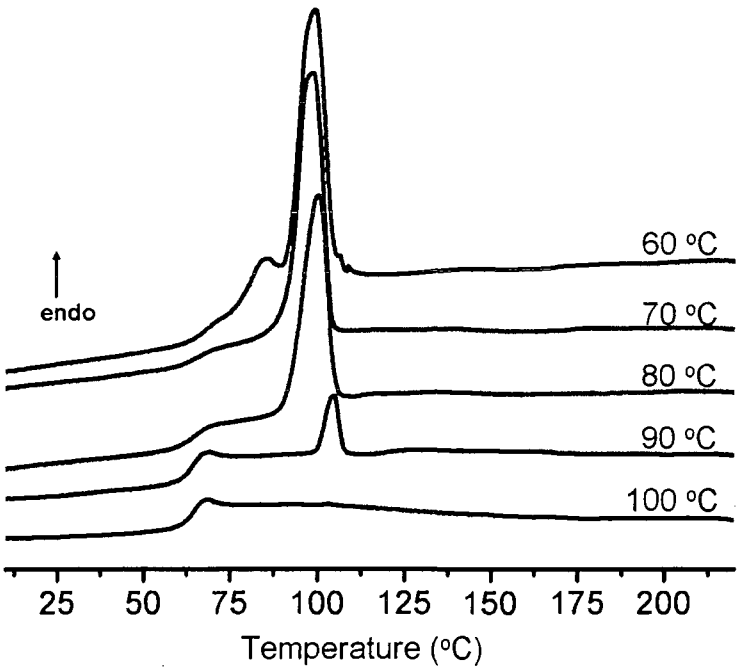

Figure 4.11. DSC thermograms of solution-cast nylon 18 ADA annealed at various temperatures for 2 h.

Figure 4.11 shows the DSC scans of nylon 18 ADA samples annealed at different temperatures for 2 hours in the range of 60 to 100 °C. Annealing temperatures higher than 100 °C gave similar thermograms to that obtained at 100 °C. Two distinct peaks are observed for the sample annealed at 60 °C. The lower endothermic peak disappears and the heat of fusion increases once the

annealing temperature is 70 °C. The heat of fusion of melting decreases with higher annealing temperatures and no melting peak is observed once the annealing temperature is100 °C or above. On the other hand, the melting peak shifts slightly to higher temperatures with increasing annealing temperatures.

Two peaks for the sample annealed at 60 °C may be related to two distinct crystal populations with different degrees of perfection and size. Smaller and less perfect crystals may grow into more stable and thicker crystals. This may explain the increase in the heat of fusion for the sample annealed at 70 °C. It is interesting to note that once the melting of these crystals occurs, the polymer chains do not rearrange to form crystals under the conditions indicated, possibly due to bulky adamantane groups in the backbone inhibiting chains getting closer in the time frame of DSC analysis. During solvent casting, nylon 18 ADA chains are more mobile and have enough time and flexibility to form limited amounts of ordered structures which they do not from the melt. This may explain why there is only a small endothermic peak with higher melting point observed once the sample is annealed at 90 °C. At this temperature, most of the crystals melt, and the peak observed is only for the most perfect crystals which have higher melting points and are still stable at this temperature. The glass transition for nylon 18 ADA is always observed at 64 °C which is higher than the other long alkyl chain nylons examined to date, possibly due bulky adamantane groups inhibiting segmental motion.

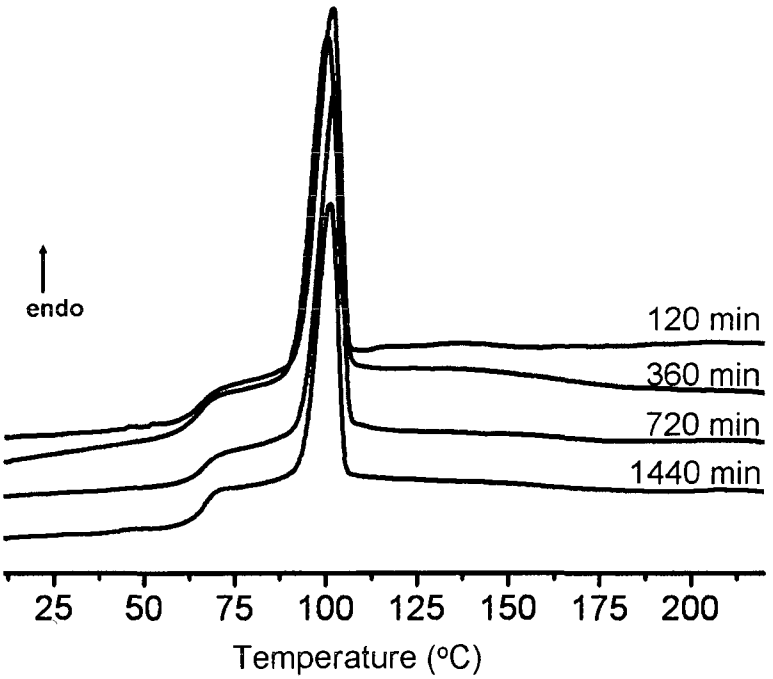

Figure 4.12. DSC thermograms of solution-cast nylon 18 ADA annealed at 80 °C for various times.

Figure 4.12 shows the DSC traces of nylon 18 ADA annealed at 80 °C for different periods of time. The heat of fusion and the melting point slightly increase with annealing time. The melting point shifts from 99 to 102, while the heat of fusion of the melting increases from 15 to 18 J/g. These changes are not significant. There are also slight differences observed for the samples annealed at 90 °C for different time periods. These results indicate that there is little or no change in crystallinity with time using the annealing conditions described here.

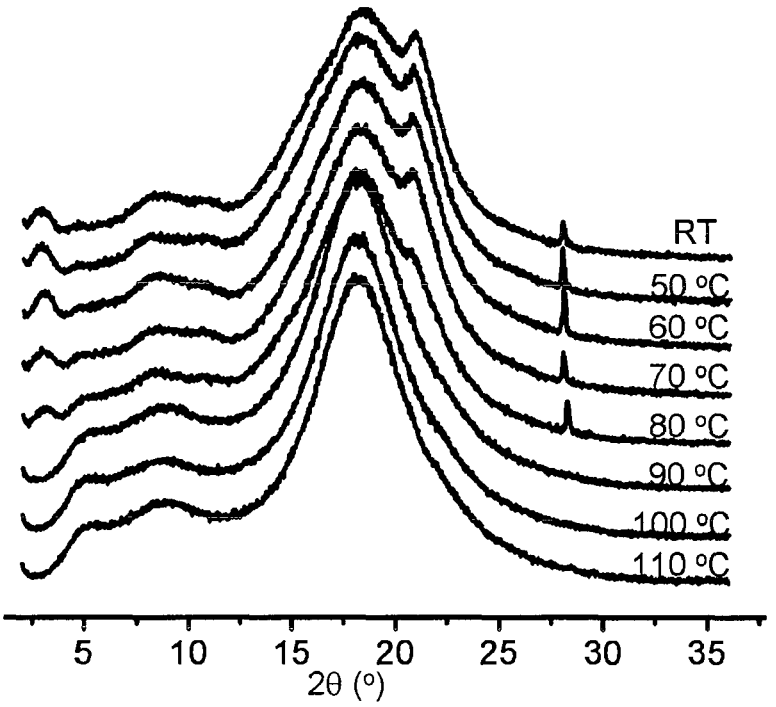

Figure 4.13. The WAXD patterns of solution-cast nylon 18 ADA annealed at various temperatures for 2 h.

A series of WAXD pattern, recorded at room temperature, of solution-cast nylon 18 ADA samples annealed at various temperatures for 2 h is given in Figure 4.13. The as-cast sample (without further thermal treatment) shows an amorphous halo in addition to a sharp peak at 21.04° and possibly a higher order peak at 28.08°. The WAXD patterns follow the same trends as the DSC thermograms (Figure 4.11). The peak intensities are almost unchanged with annealing up to 70 °C, and then the intensity of the peak at 21.04° decreased for the sample annealed at 80 °C. Once the annealing temperature is 90 °C and higher, only an amorphous halo is observed.

Thermogravimetric Analysis

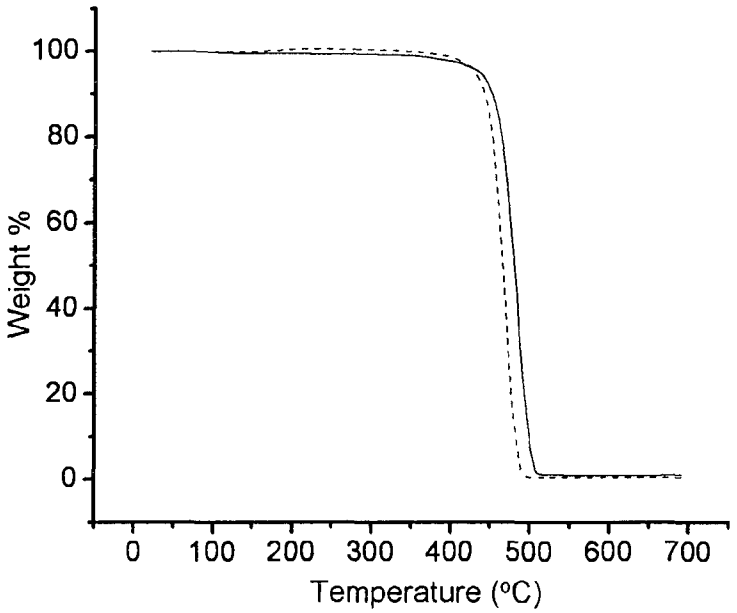

Figure 4.14. TGA thermograms in N_2 with heating rates of 10 °C/min. Dashed line is Nylon 18 18, solid line is Nylon 18 ADA.

Both polymers showed good thermal and thermo-oxidative stability. Figure 4.14 shows typical TGA traces for nylon 18 18 and Nylon 18 ADA with heating rates of 10 °C/ min in N_2. The temperature at 5 wt-% loss is 429 °C, and the temperature at 10 wt-% loss is 440 °C for nylon 18 18 in N_2. Nylon 18 ADA shows a slightly enhanced thermal stability compared to Nylon 18 18. The temperature at 5 wt-% loss is 434 °C , and the peak decomposition temperature is 485 °C which is about 18 °C higher than the peak decomposition temperature of Nylon 18 18. The change in thermal stability of Nylon 18 18 in air is insignificant, and no change is observed in thermal stability of Nylon 18 ADA.

Mechanical Analysis

Figure 4.15 shows typical stress-strain curves for Nylon 18 18 and nylon 18 ADA. The initial modulus values are measured as 820 MPa and 486 MPa for nylon 18 ADA and Nylon 18 18, respectively. The Young's modulus for nylon 18 18 is in the range of the nylon X 34 series which was given as 500-700 MPa.[26] The analysis also indicates elongation at the breaking point increased by 300% for nylon 18 ADA, while initial modulus is almost doubled compared to nylon 18 18. This remarkable improvement in mechanical properties confirms the reinforcing effect of the adamantyl moiety in polyamide backbones. The stress-strain curves of nylon 6 18 and nylon 8 18 are also given in Figure 4.15 for comparison. The elongations at break for nylon 6 18 and 8 18 are 550 and 750%, respectively.

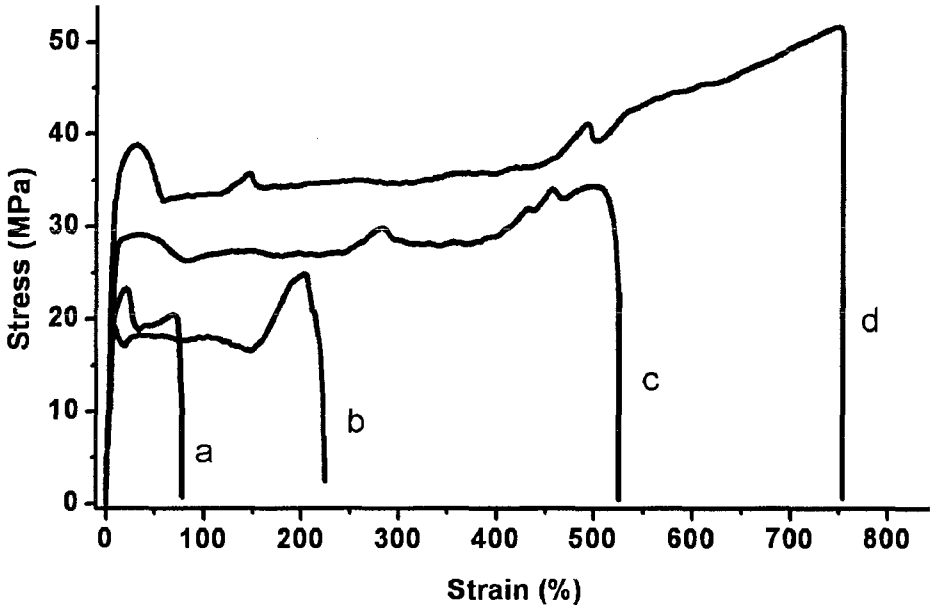

Figure 4.15. Stress-strain curve for a) nylon 18 18, b) nylon 18 ADA, c) nylon 8 18, and d) nylon 6 18.

Figure 4.16-A shows the storage module as a function of temperature for nylon 18 18. For comparison, the data are given for two other nylons, nylon 6 18 and nylon 8 18, also synthesized in our laboratory. As expected, the storage modulus increases with increasing amide density for these nylons. The increase is significant for nylon 6 18, and is almost 300% higher compared to nylon 18 18. Figure 4.16-B shows the loss tangent delta dependence on temperature for these nylons. The glass transitions obtained by DMA are in the same range of 43-45 ^{o}C. The small increase in T_g for nylon 18 18 may be a result of lower amide density of this polymer which leads to lower water absorption.

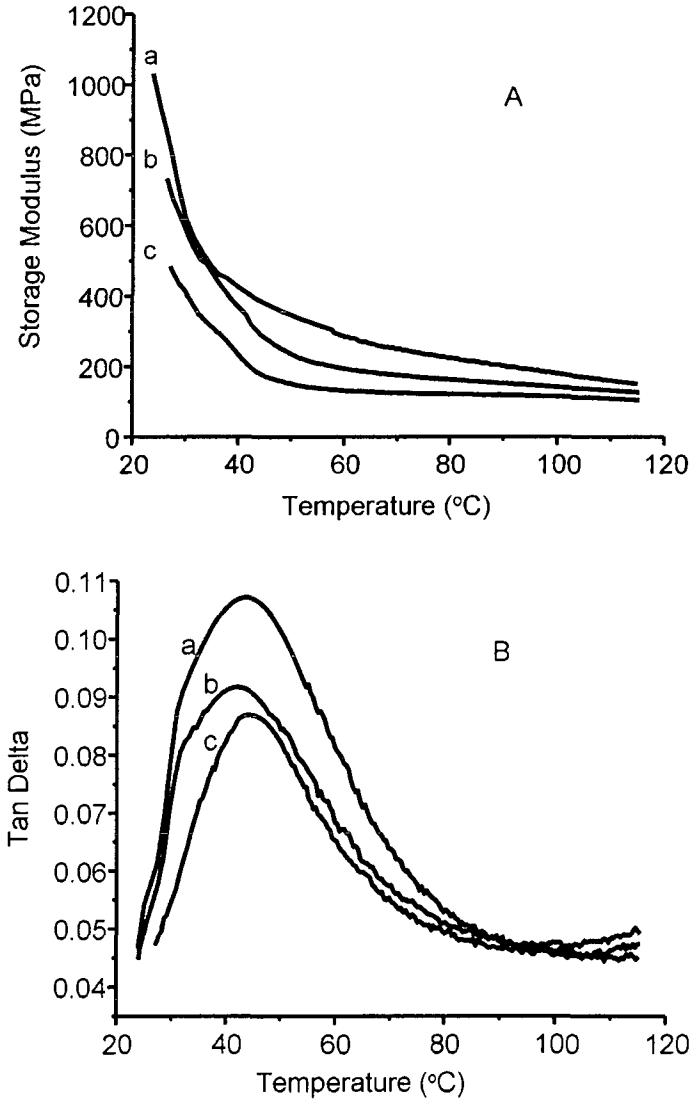

Figure 4.16. DMA curves of a) nylon 6 18, b) nylon 8 18, and c) nylon 18 18 (A- Storage modulus vs. temperature, B- Tan delta vs. temperature)

Conclusions

Two novel aliphatic nylons have been successfully synthesized. The high-aliphatic nylon with near-uniform spacing of the amide units, nylon 18 18, approaches the properties expected for polyethylene with periodic hydrogen bonds substituted along the backbone. Resistance to typical organic solvents

increases over other aliphatic nylons as a result of the increased polymethylene content. Quantitative ^{13}C solution NMR analysis confirmed a continued increase in the population of *cis* amide units as the aliphatic content increases. Non-isothermal DSC experiments point to a two-component system with two major melting and crystallization phenomena, the lower associated with van der Waals forces and the higher with amide hydrogen bonds. Combined, the regular placement of amide groups and long methylene segment lengths results in a higher-than-expected T_m, with a higher enthalpy (and higher degree of crystallinity) than most of the other nylons *X* 18. Nylon 18 ADA, on the other hand, is totally amorphous from the melt. However, solution-cast samples of nylon 18 ADA shows some ordered structures that can grows into more stable crystals with annealing. Incorporation of adamatyl moieties in the polymer's main chain enhanced both the thermal stability and mechanical properties.

Acknowledgments

The authors would like to thank Cognis Corp. for funding and materials. Partial support was also provided by the NSF IGERT grant 0333136. We also acknowledge NSF-MRI grant award 0079450 for funding to purchase the Varian ^{UNITY}*INOVA* 500 MHz NMR spectrometer and upgrade other university NMR systems.

References

1 Bermudez, M.; Vidal, X.; Munoz-Guerra, S. Synthesis, Structure and Crystal Morphology of Nylon 16. *Macromol. Chem. Phys.*, **1999**, 200, 964-971.

2 Cojazzi, G.; Drusiani, A. M.; Fichera, A.; Malta, V.; Pilati, F.; Zannetti, R. Synthesis and Some Structural Data of Nylon 18. *Eur. Polym. J.*, **1981**, 17, 1241-1243.

3 Li, W.; Yan, D. Synthesis and Characterization of Nylons Based on Hexadecane Diacid. *J. Appl. Polym. Sci.*, **2003**, 88, 2462-2467.

4 Saotome, K.; Komoto, H. Polyamides Having Long Methylene Chain Units. *J. Polym. Sci. Pt. A-1,* **1966**, 4, 1463-1473.

5 Bennett, C.; Mathias, L. J. Synthesis and Characterization of Polyamides Containing Octadecanedioic Acid: Nylons 2 18, 3 18, 4 18, 6 18, 8 18, 9 18, and 12 18. *J. Polym. Sci., Part A: Polym. Chem.,* **2005**, 43, 936-945.

6 Huang, Y.; Li, W.; Yan, D. Preparation and characterization of a series of polyamides with long alkylene segments: Nylons 12 20, 10 20, 8 20, 6 20, 4 20 and 2 20. *Polym. Bull.*, 2002, 49, 111-118.

7 Zhang, G.; Yan, D. Morphology and Structure of Chain-Folded Lamellar Crystals of Nylons 2 22, 4 22, 6 22, 8 22, 10 22, and 12 22. *Cryst. Growth Des.,* **2004**, 4, 383-387.

8 Ehrenstein, M.; Smith, P.; Weder, C. Polyamides X 34: A New Class of Polyamides with Long Alkane Segments. *Macromol. Chem. Phys.,* **2003**, 204, 1599-1606.

9 Ehrenstein, M.; Sikorski, P.; Atkins, E. D. T.; Smith, P. Structures of X 34-Nylons in Chain-Folded Lamellae and Gel-Spun Fibers. *J. Polym. Sci., Part B: Polym. Phys..,* **2002**, 40, 2685-2692.

10 Li, Y.; Yan, D. Influence of Crystallization Conditions on the Crystalline Transformation Behavior of Nylon 10 14. *Coll. Polym. Sci.*, **2002**, 280, 678-682.

11 Li, Y.; Yan, D.; Zhou, E. In situ Fourier Transform IR Spectroscopy and Variable-temperature Wide-angle X-ray Diffraction Studies on the Crystalline Transformation of Melt-crystallized Nylon 12 12. *Coll. Polym. Sci.,* **2002**, 280, 124-129.

12 Wang, L. H.; Porter, R. S. Thin Films of Nylon 13 13 Casted on Water: Morphology and Properties. *J. Polym. Sci., Part B: Polym. Phys.*, **1995**, 33, 785-790.

13 Johnson, C. G.; Mathias, L. J. Nylon 13 13 Analysis by X-ray and Solid State NMR: Treatment-dependent Crystal Forms. *Polymer,* **1993**, 34, 4978-4981.

14 Mathias, L. J.; Jensen, J.; Somlai, L. Copolymers of 4-Adamantylphenyl Metahcrylate Derivatives with Methyl Methacrylate and Styrene. *Polymer*, **2001**, 42, 6527-6537.

15 Mathias, L. J.; Reneen, J. van A.; Coetzee, L. Polymerization of Olefins with Bulky Substituents.1. Homo- and Copolymerization of 3-(1-Adamantyl)propene. *Polymer,* **2004**, 45, 799-804.

16 Mathias, L. J.; Reichert, V. R. Highly Cross-linked Polymers Based on Acetylene Derivatives of Tetraphenyladamantane. *Macromolecules,* **1994**, 27, 7030-7034.

17 Liaw, B.; Liaw, D. Synthesis and Characterization of New Polyamide-imides Containing Pendent Adamantyl Groups. *Polymer*, **2001**, 42, 839-845.

18 Kao, S. C.; Shiue, H.; Chern, Y. Synthesis and Characterization of New Polyamides Containing Adamantyl and Diamantyl Moieties in the Main Chain. *J. Polym. Sci., Part A: Polym. Chem.*, **1998**, 36, 785-792.

19 Steadman, S. J.; Mathias, L. J. A New Non-acidic Mixed Solvent System for Nylon Nuclear Magnetic Resonance: *cis* Amide Quantitation in Nylons and Model Amides. *Polymer*, **1997**, 38, 5297-5300.

20 Davis, R. D.; Steadman, S. J.; Jarrett, W. L.; Mathias, L. J. Solution ^{13}C NMR Characterization of Nylon 6 6: Quantitation of *cis* Amide Conformers, Acid and Amine End Groups, and Cyclic Unimers. *Macromolecules*, **2000**, 33, 7088-7092.

21 Van Krevelen, D. W. *Properties of Polymers*, 3rd ed.; Elsevier: New York, **1990**.

22 Brandrup , J.; Immergurt , E. H. *Polymer handbook*, 3rd ed. ; John Wiley & Sons, Inc.: New York, **1989**.

23 Zhou, Hongyi; Wilkes, G. L. Comparison of Lamellar Thickness and Its Distribution Determined from DSC, SAXS, TEM and AFM for High-density Polyethylene Films Having a Stacked Lamellar Morphology. *Polymer*, **1997**, 38, 5735-5747.

24 Jones, N. A.; Atkins, E. D. T.; Hill, M. J. Comparison of Structures and Behavior on Heating of Solution-Grown, Chain-Folded Lamellar Crystals of 31 Even-Even Nylons. *Macromolecules,* **2000**, 33, 2642-2650.

25 Skrovanek, Daniel J.; Painter, Paul C.; Coleman, Michael M. Hydrogen Bonding in Polymers. 2. Infrared Temperature Studies of Nylon 11. *Macromolecules,* **1986**, 19, 699-705.

26 Ehrenstein, Moritz; Smith, Paul; Weder, Christoph. Polyamides X 34: A New Class of Polyamides with Long Alkane Segments. *Macromol. Chem. Phys.*, **2003**, 204, 1599-1606.

CHAPTER V

INVESTIGATION OF MELTING BEHAVIORS AND CRYSTALLINITY OF LINEAR POLYAMIDE WITH HIGH ALIPHATIC CONTENT

Abstract

The melting behaviors and crystal structures of a long alkyl chain polyamide, nylon 18 18, were investigated under annealing and isothermal crystallization conditions. Nylon 18 18 showed multiple melting peaks in DSC thermograms depending on thermal history of the samples. The origin of the multiple melting peaks may be a result of a melting and recrystallization mechanism during DSC scans. WAXD patterns showed two new diffraction peaks which appeared at 0.44 and 0.37 nm and are characteristic peaks of α-form (triclinic structure) of even-even nylons with increasing annealing temperature. The intensities of these peaks increased, and they split further apart, with elevated annealing temperatures. The solid state ^{15}N CP/MAS NMR spectra of the nylon 18 18 samples that had been quenched and annealed also confirmed the α crystalline form.

Introduction

Nylons have excellent mechanical properties resulting from backbone symmetry and total amide density combined with processing induced morphology. The backbone symmetry determines if the polymer can be crystalline or amorphous while the processing controls the orientation of the polymer chains and the degree of crystallinity. Amide density affects T_m, and to some extent, T_g. In recent years, there have been several reports on nylons with low amide unit density.[1,2,3,4] This is desirable to improve certain properties such as hydrophophobicity, solvent resistance and processing conditions. These nylons may be thought of as backbone-functionalized polyethylene: They posses the hydrophobic character of polyethylene along with improved thermal properties due to the hydrogen bonding amide units. These long alkyl chain nylons have also been considered as compatibilizers between polyamides and polyolefins.[5] Previous work by our group and others, has emphasized synthesis and crystal structures of nylons with long alkyl chains.[1,6,7,8] However, there have been no reports on the affect of crystallization conditions on melting behavior of long alkyl chain nylons.

Multiple melting peaks have been reported for many semicrystalline polymers such as poly(ethylene terepthalate),[9,10,11] poly(butylene terepthalate),[12,13] poly(ether ether ketone) (PEEK)[14,15,16] and traditional nylons[17,18]. There have been several interpretations proposed for these multiple endotherms based on three hypotheses. First, the two melting endotherms may result from two different crystal morphologies (polymorphism).[19,20] For instance,

nylon 12 was shown to have two separate peaks depending on the history of the samples.[20] These two peaks were attributed to α and γ crystalforms of the polymer. The melting point of α nylon 12 was given as 173 °C, while the γ form of nylon 12 melted at around 200 °C. The multiple peaks seen during DSC scans were explained by recyrstallization to γ form after melting of α form.

The second hypothesis was associated with crystal structures having different lamellar thicknesses, and therefore, different thermodynamic stabilities.[21] For this scenario, the main crystal population, grown first during isothermal crystallization, is overlaid by a smaller population of crystallites formed in intermediate spaces, perhaps nucleated at the surfaces of the primary crystals. The third interpretation for multiple endotherm during DSC scans is related to melting and recyrstallization of one initial morphology as a result of prior thermal history of the samples.[22] According to this explanation, the lower endotherm involve the onset of melting of the characteristic crystals which formed rapidly during initial cooling and are less perfect. These crystals experience continuous melting and recyrstallization during the DSC analysis to give a trace in which the peak shape observed is the combination of continuously overlapping melting and recrystallization processes.

In this paper, the change in melting behavior and crystal morphology of nylon 18 18 was investigated with various annealing and isothermal crystallization conditions. Unlike the other long alkyl chain nylons described in litrature, nylon 18 18 possesses relatively even distribution of amide units along the polymer chains. Melting behaviors of this long alkyl chain nylon were studied

on samples either crystallized from the glassy state or from the melt. The samples later were either quenced from melt and annealed at certain temperature, or cooled to a certain temperature and isothermally crystallized for a given time. The multiple endotherms is discussed with respect to changes in crystal morphology as seen by WAXD, FTIR, CP/MAS solid state ^{15}N and ^{13}C NMR.

Experimental

Synthesis of nylon samples. Nylon 18 18 was produced here by a melt polycondensation technique. 1,18-Octadecanediamine and 1,18-octadecanedioic acid were supplied by Cognis Corporation and were used as received. The monomers were mixed together in equimolar amounts (~ total 4-5 g) and heated under nitrogen purge using a silicon oil bath at 170-180 °C for 4 hours, then at 220-230 °C for 4 hours. At this point, no bubbling was visible in the melt and a vacuum was applied for 0.5 hours. The sample was cooled under vacuum. The resulting material was opaque and white in color. The intrinsic viscosity was determined to be 0.54 dL/g in dichloroacetic acid.

Instrumentation and techniques. Dilute solution viscometry (DSV) was performed using a Cannon-Ubbelohde 1C C628 viscometer, with dichloroacetic acid as the solvent. Efflux times were recorded at a temperature of 35±0.2 °C.

Nylon 18 18 was melted at 190 °C for 3 mins and quenched between two cold metal plates. For DSC experiment, all thermal treatment was performed in TA Instruments 2920 using aluminum pans. For all other experiment, the samples were annealed in a conventional oven with an automated temperature

controller. The samples were placed in aluminum holder which was purged with argon for 10 mins and sealed after purging to minimize oxidation of the samples. For consistency, the samples annealed using the conventional oven were analyzed by DSC and the data compared with those annealed in the DSC.

Transmission FTIR spectroscopy was carried out on a Mattson Galaxy Series FTIR 5000 and 256 transients. Differential scanning calorimetry (DSC) experiments were performed on a TA Instruments 2920 using pierced-lid crimped aluminum pans. The temperature and heat capacity were calibrated with indium and sapphire standards, respectively. Unless otherwise stated, DSC analyses were recorded at a ramp rate of 10.0 °C/min for both heating and cooling. For a typical DSC analyses, small pieces (~6 mg) were cut and placed in an aluminum DSC pan. The samples were heated at 10 °C/min to a given temperature and annealed at that temperature for 2 h. They were cooled down to 20 °C at a cooling rate of 10 °C/min, and heated again with a heating rate of 10 °C/min trough complete melting. Each sequence of thermal scans was recorded at least three times for reproducibility. The melting temperature was taken as the endotherm maximum, and the crystallization temperature was taken as the exotherm maximum. The overlapped peaks of thermograms were separated by fitting with multiple Gaussian function using Origin 7.0 data-analysis and plotting software.

Wide angle X-ray diffraction (WAXD) measurements were obtained with a Rigaku Ultima III diffractometer operated at 40 kV and 44 mA. Melt pressed samples were quenched and run with a scan speed of 0.5° per minute from 2 to

45°. The thermal treatments of these samples were as similar as possible to those analyzed by other methods.

CP/MAS solid state ^{15}N and ^{13}C NMR experiments were performed on a Bruker MSL 400 MHz spectrometer and peaks were referenced to the amide nitrogen of ^{15}N labeled glycine at δ=0.0 ppm and adamantane methane at 29.5 ppm, respectively, as external standards.

Results and Discussion

The melting behaviors and crystal structures of various nylon 18 18 samples were considered to be the result of both amide group content and the spacing of polymethylene segments between these amide units. Unlike other nylons with shorter alkyl chains, the comformational and librational motions of the polymethylene chains enhances mobility of the hydrogen bonding amides, enhancing the reordering process during annealing. This may be the reason for the broad melting endotherm seen between 120-140 °C, most likely associated with melting of ordered domains of less perfect crystallinity then that of the main crystalline regions. This peak occurs in each trace at roughly 5 °C above the annealing temperature, consistent with gradual increase in the size and/or perfection of these domains, which is followed by a cold crystallization exotherm around 140 °C.[23] Based on this observation and experimental data given in this paper, the DSC results for annealed nylon 18 18 samples were divided into two section.

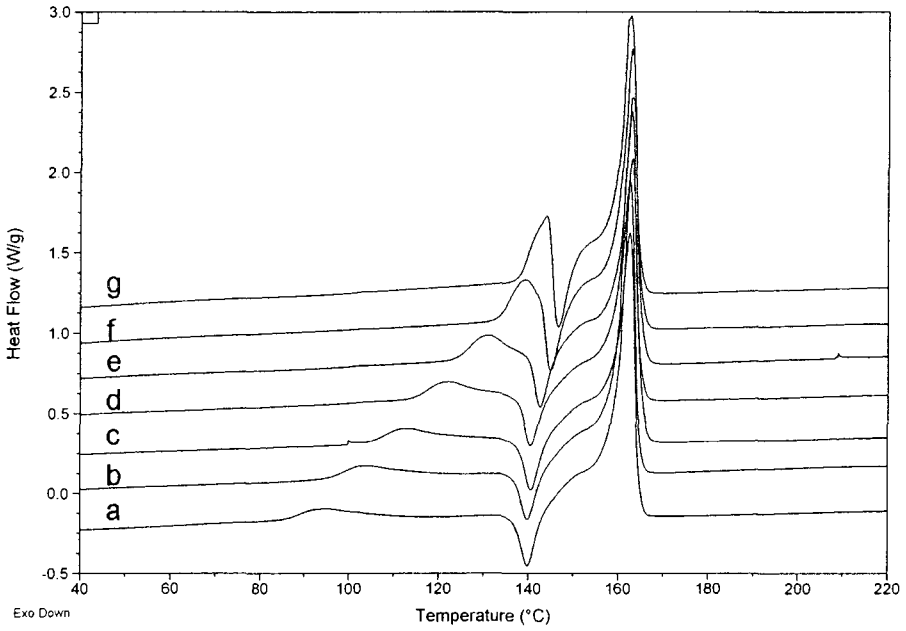

Figure 5.1. DSC thermograms of nylon18 18 annealed for 2 h at a) 80 °C, b) 90 °C, c) 100 °C, d) 110 °C, e) 120 °C, f) 130 °C, and g) 135 °C (samples annealed in DSC).

Table 5.1

DSC parameters of nylon 18 18 samples annealed between 80 to 135 °C

T_a[a] (°C)	T_m1[b] (°C)	T_m2[b] (°C)	ΔH_m1[c] (J/g)	ΔH_m2[c] (J/g)	X_{DSC}%[d]
80	94	162.5	4.7	66.96	19.8
90	102.4	162.5	5.6	65.11	19.2
100	112	162.9	7.1	63.05	18.6
110	122.4	162.6	10	61.45	18.2
120	131.2	162.9	11.4	59.65	17.6
130	139.3	162.8	12.2	59.87	17.7
135	143.9	162.4	12.6	59.66	17.6

[a] annealing temperature
[b] melting point of lower and higher endotherms
[c] heat of fusion of lower and higher endotherms
[d] percent crystallinity based on only ΔH_m2

Figure 5.1 shows the DSC scans of nylon 18 18 samples annealed at different temperatures in the range of 80 to 135 °C. The samples were first quenched between two cold metal plates from the molten state before DSC analysis. All curves have a sharp endothermic peak resulting from melting of the main crystal population at around 163 °C. They also posses another wide endotherm as a result of smaller crystal population found approximately 12 °C above the annealing temperature. The lower melting peak becomes stronger and sharper with increasing annealing temperature, while the higher melting peak area slightly decreases.

Overall crystallinity is not affected with increasing annealing temperature for given time periods. The percent crystallinity (X%) was calculated using a procedure based on group additivity values from Van Krevelen[24] to give the theoretical ΔH_f. The equilibrium heat of fusion, ΔH_f, was calculated by adding two amide groups (67.4 J/g each) and thirty-four methylene groups (at 270.8 J/g each), to give a total of 338.2 J/g. The calculated percent crystallinity is lower than for typical commercial polyamides which may be a result of high conformational mobility of the polymethylene chains kinetically inhibiting crystallization. Samples annealed up to 135 °C showed the same percent crystallinity which meant even at 135 °C the temperature was not high enough for the extensive molecular motion required to form proper register of amide groups into a lamella structure. However, imperfections such as gauche conformations in the polymethylene chains can be excluded under this low temperature annealing conditions. In addition, the perfection and narrower distribution of the crystals

may occur as a result of the fact that the temperature in this region was high enough to give polymer chains enough mobility to form high ordered crystals.

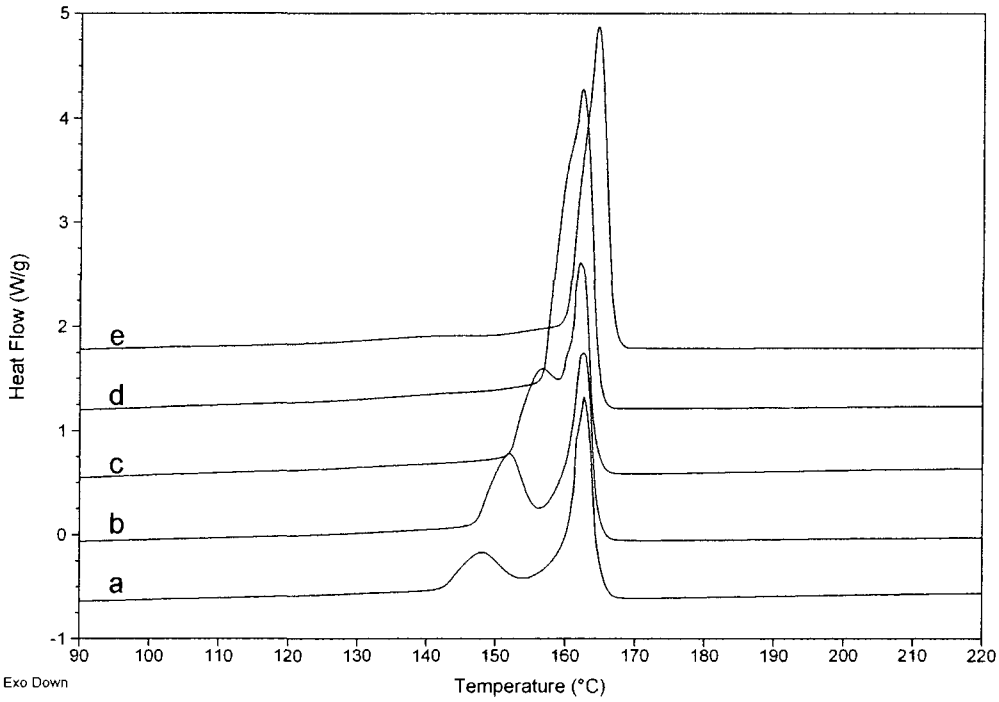

Figure 5.2. DSC thermograms of nylon18 18 annealed for 2 h at a) 140 °C, b) 145 °C, c) 150 °C, d) 155 °C, and e) 158 °C (samples annealed in DSC).

Table 5.2

DSC parameters of nylon 18 18 samples annealed between 140 to 158 °C.

T_a[a] (°C)	T_m1[b] (°C)	T_m2[b] (°C)	ΔH_m1[c] (J/g)	ΔH_m2[c] (J/g)	H_m[d] (J/g)	X_{DSC}%[e]
140	147.9	162.6	16.4	47.6	77.7	23
145	151.9	162.5	24.3	43.1	87.8	26
150	156.6	162	36.1	34.3	93.1	27
155	160.7	162.2	52.3	28.5	115.8	34
158	163.1	164.4	29.6	36.6	95.7	28

[a] annealing temperature
[b] melting point of lower and higher endotherms
[c] heat of fusion of lower and higher endotherms
[d] total heat of fusion (the beginning of the melting was taken as 110 °C)
[e] Percent crystallinity

DSC scans of nylon 18 18 that had been annealed for 2 h at higher temperatures are shown in Figure 5.2. Two distinct peaks are observed for those samples annealed in the range of 140-158 °C. The lower endothermic peak was 5-7 °C higher than the annealing temperature, and increased linearly with annealing temperature until it merged with the higher peak at an annealing temperature 158 °C.

The low temperature endotherm also increased continuously in size with increasing annealing temperature, while the heat of fusion of the high temperature endotherm decreased. These changes are more pronounced compared to the results obtained for low temperature annealing. The heat of fusion for each endotherm, the melting points, and total crystallinity are given in Table 5.2. Overlapped peaks were separated by fitting with a multiple Gaussian function. The heat of fusion of the higher melting domains is almost independent of the annealing temperature below 135°C but decreased with

higher annealing temperatures. This result can not be explained by the increased heat of fusion of the lower endotherm at the expense of the higher endotherm since the transformation of the higher melting crystals to lower melting crystals is prohibited by thermodynamics. However, it clearly shows that two endotherms are somehow associated, and the melting/recrystallization hypothesis may be well suited to explain this result.

It is noteworthy that, unlike the low temperature annealing, the total percent cystallinity also increases as the annealing temperature increased. The minimum temperature required for the polymer chains to overcome the energy barrier to form larger crystalline domains of nylon 18 18 may be around 140 °C. Once the annealing temperature reaches 158 °C, only one endotherm is observed and the melting point was increased to 164 °C. This may be due to the fact that at this temperature, defects can be excluded and the chains can be reorganized to form thicker crystals with a higher melting point.

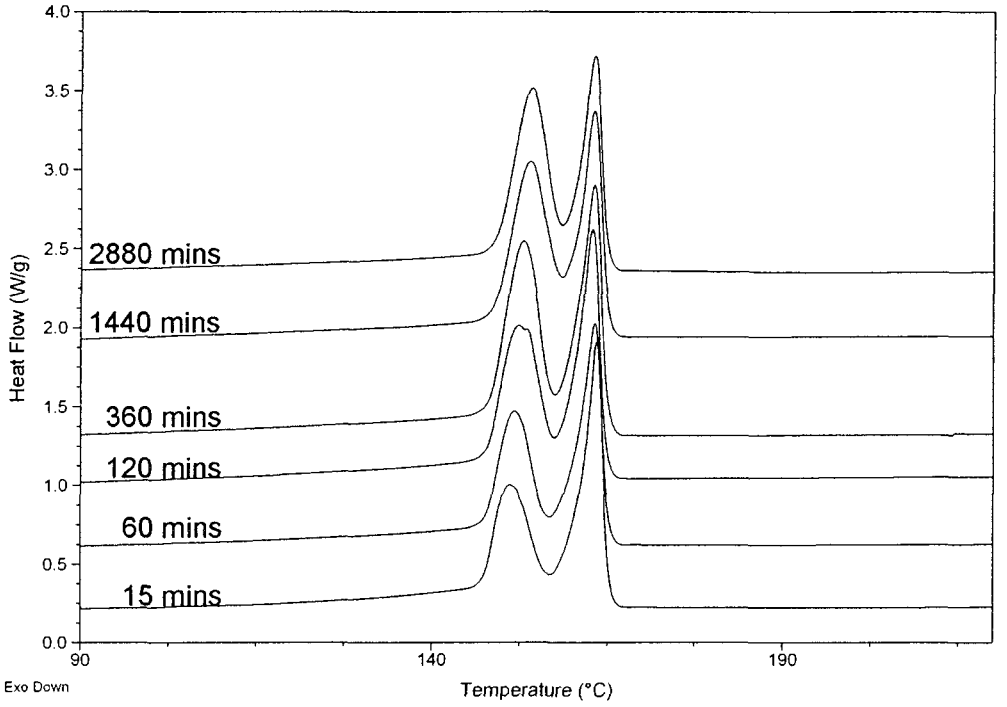

Figure 5.3. DSC heating thermograms of nylon18 18 annealed at 145 °C for 15, 60, 120, 360, 1440, and 2880 mins from bottom to top.

Figure 5.3 shows the DSC traces of nylon 18 18 annealed at 145°C for different periods of time. The upper endothermic peak was nearly constant at 163 °C, while the lower temperature melting peak gradually shifted from 151 to 154 °C with increasing annealing time. The heat of fusion for the lower endotherm also increased with the annealing time from 18 to 27 J/g. By contrast, the heat of fusion of the upper endothermic peak decreases with time from 30 to 20 J/g. These changes may be attributed to the perfection and/or thickening of the thinner lamellar crystals produced by annealing the sample. The total crystallinity on the other hand, is almost invariant with annealing time in range of 22-25 %. This result may indicate that at this specific temperature melting/ recrystalization is in equilibrium.

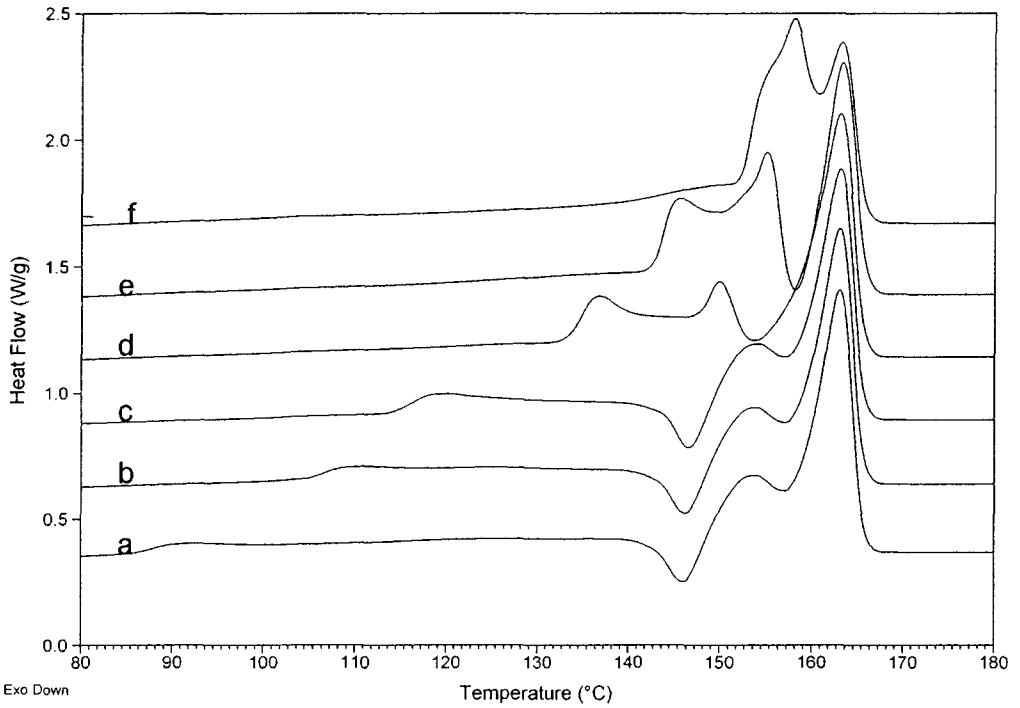

Figure 5.4. DSC thermograms of nylon18 18 isothermally crystallized from melt for 2 h at a) 80 °C, b) 100 °C, c) 110 °C, d) 130 °C , e) 140 °C, and f) 150 °C (cooling rate is 60 °C/min).

The DSC heating curves of Nylon 18 18 samples, isothermally crystallized from the melt, are given in Figure 5.4. The samples were heated to 190 °C with a heating rate of 10 °C/min and held at this temperature for 5 mins to erase thermal history of the samples. Then, they were cooled to a given temperature with a cooling rate of 60 °C/min and held at that temperature for 2 h. After being isothermally crystallized at the specified temperature for 2 h, the samples were cooled with a rate of 60 °C/min to 20 °C, and then heated up to 190 °C with a heating rate of 10 °C/min. Thermograms obtained from isothermal crystallization of nylon 18 18 from the melt are totally different those obtained by annealing from the glassy state. Unlike the quenched samples which shows slight variations in

DSC traces even at lower temperatures, the samples isothermally crystallized up to 110 °C gave almost the same thermograms with a higher cold crystallization peak. A higher cold crystallization peak is not surprising considering crystallization during cooling was not as fast as for the quenched sample, this leads to more organized chains melted and recrystallized at a higher temperature. Once the isothermal crystallization temperature reaches 130 °C, there are three distinct peaks and no crystallization peak.

The two lower endotherms may be attributed to different sizes of crystals. The lower peaks are at the same position as the lower peak resulting from annealing from the glassy state. This endotherm may result from annealing at a given temperature. The middle peak, on the other hand, must be a result of both melting of the crystals formed during the cooling process and recrystallization of smaller, imperfect crystals into more stable and thicker lamellae. The same observation was given for nylon10 14[25]. When nylon 10 14 was isothermally crystallized from the glassy state, three distinct peaks were observed. Two lower endotherms were attributed to different thicknesses and perfection of the crystals formed during isothermal crystallization. The position of the main melting endotherm was constant regardless of the isothermal crystallization temperature.

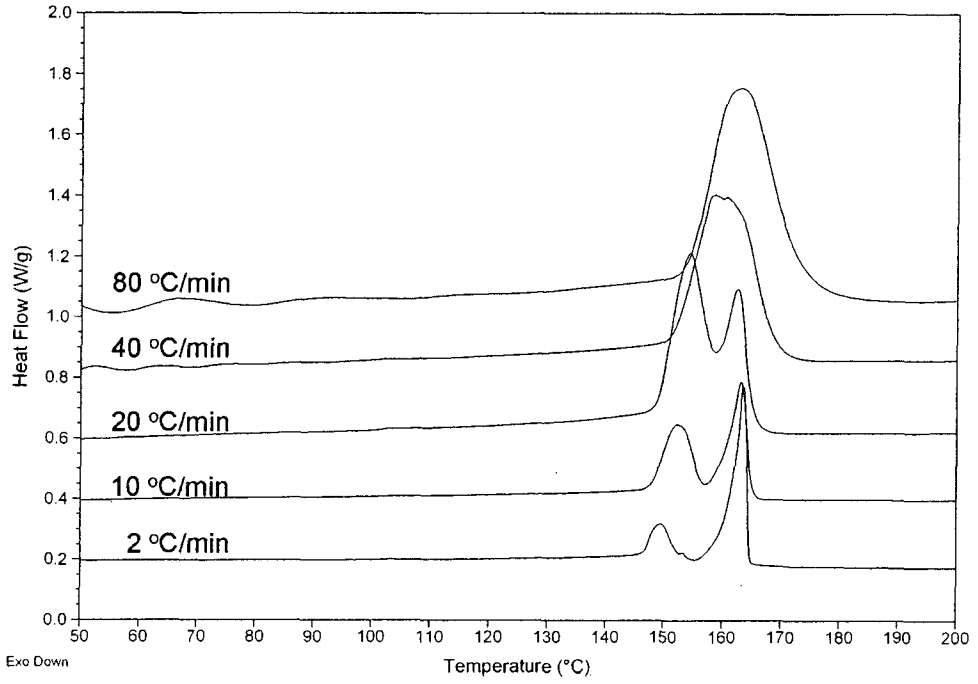

Figure 5.5. DSC thermograms of nylon18 18 annealed at 145 °C for 2 h and scanned with different heating rates.

Table 5.3

DSC parameters of nylon 18 18 samples annealed 145 °C for 2 h and scanned with different heating rates.

Scanning rate (°C/min)	T_m1^a (°C)	T_m2^a (°C)	ΔH_m1^b (J/g)	ΔH_m2^b (J/g)	ΔH_m^c (J/g)
2	149	163	13	50	84
10	152	163	31	35	81
20	154	162	46	13	74
40	158	160	-	-	76
80	163	163	-	-	71

[a] melting point of lower and higher endotherms
[b] heat of fusion of lower and higher endotherms
[c] total heat of fusion (the beginning of the melting was taken as 110 °C)

Figure 5.5 shows DSC traces of PA1818 sampled annealed at 145 °C for 2 h with heating rates in the range of 2 to 80 °C/min. As the heating rate was increased, the lower endothermic peak shifted to higher temperature and the area under this endotherm gradually increased. On the other hand, the higher melting peak shifted to lower temperature and decreased in size with increasing heating rate. This behavior can be explained by simultaneous melting, recrystallization and then melting of recrystallized lamellas. With increasing heating rate, the time needed for reorganization was restricted. With a heating rate of 40 °C/min, the two endotherms almost merged into a single peak. The peak position is between the two initial endotherms.

This, same behavior was discussed for several different polymers. The melting mechanism proposed by Runt[26] to account for the heating rate dependence of melt-crystallized poly(caprolactone)/poly(styrene-co-acrylonitrile) is well suited the melting behavior of nylon 18 18 with varied heating rates. If the heating rate increased even more, the peak shifted to higher temperature. This can be explained by the low thermal conductivity of the polymer.

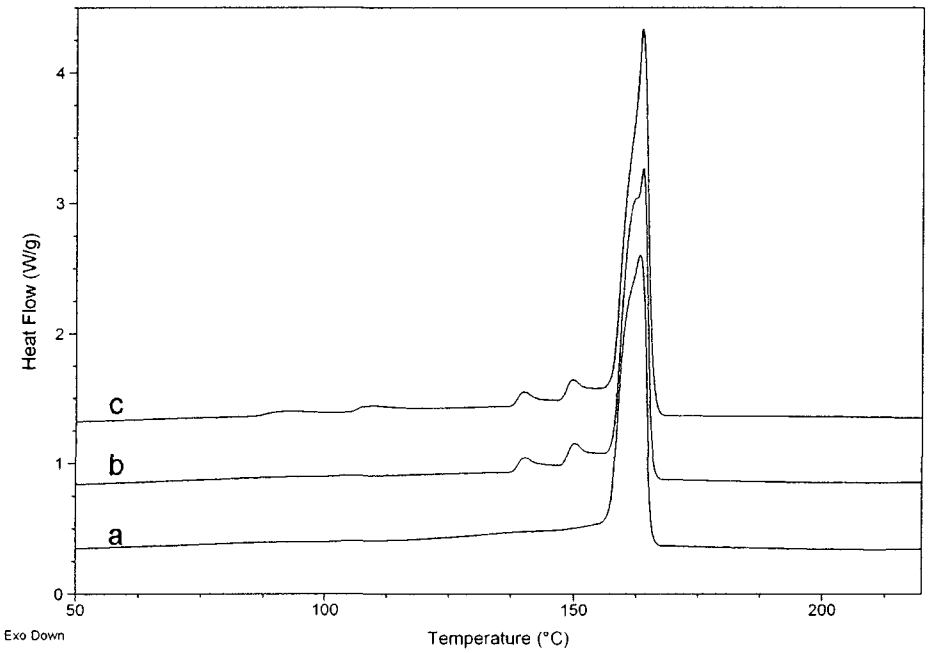

Figure 5.6. DSC thermograms of nylon18 18 sequentially annealed a) 80 °C, 100 °C, 135 °C, 145 °C, and finally 155 °C for 2 h each, b) first 155 °C then 145 °C, and 135 °C for 6 h each, and c) first 155 °C then 145 °C, 135 °C, 100 °C, and 80 °C for 2 h each.

Figure 5.6 shows the DSC curves for the stepwise annealed samples of nylon 18 18. The top thermogram is of the sample first annealed at 155 °C for two hours and then progressively annealed at 145, 135,100, and 80 °C for another two hours at each annealing temperature. The sample annealed first at 155 °C for two hours and then progressively annealed at 145 and 135 °C for six hours gave the middle thermogram. After the stepwise annealing of the sample at lower temperatures, multiple melting endotherms were observed and the number of melting endotherms was dependent on the number of annealing steps with the number of endothermic peaks increasing with the number of annealing steps. The bottom thermogram was of the sample annealed progressively at

80,100, 135, 145, and 155 °C for two hours. It showed only a main endothermic peak due to the fact that the crystals formed during lower annealing steps transformed to thicker lamellae with each step. It is noteworthy to mention that the main melting peak was almost invariant for both annealing process, and the heat of fusion for the thinner lamella was much lower compared to those samples at specific temperature.

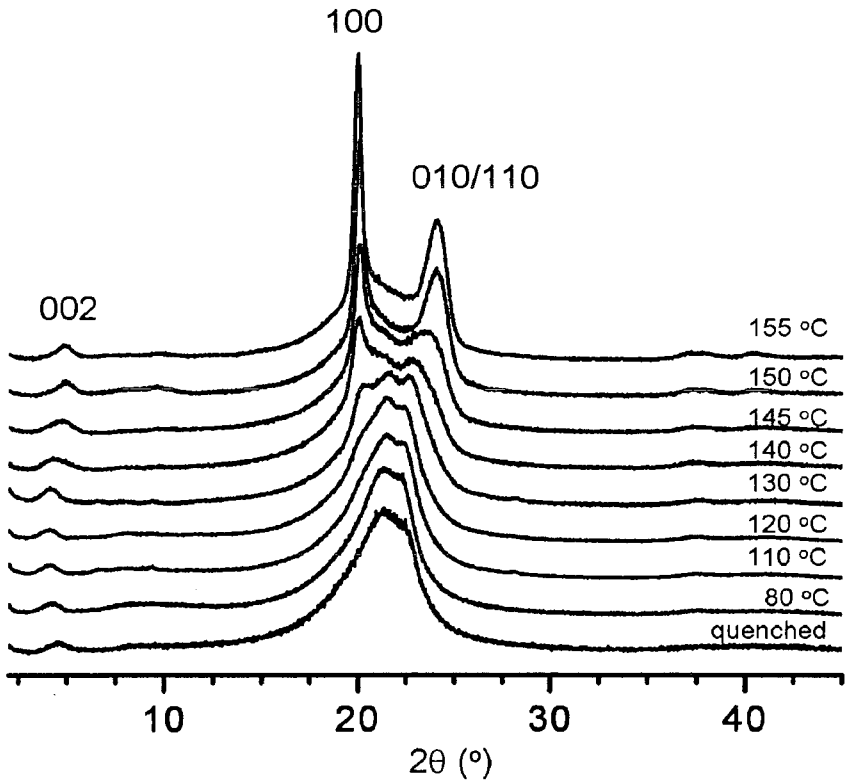

Figure 5.7. The WAXD patterns of the nylon 18 18 annealed at various temperatures for 2 h from bottom to top: quenched, 80, 110, 120, 130, 140, 145, 150, and 155 °C.

A series of WAXD patterns, recorded at room temperature, of the annealed nylon 1818 at various temperatures for 2 h is shown in Figure 5.7. The sample quenched from the molten state without further thermal treatment is also presented for comparision. The quenched sample shows only an amorphous

halo. The samples annealed up to 130 °C show partially ordered structures but still are mostly amorphous. Once the annealing temperature reaches 140 °C, two new diffraction peaks appeared at 0.44 and 0.37 nm which are characteristic peaks of the α-form (triclinic structure) of even-even nylons. The (100) and (010) planes (which represent the interchain spacing within the hydrogen-bonded sheets and intersheet spacing, respectively) continuously separate as the annealing temperature increases. The intensity of the diffraction peaks also increases with increasing annealing temperature. This suggests that the crystals become more perfect as the degree of crystallinity increases.

Nylons can show different crystalline forms and can exhibit crystal-crystal transitions.[27,28,29] The WAXD patterns of nylon 11[28], for instance, show α to δ and again to α transition with prolonged annealing time. Nylon 12 12[29] was reported to give a strong diffraction peak at 0.42 nm, characteristic of a pseudo-hexagonal structure (or γ form), but once crystallized at 90 °C from the melt, the γ form was transformed to the α form. No x-ray polymorphism was observed for nylon 18 18 during annealing, which suggests only one type of crystalline form develops for this polymer. Therefore, the multiple melting endotherms are not related to different crystalline structures but are a result of the melting of α form crystallites of different size and perfection. Finally, hydrogen bonding is still the most important factor controlling the crystal morphology of this nylon even with its low amide density.

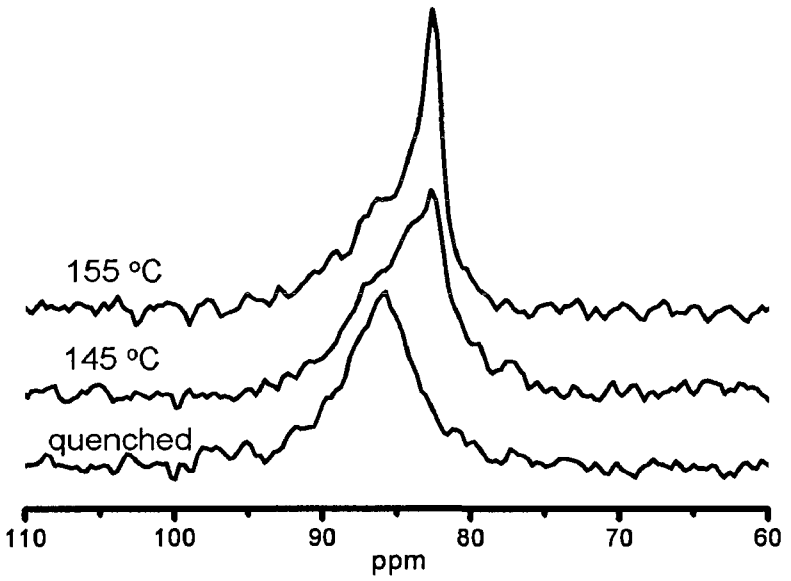

Figure 5.8. The solid state ^{15}N CP/MAS NMR spectrum of nylon 18 18 samples a) quenched, b) annealed at 145 °C, and c) annealed at 155 °C for 2 h.

Previous works by our group on various A-B and AA-BB nylons has shown that the chemical shift of the amide nitrogen is determined by crystalline form.[30,31,32,33] The α form gives a chemical shift at ~84 ppm, whereas the γ form gives a chemical shift around ~89 ppm. Most other nylon X 18 where X is even possess α form crystallinity, the thermodynamically stable form for even-even nylons. However, the even-even nylons *X* 18 previously reported show a trend toward higher amorphous content as the aliphatic content increases. Quenched nylon 18 18 gives a broad peak resulting from a highly amorphous system, with a peak value at 86 ppm (Figure 5.8). Once the sample is annealed at 145 °C for 2 h, a new peak appears at 84 ppm associated with the α structure. The peak intensity increases while the amorphous peak decreases when the sample is

annealed at 155 °C for 2 h. This result is consistent with the WAXD patterns of Figure 5.7.

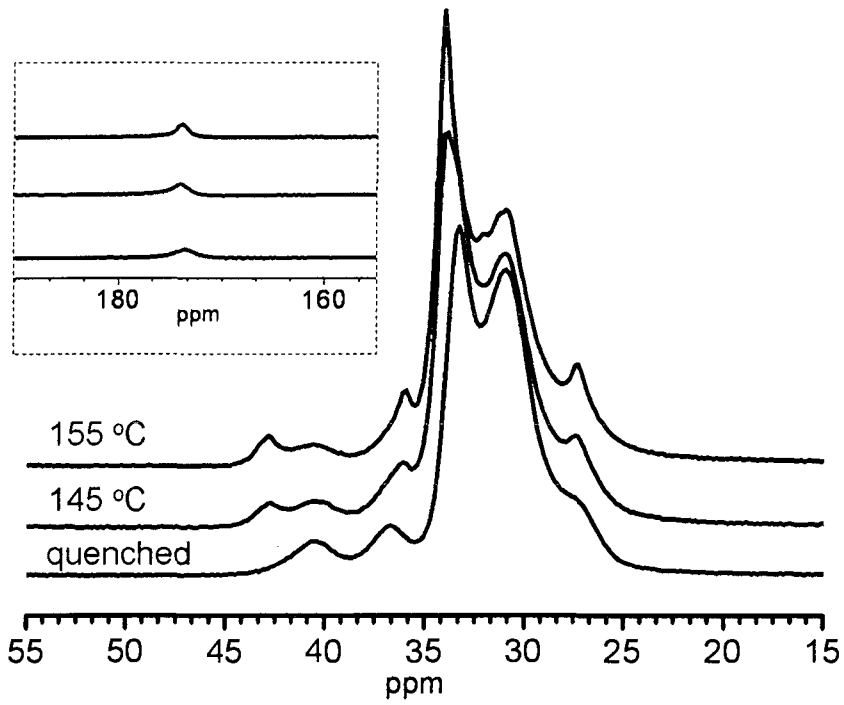

Figure 5.9. The solid state ^{13}C CP/MAS NMR spectrum of nylon 18 18 samples a) quenched, b) annealed at 145 °C, and c) annealed at 155 °C for 2 h.

The solid state ^{13}C CP/MAS NMR spectrum of the nylon 18 18 samples, neat, annealed at 145 °C, and at 155 °C, are shown in Figure 5.9. The peak at 173.5 ppm of carbonyl group is shifted to 173.9 ppm on annealing. The aliphatic regions, on the other hand, showed significant changes, especially for those carbons α to the amide nitrogen. There is one broad peak at 40.5 ppm for quenched nylon 18 18. After annealing at 145 °C, a new peak is seen at 42.9 ppm for highly crystalline regions which shifted even further and became more distinct once the sample is annealed at 155 °C. The peak at 40.5 ppm can be still

observed, but the intensity of this peak is much smaller compared to the quenched sample. Similar sharpening is seen for the all-trans polymethylene peak at 33-35 ppm and the β-CH_2 to carbonyl peak at 25-26 ppm. The peaks are narrower for the annealed samples due to the fact that increasing crystallinity leads to less conformational disorder and narrower peaks.

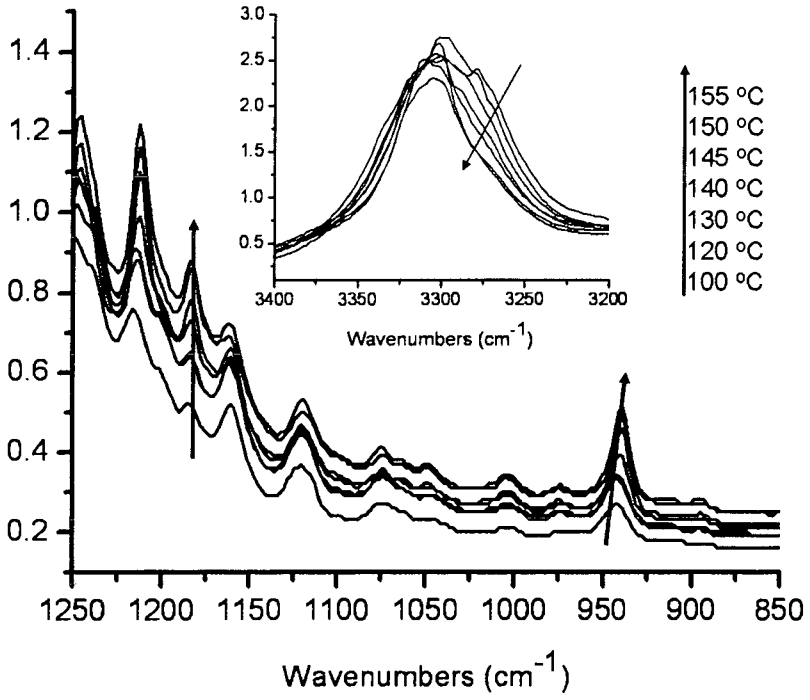

Figure 5.10. Partial FTIR spectrum of annealed nylon 18 18 with increasing annealing temperature (arrows indicate direction of increasing temperature).

FTIR spectra of annealed nylon 18 18 are given in Figure 5.10. For comparison, the same sample was used throughout the annealing process. The band at 942 cm^{-1} (amide IV, C-CO stretching mode)[27] is related to the crystalline region of the polymer. On annealing, this peak shifts to 939 cm^{-1} and becomes

more narrow as a result of restricted conformational motions of the amide group in the crystalline regions. The band at 1184 cm^{-1} is due to stretching vibration mode of C-C bonds.[27] There is no significant change on this band up to 130 °C. Once the annealing temperature reaches 140 °C, the intensity of this band is much higher and narrower. The band around 3305 cm^{-1} is due to the stretching vibration of NH groups (amide A),[34] and can be related to hydrogen bonding.[27] Enhanced vibration as a result of conformational disorder leads to a broader band, while an ordered structure will result in narrowing of this band. For nylon 18 18 samples, the annealing process lead to narrowing of this band as well as giving a more defined peak.

Conclusions

The melting behaviors and crystal structures of a long alkyl chain polyamide, nylon 18 18, were investigated under annealing and isothermal crystallization conditions. Nylon 18 18 showed multiple melting peaks in DSC thermograms depending on the thermal history of the samples. The annealed samples posses only α-form crystals which was confirmed by WAXD patterns and solid state ^{15}N CP/MAS NMR spectrum of the nylon 18 18. The multiple endotherms can be explained by the hypothesis that the origin of the multiple melting peaks may be as a result of the melting and recrystallization mechanism during DSC scans. Finally, hydrogen bonding is still the most important factor controlling the crystal morphology of this nylon even with its low amide density.

References

1 Bennett, Carl; Mathias, Lon J. Synthesis and Characterization of Polyamides Containing Octadecanedioic Acid: Nylon 2 18, Nylon 3 18, Nylon 4 18, Nylon 6 18, Nylon 8 18, Nylon 9 18, and Nylon 12 18. *J. Polym. Sci., Part A: Polym. Chem.*, **2005**, 43, 936-945.

2 Ehrenstein, M.; Dellsperger, S.; Kocher, C.; Stutzmann, N.; Weder, C.; Smith, P. New Polyamides with Long Alkane Segments: Nylon 6 24 and 6 34. *Polymer*, **2000**, 41, 3531-3539.

3 Bennett, Carl; Mathias, Lon J. Linear unsaturated polyamides: Nylons 6 u18 and 18 u18. *Macromol. Chem. Phys.*, **2004**, 205, 2438-2442.

4 Cui, Xiaowen; Li, Weihua; Yan, Deyue; Yuan, Cuiming; Di Silvestro, Giuseppe. Synthesis and Characterization of Polyamides X 18. *J. Appl. Polym. Sci.*, **2005**, 98, 1565-1571.

5 Ehrenstein, Moritz; Smith, Paul; Weder, Christoph. Polyamides X 34: A New Class of Polyamides with Long Alkane Segments. *Macromol. Chem. Phys.*, **2003**, 204, 1599-1606.

6 Ehrenstein, Moritz; Sikorski, Pawel; Atkins, Edward; Smith, Paul. Structures of X 34 Nylons in Chain-folded Lamellae and Gel-Spun Fibers. *J. Polym. Sci.: Part B: Polym. Phys.*, **2002**, 40, 2685-2692.

7 Cui, Xiaowen; Li, Weihua; Yan, Deyue. A Study of the Crystalline Transitions of Polyamides X 18. *Polymer International*, **2004**, 53, 2031-2037.

8 Li, Weihua; Yan, Deyue. Crystal Structures of Polyamides X 18 Made from Long Alkyl Dicarboxylic Acid. *Cryst. Growth Des.*, **2006**, 6, 2182-2185.

9 Flores, A.; Pieruccini, M.; Noechel, U.; Stribeck, N.; Balta Calleja, F. J. Recrystallization Studies on Isotropic Cold-Crystallized PET: Influence of Heating Rate. *Polymer*, **2008**, 49, 965-973.

10 Tanaka, Nobuyuki. Two Equilibrium Melting Temperatures and Physical Meaning of DSC Melting Peaks in Poly(ethylene terephthalate). *Polymer*, **2008**, 49, 5353-5356.

11 Sweet, G. E.; Bell, J. P. Multiple Endotherm Melting Behavior in Relation to Polymer Morphology. *J. Polym. Sci., Polym. Phys. Ed.*, **1972**, 10, 1273-83.

12 Yeh, J. T.; Runt, J. Multiple Melting in Annealed Poly(butylene terephthalate). *J. Polym. Sci.: Part B: Polym. Phys.*, **1989**, 27, 1543-1550.

13 Kim, Junkyung; Nichols, Mark E.; Robertson, Richard E. The Annealing and Thermal Analysis of Poly(butylene terephthalate*). J. Polym. Sci.: Part B: Polym. Phys.*, **1994**, 32, 887-899.

14 Lee, Youngchul; Porter, Roger S. Double-melting Behavior of Poly(ether ether ketone). *Macromolecules,* **1987**, 20, 1336-1341.

15 Lee, Youngchul; Porter, Roger S.; Lin, J. S. On the Double-Melting Behavior of Poly(ether ether ketone). *Macromolecules,* **1989**, 22, 1756-1760.

16 Ko, Tong Y.; Woo, E. M. Changes and Distribution of Lamellae in the Spherulites of Poly(ether ether ketone) upon Stepwise Crystallization. *Polymer,* **1996**, 37, 1167-1175.

17 Yang, Jun; Liu, Shue; Guo, Xingyuan; Luan, Yucheng; Su, Wenhui; Liu, Jingjiang. Annealing of Nylon 10 10 under High Pressure. *Macromol. Chem. Phys.,* **2002**, 203, 1081-1087.

18 Franco, Lourdes; Puiggali, Jordi. Structural Data and Thermal Studies on Nylon 12 10. *J. Polym. Sci.: Part B: Polym. Phys.*, **1995**, 33, 2065-2073.

19 Yen, Kai C.; Woo, Eamor M. Thermal, Spectroscopy, and Morphological Studies on Polymorphic Crystals in Poly(heptamethylene terephthalate). *Polymer,* **2009**, 50, 662-669.

20 Ishikawa, Toshihiko; Nagai, Susumu; Kasai, Nobutami. Thermal Behavior of α Nylon12. *J. Polym. Sci., Polym. Phys. Ed.,* **1980**, 18, 1413-1419.

21 Cheng, Stephen Z. D.; Cao, M. Y.; Wunderlich, Bernhard. Glass Transition and Melting Behavior of Poly(oxy-1,4-phenyleneoxy-1,4-phenylenecarbonyl-1,4-phenylene) (PEEK). *Macromolecules*, **1986**, 19, 1868-1876.

22 Blundell, D. J. On the Interpretation of Multiple Melting Peaks in Poly(ether ether ketone). *Polymer*, **1987**, 28, 2248-2251.

23 Li, Qing-guo; Xie, Bang-Hu; Yang, Wei; Li, Zhong-Ming; Zhang, Wei-qin; Yang, Ming-Bo. Effect of Annealing on Fracture Behavior of Poly(propylene-block-ethylene) Using Essential Work of Fracture Analysis. *J. Appl. Polym. Sci.*, **2007**, 103, 3438-3446.

24 Van Krevelen, D.W. Properties of Polymers, 3rd ed; Elsevier: New York, **1990**.

25 Li, Yongjin; Yan, Deyue; Zhang, Guosheng. Crystalline Structure and Thermal Behavior of Nylon 10 14. *J. Polym. Sci.: Part B: Polym. Phys.*, **2003**, 41, 1422-1427.

26 Rim, Peter B.; Runt, James P. Melting Behavior of Crystalline/Compatible Polymer Blends: Poly(ε -caprolactone)/Poly(styrene-co-acrylonitrile). *Macromolecules*, **1983**, 16, 762-768.

27 Cui, Xiaowen; Yan, Deyue. Polymorphism and Crystalline Transitions of the Novel Even-odd Nylons Derived from Undecanedioic Acid. *J. Polym. Sci.: Part B: Polym. Phys.*, **2005**, 43, 2048-2060.

28 Zhang, Q.; Mo, Z.; Zhang, H.; Liu, S.; Cheng, S. Z. D. Crystal Transitions of Nylon 11 under Drawing and Annealing. *Polymer*, **2001**, 42, 5543-5547.

29 Song, Jianbin; Zhang, Huiliang; Ren, Minqiao; Chen, Qingyong; Sun, Xiaohong; Wang, Shuyun; Zhang, Hongfang; Mo, Zhishen. Crystal Transition of Nylon 12 12 under Drawing and Annealing. *Macromolecular Rapid Communications,* **2005**, 26, 487-490.

30 Mathias, Lon J.; Davis, Rick D.; Jarrett, William L. Observation of α and γ Crystal Forms and Amorphous Regions of Nylon 6-Clay Nanocomposites Using Solid State ^{15}N Nuclear Magnetic Resonance. *Macromolecules*, **1999**, 32, 7958-7960.

31 Johnson, C. Gregory; Cypcar, Christopher C.; Mathias, Lon J..^{13}C and ^{15}N Solid State NMR of Copolymers of Nylons 6 and 7: Observation of a Stable Pseudohexagonal Phase. *Macromolecules*, **1995**, 28, 8535-8540.

32 Johnson, C. Gregory; Mathias, Lon J.. Nylon 13 13 Analysis by X-ray and Solid State NMR: Treatment-dependent Crystal Forms. *Polymer,* **1993**, 34, 4978-4981.

33 Powell, Douglas G.; Sikes, Allison M.; Mathias, Lon J. Natural-abundance Nitrogen-15 CPMAS NMR of Solid Polyamides: A Technique Sensitive to Composition and Conformation in the Solid State. *Polymer,* **1991**, 32, 2523-2533.

34 Skrovanek, Daniel J.; Painter, Paul C.; Coleman, Michael M. Hydrogen Bonding in Polymers. 2. Infrared Temperature Studies of Nylon 11. *Macromolecules,* **1986**, 19, 699-705.

CHAPTER VI

PREPARATION, CHRACTERIZATION, AND COPOLYMERIZATION OF 12-MEMBERED CYCLIC DIAMIDE: 1,6-DIAZACYCLODODECANE-2,5-DIONE

Abstract

The 12-membered cyclic diamide was successfully synthesized with a fairly high yield (~ 45%). The synthesis conditions were varied to see the affect of the reactants on yield. Three fold excess HDA gave the highest yield, while further increasing the amount of HDA decreased the yield. Using diisopropylethylamine (DPEA) as acid scavenger resulted in formation of two different cyclic diamides which were fully analyzed by ^{1}H and ^{13}C solution NMR, and mass spectrometry. Copolymerization of cyclic diamides with ε-caprolactam via an anionic route gave a block copolyamide with a two distinct endotherms in the DSC analysis. However, copolymerization by the hydrolytic route gave only nylon 6 with a terminal 6 4 units.

Introduction

Cyclic amides are research topic of polymer science for two main reasons; they are either part of step-growth polymerization as a minor component, or they are used for ring-opening polymerization.[1] Cyclic diamide can be obtained in several ways including direct cyclization of dicarboxylic acid derivatives with a diamine,[2,3,4] depolymerization of polyamides,[5] and rearrangement of another cyclic.[6] One of the complication of homopolymerization of cyclic diamides are that they usually have high melting points especially those with small rings which may be very close to degradation temperatures.[7]

Nylon 6 4 is of interest because of its high melting point compared to commercial nylon 6 6. Unlike nylon 4 6 which has been commercialized by DSM under the trade name Stanyl®,[8] nylon 6 4 has not been manufactured possibly due to the side reactions which inhibits to obtain high molecular weight polymer via polycondensation reaction. Therefore, an alternate route to obtain high molecular nylon 6,4 is still needed. Ring-opening polymerization of the 12-membered cyclic monomer of nylon 6 4 may be an alternative way to obtain a high molecular weight homo, or copolymers of nylon 6 4.

Herein, we reported the synthesis and characterization of the 12-membered cyclic diamide; 1,6-diazacyclododecane-2,5-dione. The affect of the reactant on yield and products was studied. Ring opening reactivities of this cyclic diamide were also explored. For this purpose, copolymerization of the 12-membered cyclic diamide with caprolactam was investigated with different ring opening polymerization methods.

Experimental

Materials. All reagents were used as received. Succinyl chloride, N,N-diisopropylethylamine (DPEA), 4-dimethylaminopyridine (DMAP), succinic anhydride, *N*-acetylcaprolactam, 2,2,2-trifluoroethanol (TFE), and choloroform-d were purchased from Aldrich. 1,6-Hexamethylene diamine (HDA) and chloroform was purchased from Fluka. ε-Caprolactam purchased from ACROS was recrystallized from acetone and the crystals were dried at 70°C under reduced pressure overnight before use.

Instrumentation and techniques. Routine solution ^{13}C nuclear magnetic resonance (NMR) was performed on a Varian *Mercury*^{PLUS} 200 and 500 MHz spectrometer. Transmission Infrared measurements were carried out on a Mattson Galaxy Series FTIR 5000 using KBr as reference and 256 transients. Differential scanning calorimetry (DSC) experiments were performed on a TA Instruments 2920. The temperature was ramped at a heating rate of 10 °C/min under nitrogen.

Wide angle X-ray diffraction (WAXD) measurements were obtained with a Rigaku Ultima III diffractometer operated at 40 kV and 44 mA. Powder samples were run with a scan speed of 2° per minute from 2 to 45°.

The molecular weight of cyclic diamide I and II were determined by a ThermoFisher LXQ Ion-Trap instrument running in positive mode. The samples were prepared by placing ~10 mg of cyclic diamide I or II in an Eppendorf tube and 1 mL of 1:1 THF:MeOH with NaCl was added. The sample was vortexed for 1 minute to ensure a homogenous solution. 100 uL of this sample was then

diluted to 1 mL with 900 uL of the 1:1 THF:MeOH NaCl solution (the NaCl concentration in the THF:MeOH is approx. 1 uM), The diluted sample was then infused into the spectrometer at a rate of 10 uL/min to observe a stable spectrum. The spectrum was then optimized on the sodium adduct of cyclic diamide I or II using the autotune function in the XCalibur software which controls the instrument. The final spectra are the average of several collected spectra.

Synthesis of 1,6-diazacyclododecane-2,5-dione. The procedures for synthesis of the cyclic monomers are given for sample 4. All other samples were synthesized using the same procedure except the ratio of reactant or the amounts of solvent were varied. Hexamethylenediamine (HDA) (2.16 g, 116 g/mol), N,N-diisopropylethylamine (DPEA) (4.38g, 129.24 g/mol), and 4-dimethylaminopyridine (DMAP) (0.2 g, 122.17 g/mol) were dissolved in 50 mL chloroform and charged to a syringe. A second syringe was charged with succinyl chloride (2.62 g, 154.98 g/mol) in 50 mL chloroform. These two syringes were placed in a syringe pump and their content added very slowly (addition rate-0.5 mL/min) to 500 mL chloroform in a three-necked round bottom flask under nitrogen. After the reaction was complete, the precipitant was removed by filtration. Solvent was removed under reduced pressure at 50 ^{o}C and the remaining solid was washed with acetone several times. The final product was obtained as white powder. It was recrystallized from acetonitrile. The melting point of the 12-membered cyclic diamide was obtained as 290 ^{o}C by using DSC.

Synthesis of HAD-bisimide. Hexamethylene diamine (HDA) (34 mmol, 116 g/mol) and succinic anhydride (72 mmol, 100.07 g/mol) were dissolved in 20 mL

ionized water. The mixture was refluxed for 2 h and then vacuum (to remove water) was applied while the temperature increased to 150 °C. The reaction was carried out for another 2 h. After completion, the crude product was allowed to cool down to room temperature and washed with water several times. After filtration, the crude product was recrystallized from water twice which gave the final product as white crystals in 70% yield. ^{13}C NMR (200 MHz, TFE:$CDCl_3$): 179.1, 38.2, 27.5, 26.6, 25.7 ppm.

Synthesis of HAD-bisamide acid. Hexamethylene diamine (HDA) (34 mmol, 116 g/mol) and succinic anhydride (136 mmol, 100.07 g/mol) were dissolved in 100 mL ionized water. The mixture was stirred at room temperature for 6 h. After the reaction was complete, the precipitant was removed by filtration, and washed with hot water several times. After washing with acetone one more time, the final product was allowed to dry in a vacuum oven overnight. The product was obtained as white powder in 50% yield. ^{13}C NMR (200 MHz, TFE:$CDCl_3$): 176.8, 174.4, 39.8, 30.3, 29.5, 28.6, 26.1 ppm.

Synthesis of copolymer nylon (6-co-64) via the anionic polymerization method. Caprolactam (2 g) and 10 w-% cyclic diamide (0.2 g) were charged to a test tube. Another test tube was charged with caprolactam (0.3 g) and dry sodium hydride (0.2 g). Nitrogen was bubbled through both test tubes for 15 min before heating. Both test tubes were placed in a previously heated oil bath at 140 °C. After melting, 0.3 mL *N*-acetylcaprolactam was added to caprolactam/cyclic diamide mixture by a syringe and the mixture was allowed to stir for another 10 min. The caprolactam/sodium hydride mixture was then added

to this mixture, and the reaction was carried out at 145 °C until it solidified. The product was allowed to cool down to room temperature under nitrogen, and was then powdered and washed with refluxing ethanol overnight to remove unreacted monomers. After washing with ethanol one more time, the final product was dried in a vacuum oven for 12 h at 100 °C.

Synthesis of copolymer nylon (6-co-64) via hydrolytic polymerization method. Caprolactam (2 g), 10 w-% cyclic diamide (0.2 g), 10 mol-% aminocaproic acid, and 1 mL ionized water were charged to a test tube. Nitrogen was bubbled through the mixture for 15 min before heating. The temperature was maintained at 250 °C for 4 h in a sand bath. The product was allowed to cool down to room temperature under nitrogen, and was then powdered and washed with refluxed ethanol overnight to remove unreacted caprolactam and cyclic diamide. After washing with ethanol on more time, the final product was dried in a vacuum oven for 12 h at 100 °C.

Results and Discussion

The synthetic scheme for the 12-membered cyclic diamide is given in Scheme 6.1. The synthesis of cyclic diamides of diamines and diacid chlorides is usually obtained with high-dilution methods or slow addition of reactants into a solvent to decrease the possibility of linear oligomer or polymer formation.[3]

Scheme 6.1. Synthesis of 1,6-diazacyclododecane-2,5-dione.

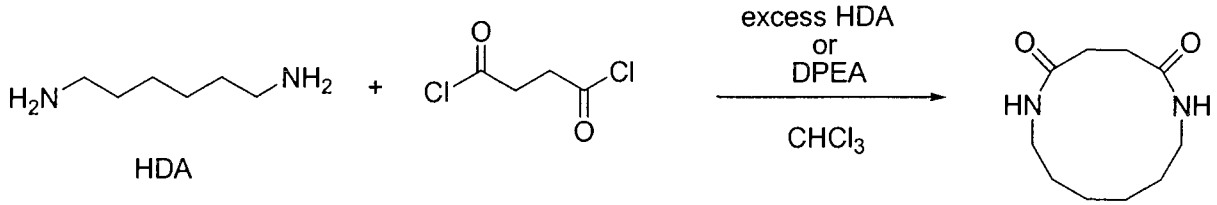

It was of interest here to explore the affect of reactants, ratio of reactants, and amount of solvent used for synthesis of the 12-membered cyclic diamide on yield. For this purpose, the amount of succinyl chloride was kept almost constant (~ X=13 mmol) and the amount of the other reactants was changed with respect to the succinyl chloride. The data are given in Table 6.1. The best yield was obtained for the samples numbered 1 and 3. The catalyst, DMAP, somehow inhibited the cyclization. Three fold-excess of HDA gave the best yield. Increasing HDA concentration even further decreased the yield of the cyclic diamide, possibly due to increasing probability that one succinyl chloride could react with two HDA leading to a linear monomer.

Table 6.1.

Synthesis of 1,6-diazacyclododecane-2,5-dione.

Sample	HDA	Succinyl chloride	Chloroform (mL)	DPEA	DMAP	Yield-%
1	3X	X	500	-	-	45
2	5X	X	500	-	-	26
3	X	X	500	2X	-	42
4	X	X	500	2X	0.1X	12
5	3X	X	1000	-	-	40
6	X	X	1000	2X	-	32

The 12-membered ring cyclic diamide obtained as a white powder is not soluble in chloroform; therefore a TFE:$CDCl_3$ mixture was used for NMR analysis. ^{13}C solution NMR of 1,6-diazacyclododecane-2,5-dione in TFE:$CDCl_3$ is given in Figure 6.1. The carbonyl carbon peak of the cyclic amide appears at 173.3 ppm. This peak and the peak assigned as "a" are a good indication of the absence of the linear compounds in the final product.

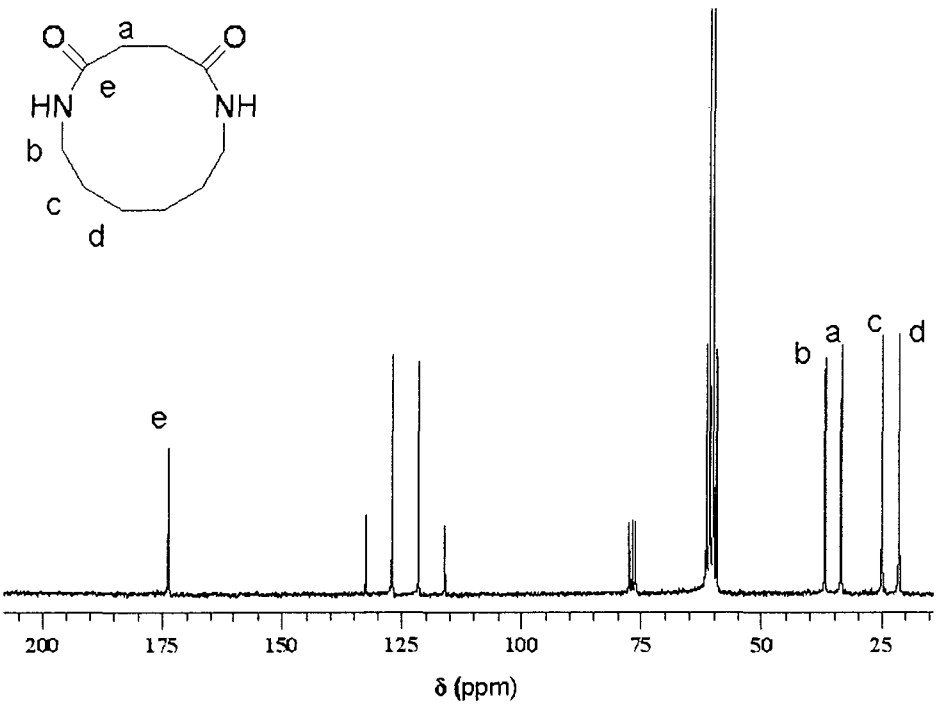

Figure 6.1. ^{13}C solution NMR spectrum of 1,6-diazacyclododecane-2,5-dione. The sample was dissolved in TFE:$CDCl_3$.

The ^{1}H solution NMR spectrum of 1,6-diazacyclododecane-2,5-dione is given in Figure 6.2. All peaks are assigned based on the molecular structure expected for the cyclic diamide. The amide NH can be seen around 6.6 ppm and there is a small shoulder of this peak at 6.9 ppm. The protons α to the amide NH

can be observed at 3.3 ppm, and this peak also has a small shoulder around 3.2 ppm. The shoulder may be related with a higher order macrocycle formation which cannot be observed easily with ^{13}C solution NMR.

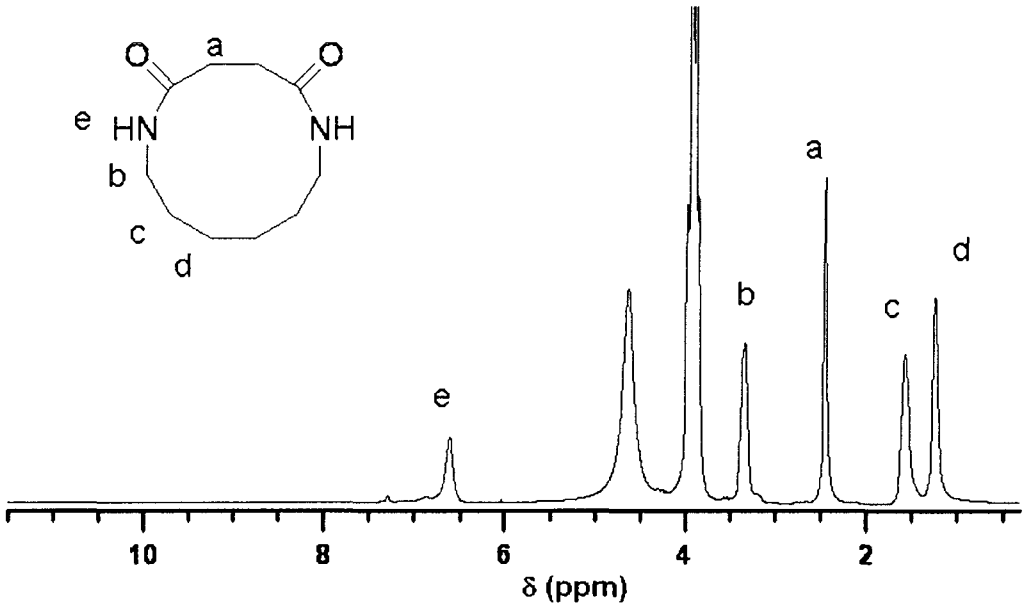

Figure 6.2. ^{1}H solution NMR of 1,6-diazacyclododecane-2,5-dione. The sample was dissolved in TFE:$CDCl_3$.

The infrared spectra for the 12-membered cyclic diamide made here displayed the characteristic peaks of amide groups and methylene groups, as shown in Figure 6.3. Peaks were found at 3313 cm^{-1} (N-H stretching), 3095 cm^{-1} (overtone of N-H in-plane bending), 2834-3000 cm^{-1} (C-H stretching), 1644 cm^{-1} (C=O stretch), 1538 cm^{-1} (C-N stretch and CO-N-H bend).[9]

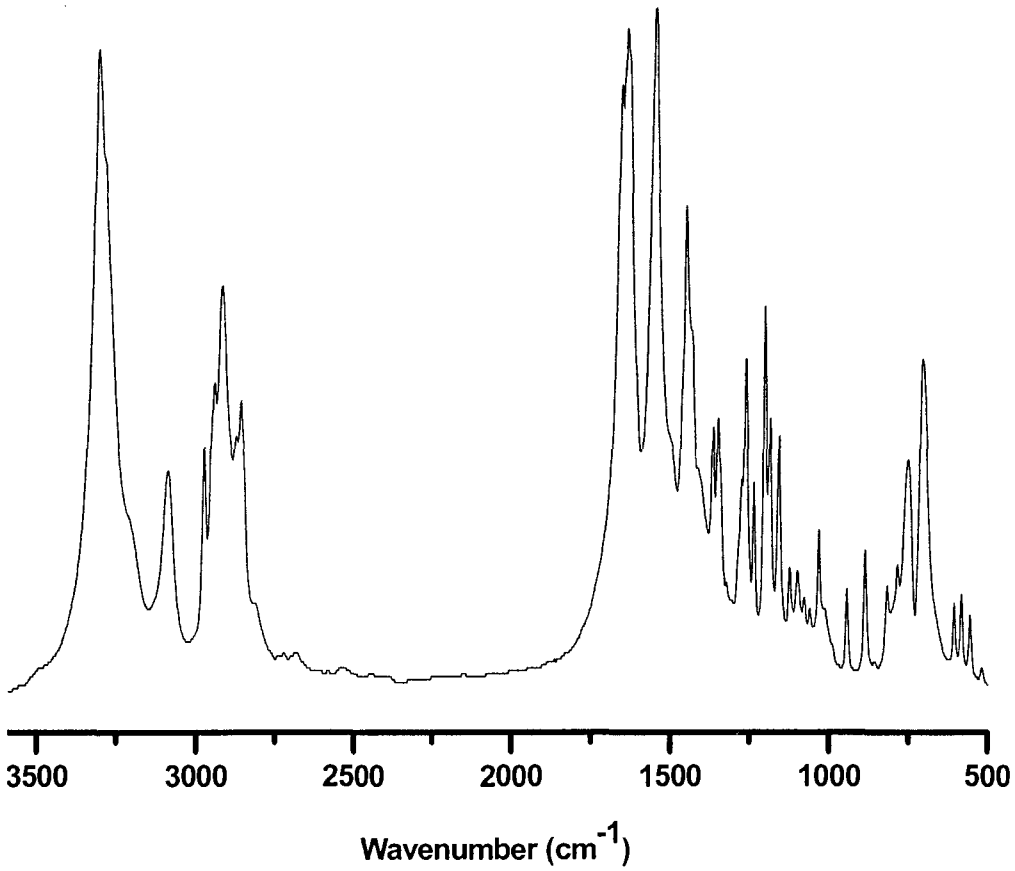

Figure 6.3. FTIR spectrum 1,6-diazacyclododecane-2,5-dione.

For the reaction of HDA with succinyl chloride, only one kind of cyclic product is obtained. The second product, which gives a peak around 6.9 ppm in the ^{1}H NMR spectrum, was speculated as being due to higher order cyclics formation. However, the same reaction with DPEA gives a 50/50 mixture of cyclic diamide I and cyclic diamide II. Cyclic diamide I is the same 12-membered cyclic compound obtained without DPEA. Cyclic diamide II, on the other hand, can be obtained nearly quantitatively as a white powder with a melting point of 250 °C after recrystallization of the 50/50 mixture from acetonitrile. Using mass spectrometry, the molecular weight of cyclic diamide I and cyclic diamide II were determined being 198.18 g/mol and 396.41 g/mol, respectively, corresponding to

mono- and biscyclic diamides. Triethyl amine, which is commonly used in synthesis to obtain cyclic diamide[10] instead of DPEA gives negligible yield of cyclic product. This may be due to higher reactivity of succinyl chloride compared to other aliphatic diacid chlorides.[3]

Figure 6.4 shows the ^{13}C solution NMR spectra of the mixture and cyclic diamide II in TFE:$CDCl_3$ mixture. All peaks are assigned based on the expected structures of the cyclic monomers. It can be seen that there are two set of peaks with same number of peaks of roughly equal intensities. However, the peak intensities of the carbonyl carbons are not the same, perhaps due to different relaxation times for these carbons. The peaks associated with cyclic diamide I appear exactly at the same chemical shifts as for the cyclic monomer obtained without DPEA and are assigned with the same letters. The carbonyl carbon peak of cyclic amide II appears at 173.5 ppm. Compared to cyclic diamide I, peaks related to cyclic diamide II are shifted significantly. The peak α to the amide groups of cyclic diamide I assigned as "b" (observed at 36.7 ppm) shifts to 38.4 ppm for the cyclic diamide II. A similar but upfield shift is observed for the methyl group α to the carbonyl which shifts from 34.5 to 31.4 ppm. The significant differences of chemical shifts for cyclic diamides may be a good indication of different ring strains for these two monomers.

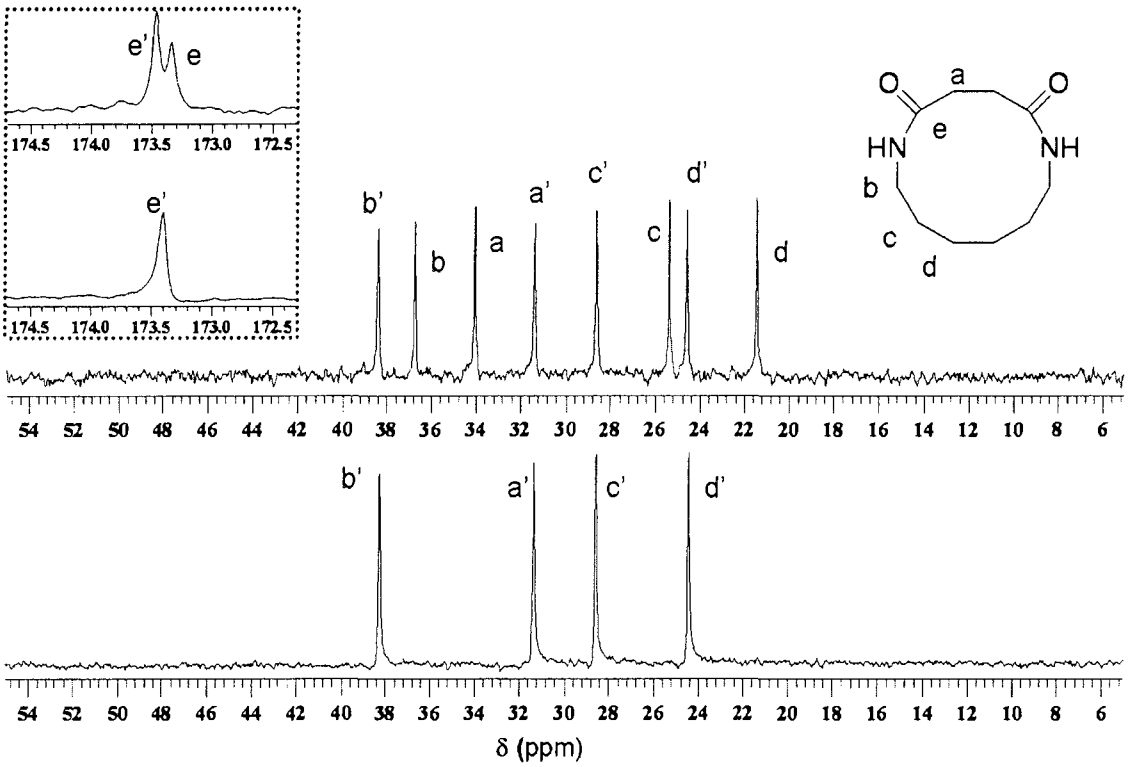

Figure 6.4. ^{13}C solution NMR of the 50/50 mixture (top) and cyclic diamide II (bottom). The sample was dissolved in TFE:$CDCl_3$.

The solution ^{1}H NMR spectra of the mixture and cyclic diamide II are given in Figure 6.5. Two sets of peaks with the same number and roughly equal intensities are also observed in the ^{1}H NMR spectra. All peaks are assigned based on the molecular structure of cyclic diamides. The peaks associated with the protons α to the amide NH, which can hardly observed in Figure 6.2, are of equal intensities. Splitting of the peaks associated the same protons of cyclic diamide I is seen at 3.3 ppm. The amide NH which can be observed around 6.6 ppm for cyclic diamide I shifts downfield to 6.9 ppm for cyclic diamide II. Similar downfield shifts were observed for various ring size cyclic oligo(undecanamide)s.[1] Hovewer, the shifts are not as pronounced for cyclic

oligo(undecanamide)s of different sizes. This may be due to the fact that the ring strain is more crucial for cyclic diamides in this study.

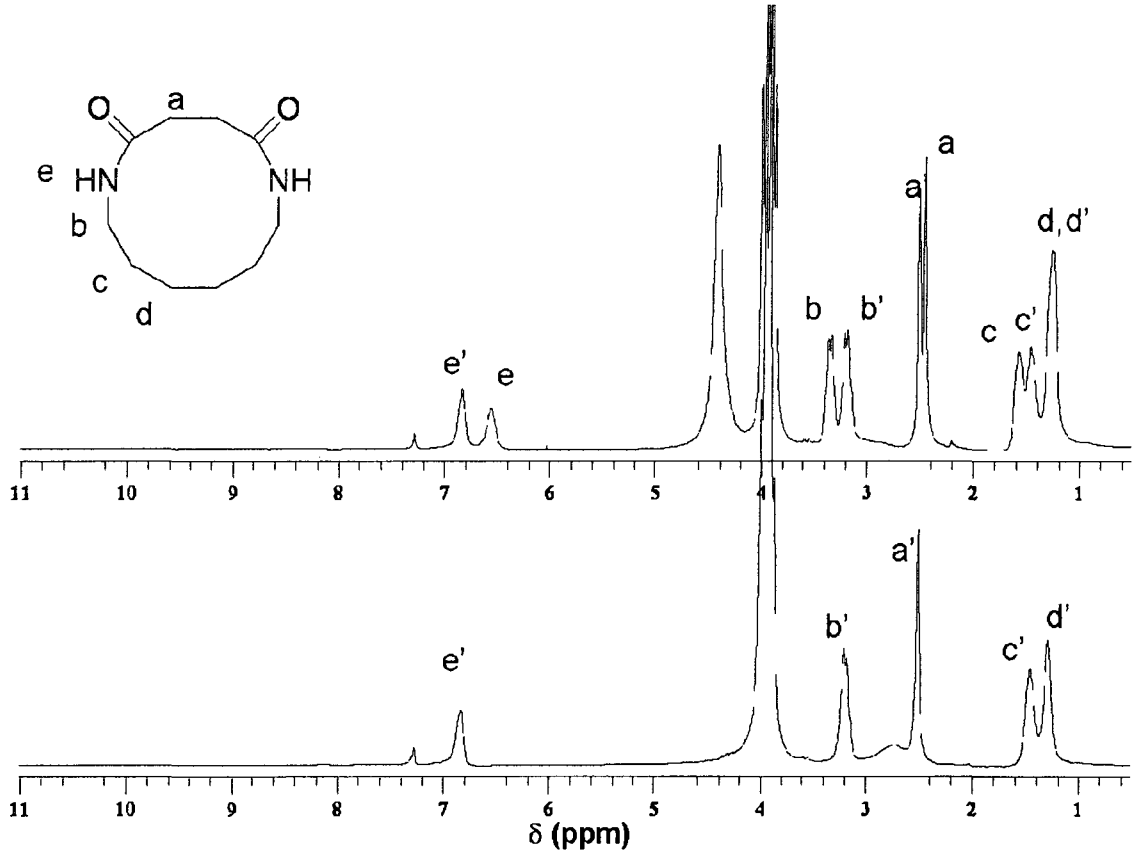

Figure 6.5. ^{1}H solution NMR of 50/50 mixture (top) and cyclic diamide II (bottom). The sample was dissolved in TFE:$CDCl_3$.

FTIR spectra of the 50/50 mixture and pure cyclic diamide II are given in Figure 6.6. As anticipated, the two spectra are almost identical with only minor differences which associated with cyclic diamide I. Most changes are observed for the stretching vibration of NH groups, as seen by comparing the FTIR spectra of cyclic diamide I (Figure 6.3) with FTIR spectra of cyclic diamide II. For cyclic diamide I, this band is narrower and shows only one peak at 3313 cm^{-1} with a small shoulder, while two peaks at 3301 and 3334 cm^{-1} are observed for the

cyclic diamide II. This band is very sensitive to hydrogen bonding and generally enhanced vibration is a result of conformational disorder which leads to a broader band, while an ordered structure will show a narrow band.[11,12] Based on the shape and frequency of this band, it may be stated that cyclic diamide I is more ordered compared to cyclic diamide II. The difference may also be related with types of inter- and intramolecular hydrogen bonding of the different cyclic structures. [2]

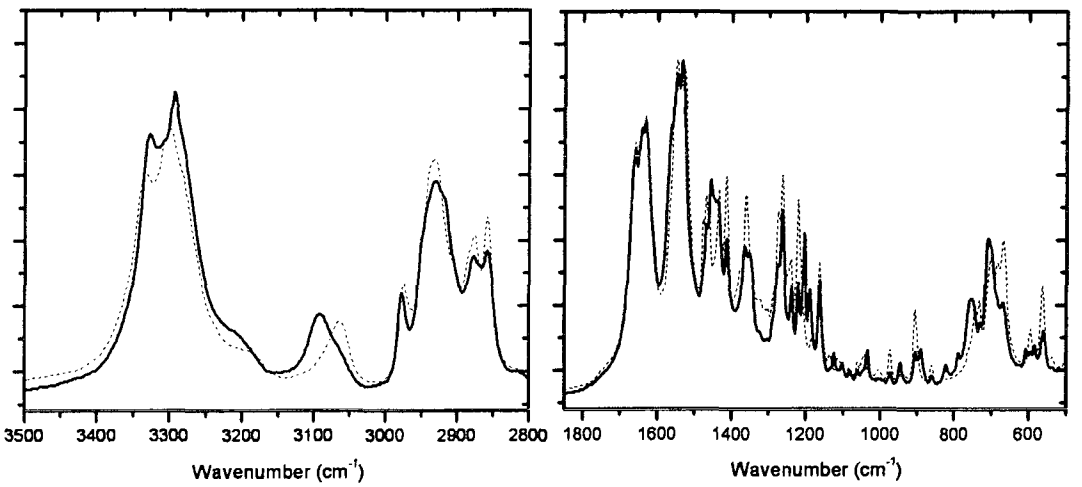

Figure 6.6. Partial FTIR spectra of the 50/50 mixture (solid line) and cyclic diamide II (dashed line).

Crystal packings of cyclic diamides were investigated using WAXD and are completely different for each cyclic monomer. WAXD patterns recorded at room temperature of the 50/50 mixture, and purified cyclic diamide I and cyclic diamide II, are shown in Figure 6.7. Cyclic diamide II was obtained after recyrstallization from a 50/50 mixture and WAXD pattern shows exactly the same peaks of 50/50 mixture except those associated with the cyclic diamide I. Cyclic diamide I, on the other hand, shows only three distinct peak at 13, 23, 27°.

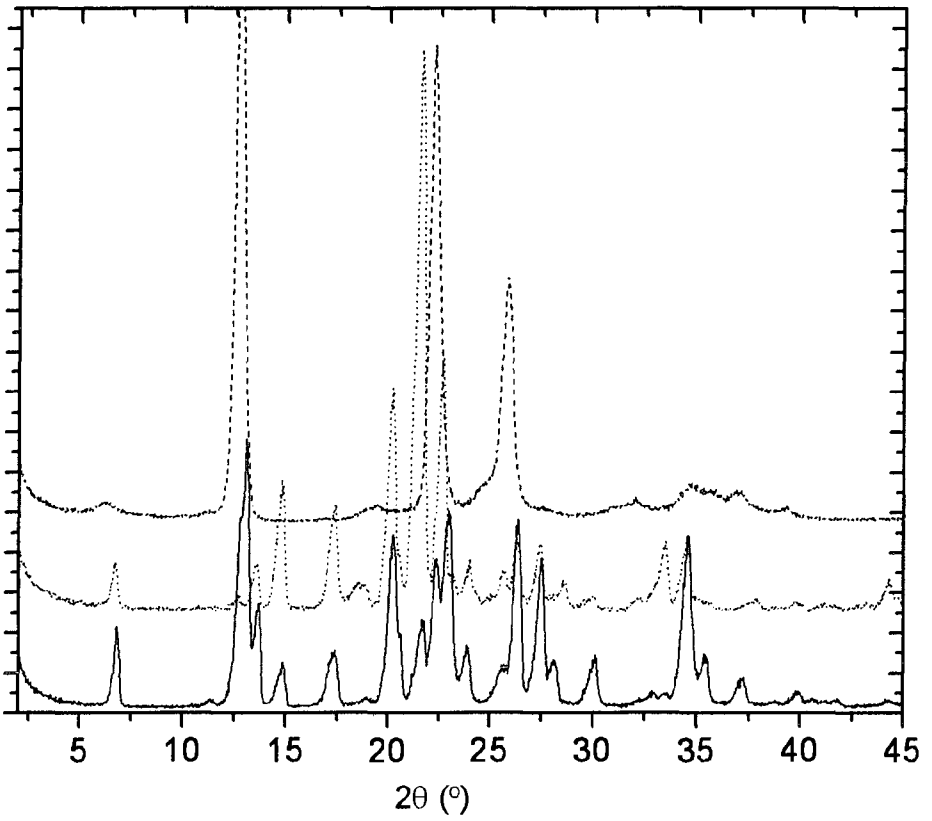

Figure 6.7. The WAXD patterns of 50/50 mixture (bottom) and cyclic diamide II (middle), and cyclic diamide I (top).

Copolymerization of 1,6-diazacyclododecane-2,5-dione

Homopolymerization of these cyclic diamides in the molten state is difficult due to the fact that the melting point of these monomers is so high, especially for the 12 member cyclic diamide which is around 290 °C and in the range of nylon 6 4. For this reason, we first explored the copolymerization of caprolactam with these cyclic monomers to investigate ring opening abilities and effect of nylon 6 4 repeat units on possible improvement of thermal and mechanical properties of nylon 6.

Copolymerization of 1,6-diazacyclododecane-2,5-dione with ε-caprolactam was carried out by both anionic and hydrolytic polymerization

methods to investigate the effect of the reaction mechanism on final copolymers. The details of the copolymerization are described in the experimental section. Since anionic polymerization is faster and carried out at lower temperature, it was expected to give fewer side products. Cyclic diamides used for polymerization mostly contained a single type of cyclic diamide.

The ^{13}C solution NMR spectrum of a copolymer synthesized by anionic polymerization is shown in Figure 6.8. The spectrum of homopolymer nylon 6 is included for comparison. The carbonyl carbon peak of the cyclic amide observed at 173.3-173-5 ppm shifts downfield to 174 ppm in the polymer backbone. The peaks assigned as a and c of cyclic diamide I are observed at 34.05 and 25.4 ppm, respectively. These peaks appear at 31.5 and 28.8 ppm, respectively, in the copolymer and are very close to the chemical shifts of these same carbons of cyclic diamide II. This is a good indication that chemical shifts of cyclic diamide II are related to the higher order macrocycle with less ring strain. The chemical shifts in the NMR spectrum will be more like their linear counterpart due to reduced ring-strain. Based on the intensity of the carbonyl carbon peak, the incorporation of nylon 6 4 is calculated as being 12 mol-%. The actual intensity of the carbonyl carbon of nylon 6 4 units is divided by two based on the assumption that there are two carbonyl carbon for nylon 6 4 units while only one for nylon 6 units.

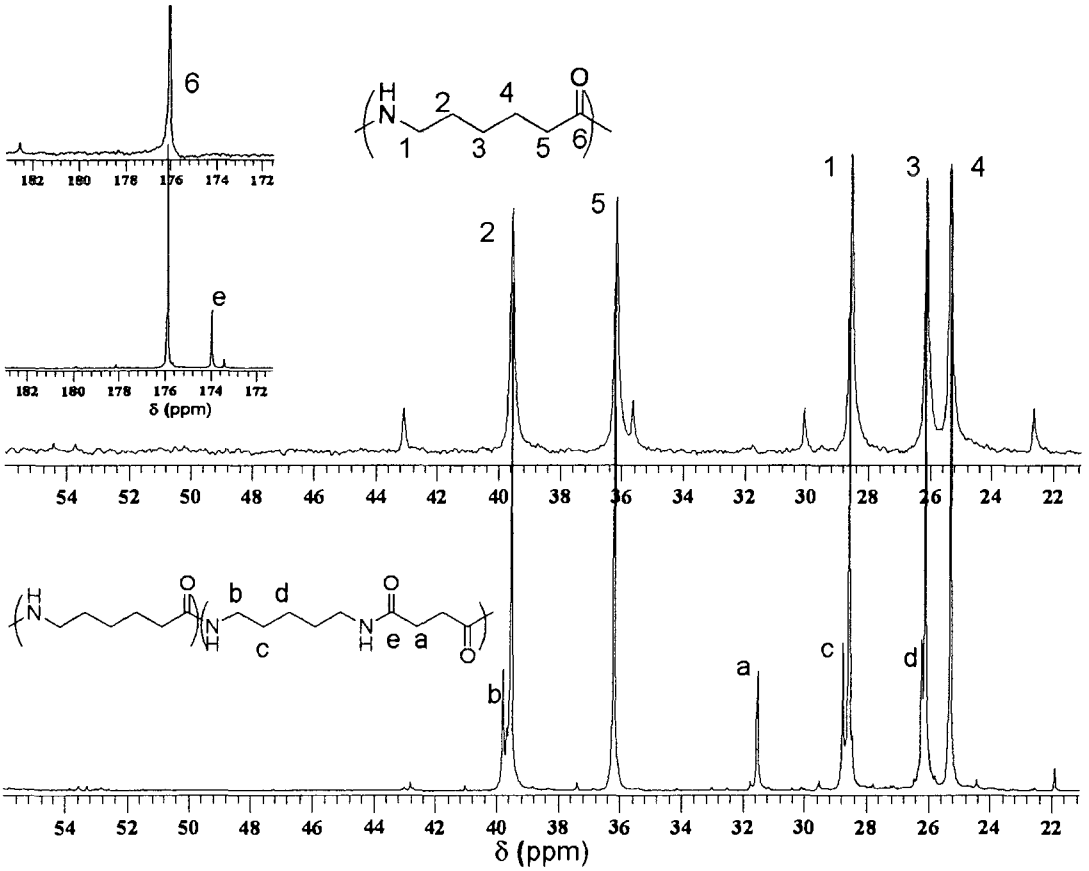

Figure 6.8. ^{13}C solution NMR of neat nylon 6 (top) and nylon (6-co-64) (bottom) by anionic polymerization method; 3:1 TFE:$CDCl_3$ NMR solvent.

As expected, copolymerization using the hydrolytic polymerization method is more complicated and results in several side products. To identify the peaks of copolymers, two novel model compounds was synthesized and the chemical shifts of copolymers analysized based on the chemical shift of these compounds in same solvent system (3:1 TFE:$CDCl_3$). The structures of these compounds are shown in Figure 6.9.

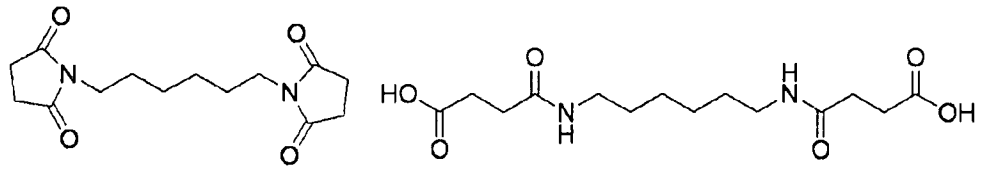

a b

Figure 6.9. Chemical structures of a) HAD-bisimide and b) HAD-bisamide acid.

The ^{13}C solution NMR spectrum of the copolymer with 10 w-% cyclic diamide synthesized by hydrolytic polymerization is shown in Figure 6.10. All peaks are assigned based on the chemical shifts of model compounds and nylon (6-co-64) obtained by anionic polymerization. Four distinct carbonyl peaks are observed including the carbonyl carbon of nylon 6. The carbonyl peak of acid-end groups appears at 178 ppm, while the carbonyl peak of imide-end group appears at 179.8 ppm. The peak associated with nylon 6 4 carbonyl is observed at 173.9 and split into two; one probably in the backbone, and the other the carbonyl carbon close to the carboxylic acid end-group. The splitting can be observed easily for the methyl carbon α to the carbonyl assigned as a. There are three peaks observed for this carbon in which one is associated with the carbon α to carboxylic acid end-groups and the others are associated with carbons α to backbone amides and amides close to carboxylic acid end-groups. Considering the intensities of the peaks, the cyclic diamide reacted only once and formed either imide or carboxylic acid terminal units.

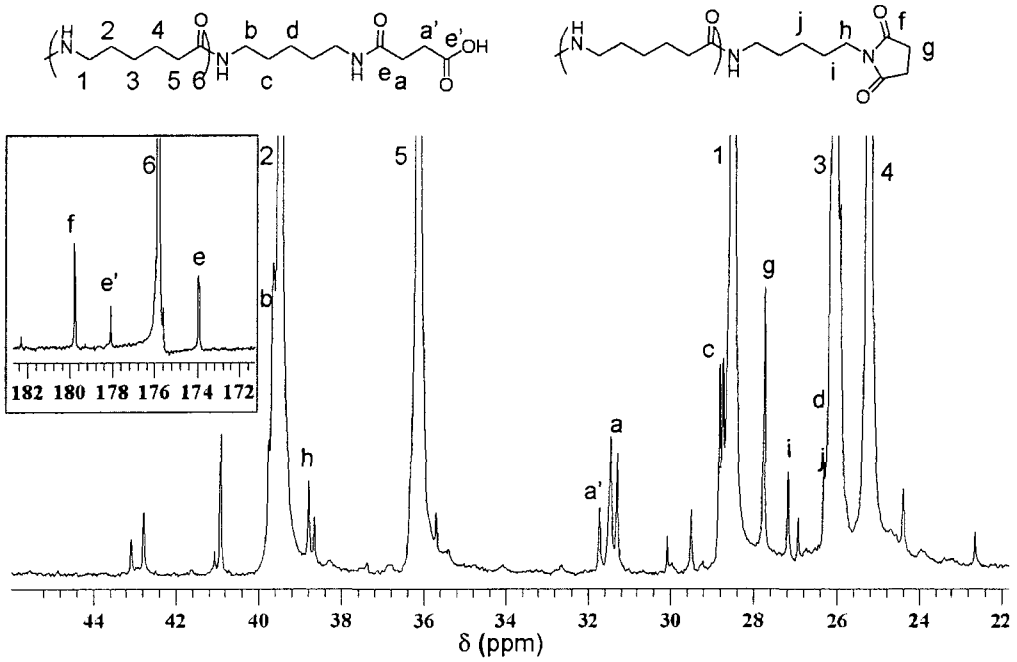

Figure 6.10. ^{13}C solution NMR of nylon (6-co-64) by hydrolytic polymerization method. The sample was dissolved in 3:1 TFE:$CDCl_3$.

The DSC heating thermograms of Nylon (6-co-64) by hydrolytic polymerization and anionic polymerization are given in Figure 6.11. Nylon (6-co-64) by anionic polymerization shows two distinct peaks at 217 and 280 °C indicating two different crystal populations. The higher endotherm is almost the same as the melting point of nylon 6 4 which was reported as 278 °C.[1] In addition to ^{13}C solution NMR spectrum of the copolymer synthesized by anionic method, which shows one peak and no splitting for nylon 6 4 repeat units, two distinct peak in the DSC similar to each homopolymer strongly suggests that the copolymer is a block copolyamide, and the reactivity of 1,6-diazacyclododecane-2,5-dione and ε-caprolactam are significantly different. Two distinct peaks at 195 and 218 °C are also observed in the DSC heating thermogram of nylon (6-co-64) obtained by hydrolytic polymerization and no endotherm is observed over the

temperature higher then the melting of nylon 6. The lower endotherm must be related with the melting of terminal nylon 6 4 units.

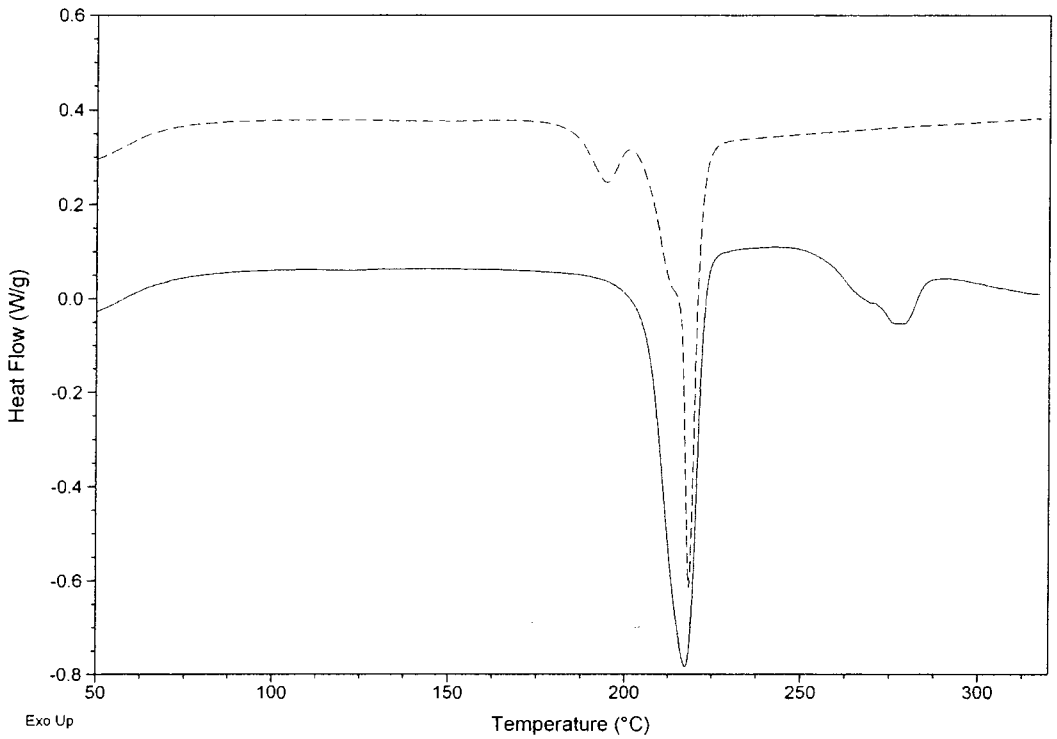

Figure 11. DSC heating thermograms of nylon (6-co-64) by hydrolytic polymerization (dashed line), and anionic polymerization (solid line).

Conclusions

The 12-membered cyclic diamide has been successfully synthesized in fairly high yield. The yield and the ring size of cyclic diamide can be varied by altering the reactants and reactant ratios. The synthesis of cyclic diamide with DPEA gave two different cyclic structures which can be easily isolated by recrystallization. The crystal packing as well as the melting points of each diamide were totally different. These cyclic diamides were shown to copolymerize with caprolactam, resulting in a block copolymers of nylon 6 and 6 4.

Acknowledgments

The authors would like to thank Dr. Douglas Masterson for help using mass spectrometry.

References

1_Peng, Puping; Hodge, Philip. Cyclic Oligo(undecanamide)s (Nylon 11s) and Cyclic Alternating Oligo(undecanamide-undecanoate)s: Their synthesis Using High Dilution Conditions and Their Analysis. *Polymer*, **1998**, 39, 981-990.

2 Salanski, P.; Krajewski, J. W.; Gluzinski, P.; Kasprzyk, S.; Stankiewicz, T.; Jurczak, J. Synthesis, Nuclear Magnetic Resonance, and X-ray Investigations of 1,10-Diazacyclooctadeca-2,9-dione. *Journal of Crystallographic and Spectroscopic Research*, **1991**, 21,195-200.

3 Vogl, O.; Knight, A. C. Polyoxamides. I. Preparation and Characterization of Cyclic Oxamides. *Macromolecules*, **1968**, 1, 311-315.

4 Vogl, O.; Knight, A. C. Polyoxamides. II. Polymerization of Cyclic Diamides. *Macromolecules*, **1968**, 1, 315-318.

5 Levchik, Sergei V.; Weil, Edward D.; Lewin, Menachem. Thermal Decomposition of Aliphatic Nylons. *Polymer International*, **1999**, 48, 532-557.

6 Iwakura, Yoshio; Uno, Keikichi; Haga, Kazuo; Nakamura, Koutarou. Cyclic Diamides. II. Synthesis and Polymerizations of Perhydro-1,5-diazocine-2,4-dione and Its Derivatives. *J. Polym. Sci., Polym. Chem. Ed.*, **1973**, 11, 367-376.

7 Iwakura, Yoshio; Uno, Keikichi; Akiyama, Masayasu; Haga, K. Polymerization of Perhydro-1,5-diazocine-2,6-dione. *J. Polym. Sci.: Part A-1: Polym. Chem.*, **1969**, 7, 657-666.

8 Vulic, Ivan; Hooft, Rob W. W.; Kroon, Jan. The Structure of 1,6-Diazacyclododecane-7,12-dione, A Cyclic Monomeric Model of Polyamide 4 6. *Journal of Crystallographic and Spectroscopic Research*, **1993**, 23, 917-920.

9 Cui, Xiaowen; Yan, Deyue. Polymorphism and Crystalline Transitions of the Novel Even-odd Nylons Derived from Undecanedioic Acid. *J. Polym. Sci.: Part B: Polym. Phys.*, **2005**, 43, 2048-2060.

10 Glans, J. H.; Akkapeddi, M. K. Synthesis and Polymerization of 2,15-Diaza-1,16-dioxo[16]paracyclophane. *Macromolecules*, **1992**, 25, 5526-5527.

11 Skrovanek, Daniel J.; Painter, Paul C.; Coleman, Michael M. Hydrogen Bonding in Polymers. 2. Infrared Temperature Studies of Nylon 11. *Macromolecules*, **1986**, 19, 699-705.

12 Zhang, Q.; Mo, Z.; Zhang, H.; Liu, S.; Cheng, S. Z. D. Crystal Transitions of Nylon 11 under Drawing and Annealing. *Polymer,* **2001**, 42, 5543-5547.

13 Kagiya, Tsutomu; Izu, Masatsugu; Matsuda, Takehisa; Fukui, Kenichi. Synthesis of Polyamides by the Polyaddition of Bis-succinimides with Diamines. *J. Polym. Sci.: Part A-1: Polym. Chem.*, **1967**, 5, 15-20.